# FILTERED MULTITONE FOR SLOW FADING AND FAST FADING CHANNELS

by

Pooyan Amini

A dissertation submitted to the faculty of
The University of Utah
in partial fulfillment of the requirements for the degree of

Doctor of Philosophy

Department of Electrical and Computer Engineering

The University of Utah

May 2013

# The University of Utah Graduate School

## STATEMENT OF DISSERTATION APPROVAL

The dissertation of **Pooyan Amini**

has been approved by the following supervisory committee members:

| | | |
|---|---|---|
| **Behrouz Farhang-Boroujeny** | , Chair | **01/31/2013** Date Approved |
| **V. John Mathews** | , Member | **02/01/2013** Date Approved |
| **Rong-Rong Chen** | , Member | **02/01/2013** Date Approved |
| **Neal Patwari** | , Member | **02/01/2013** Date Approved |
| **Lawrence G. Zeng** | , Member | **02/01/2013** Date Approved |

and by **Gianluca Lazzi**, Chair of the Department of **Electrical and Computer Engineering**

and by Charles A. Wight, Dean of The Graduate School.

# ABSTRACT

The demand for high speed communication has been increasing in the past two decades. Multicarrier communication technology has been suggested to address this demand. Orthogonal frequency-division multiplexing (OFDM) is the most widely used multicarrier technique. However, OFDM has a number of disadvantages in time-varying channels, multiple access, and cognitive radios. On the other hand, filterbank multicarrier (FBMC) communication has been suggested as an alternative to OFDM that can overcome the disadvantages of OFDM. In this dissertation, we investigate the application of filtered multitone (FMT), a subset of FBMC modulation methods, to slow fading and fast fading channels.

We investigate the FMT transmitter and receiver in continuous and discrete time domains. An efficient implementation of FMT systems is derived and the conditions for perfect reconstruction in an FBMC communication system are presented. We derive equations for FMT in slow fading channels that allow evaluation of FMT when applied to mobile wireless communication systems. We consider using fractionally spaced per tone channel equalizers with different number of taps. The numerical results are presented to investigate the performance of these equalizers. The numerical results show that single-tap equalizers suffice for typical wireless channels. The equalizer design study is advanced by introducing adaptive equalizers which use channel estimation. We derive equations for a minimum mean square error (MMSE) channel estimator and improve the channel estimation by considering the finite duration of channel impulse response. The results of optimum equalizers (when channel is known perfectly) are compared with those of the adaptive equalizers, and it is found that a loss of 1 dB or less incurs.

We also introduce a new form of FMT which is specially designed to handle doubly dispersive channels. This method is called FMT-dd (FMT for doubly dispersive

channels). The proposed FMT-dd is applied to two common methods of data symbol orientation in the time-frequency space grid; namely, rectangular and hexagonal lattices. The performance of these methods along with OFDM and the conventional FMT are compared and a significant improvement in performance is observed. The FMT-dd design is applied to real-world underwater acoustic (UWA) communication channels. The experimental results from an at-sea experiment (ACOMM10) show that this new design provides a significant gain over OFDM.

The feasibility of implementing a MIMO system for multicarrier UWA communication channels is studied through computer simulations. Our study emphasizes the bandwidth efficiency of multicarrier MIMO communications .We show that the value of MIMO to UWA communication is very limited.

# CONTENTS

# LIST OF FIGURES

# LIST OF TABLES

# CHAPTER 1

# INTRODUCTION

The data traffic demand has been increasing in the past two decades with an extremely fast pace and it is expected to continue the same trend in the next decade [2–15]. This increasing need has led to the use of multicarrier techniques for high speed communications. Orthogonal frequency division multiplexing (OFDM) has been the dominant technology for broadband communications in the past [16–18]. The most important advantage of OFDM is simple equalization by using a single-tap equalizer at each subcarrier which is achieved because of the orthogonality of a different subcarrier channels. On the other hand, a number of researchers have noted the shortcomings of OFDM in time-varying channels. For instance, [19] noted that the relatively large side-lobes of the spectra of the individual subcarriers in an OFDM signal limit its applicability to cognitive radios. Also, a number of researchers have noted the limitation of OFDM in dealing with time-varying channels and have suggested the use of alternative methods that employ filterbanks for multicarrier modulation [20–26].

The extension of OFDM to orthogonal frequency multiple access (OFDMA) has also been proposed [18,27]. In OFDMA, each user transmits on a subset of subcarriers. In order to avoid intercarrier interference, all of the users should be synchronized. This synchronization may not be straightforward for uplink channels and may be impractical for cognitive radio applications.

In order to address these shortcomings, alternative systems that use filterbanks for multicarrier modulation have been proposed. Filterbank multicarrier communication systems use a bank of filters in the transmitter and receiver. These filters are a modulated version of a prototype filter. Using a prototype filter can clearly solve

the synchronization problems. In addition, filterbank multicarrier (FBMC) systems limit the interference to adjacent subcarrier bands which results in less sensitivity to Doppler effects and carrier offset.

In the rest of this chapter, we first talk about OFDM in Section 1.1. Filterbank multicarrier communications methods such as staggered modulated multitone (SMT), cosine-modulated multitone (CMT), and filtered multitone (FMT)are considered in Section 1.2. Then, we present the filtered multitone for slowly fading channels in Section 1.3. Filtered multitone for fast fading channels is presented in Section 1.4. Finally, the contributions and organization of this dissertation are described.

## 1.1 Orthogonal Frequency Division Multiplexing

The block diagram of an OFDM transceiver is presented in Fig. 1.1. Following this figure, an OFDM transmitter starts by taking the $N$-point inverse discrete Fourier transform (IDFT) of the data symbols, $s_0[n], s_1[n], \cdots, s_{N-1}[n]$.

$$S_l[n] = \frac{1}{N} \sum_{k=0}^{N-1} s_k[n] e^{-j\frac{2\pi k}{N} l}. \tag{1.1}$$

Defining $\mathbf{S}[n]$ and $\mathbf{f}_k$ as

$$\begin{aligned} \mathbf{S}[n] &= [S_0[n], S_1[n], \cdots, S_{N-1}[n]]^{\mathrm{T}} \\ \mathbf{f}[n] &= \left[1, e^{j\frac{2\pi k}{N}1}, e^{j\frac{2\pi k}{N}2}, \cdots, e^{j\frac{2\pi k}{N}(N-1)}\right]^{\mathrm{T}} \end{aligned} \tag{1.2}$$

(1.1) can be written as

$$\mathbf{S}[n] = \frac{1}{N} \sum_{k=0}^{N-1} s_k[n] \mathbf{f}_k. \tag{1.3}$$

The above equation shows that the $k$th symbol $s_k[n]$ modulates a complex carrier at frequency of $f_k = \frac{k}{N}$. It is also worth noting that the spacing between all the carriers is $\frac{1}{N}$. Assuming an ideal channel, if adding the cyclic prefix is ignored at the transmitter and receiver, an undistorted copy of $x[n]$ is received in the receiver and by applying a DFT to each frame of $x[n]$ will recover the transmitted data symbols $s_0[n]$, $s_1[n]$, $\cdots$, $s_{N-1}[n]$. Practical channels, on the other hand, almost always suffer from multipath fading. The presence of multipath fading results in intersymbol interference (ISI) among $x[n]$ samples at the receiver.

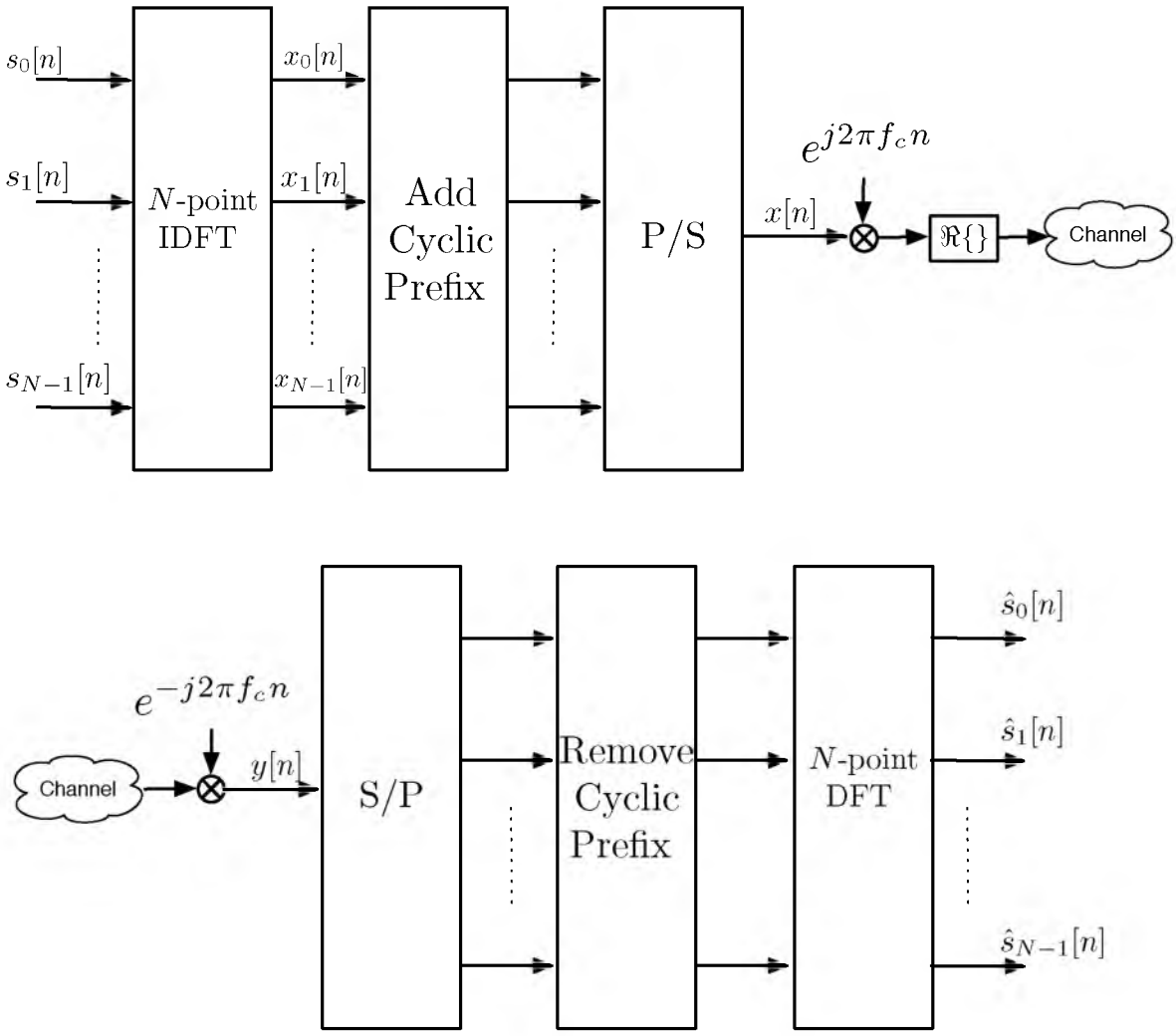


**Figure 1.1**: Block diagram of OFDM.

In order to avoid ISI, a guard interval with $N_{cp}$ samples is inserted before each OFDM symbol. This guard interval is filled with zeros or a copy of the last $N_{cp}$ samples of the output of IDFT. The later case is referred to as cyclic prefix (CP) and is more common. Thus, we focus only on OFDM with CP. The structure of CP is presented in Fig. 1.2.

Assuming that the length of the channel impulse response $L$ is less than $N_{CP}$, intersymbol interference (ISI) from adjacent OFDM symbols is avoided. Furthermore, the use of CP maintains the orthogonality of different subcarrier channels and thus allows recovery of the transmitted symbol $s_k[n]$ through a DFT operation and a single-tap equalizer per subcarrier channel in a time-invariant environment.

In order to explain the shortcomings of OFDM with CP for time-varying channels, we can write the baseband transmit signal as

$$x[n] = \frac{1}{N} \sum_{k=0}^{N} \sum_{l} s_k[l] g[n-l] e^{j2\pi(n-N_{CP})k/N} \tag{1.4}$$

where

$$g[n] = \begin{cases} 1, & n = 0, 1, \cdots, N + N_{CP} \\ 0, & \text{otherwise.} \end{cases} \tag{1.5}$$

Following the derivation of the power spectral density (PSD) in [28], it can be shown that the PSD for the transmitted OFDM signal in (1.4) is

$$\phi(f) = C \sum_{k=0}^{N} \left| \phi\left(f - \frac{k}{N}\right) \right|^2 \tag{1.6}$$

where $C$ is a constant, and

$$\phi(f) = \text{sinc}(fN). \tag{1.7}$$

(1.6) shows that for each subcarrier, $k$, there is one sinc function centered at $f_k = \frac{k}{N}$. Fig. 1.3 presents the spectrum of a subcarrier in an OFDM system. It can be seen

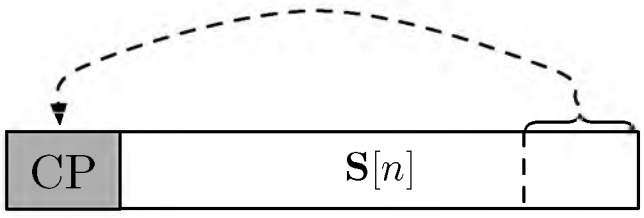


**Figure 1.2**: Structure of cyclic prefix.

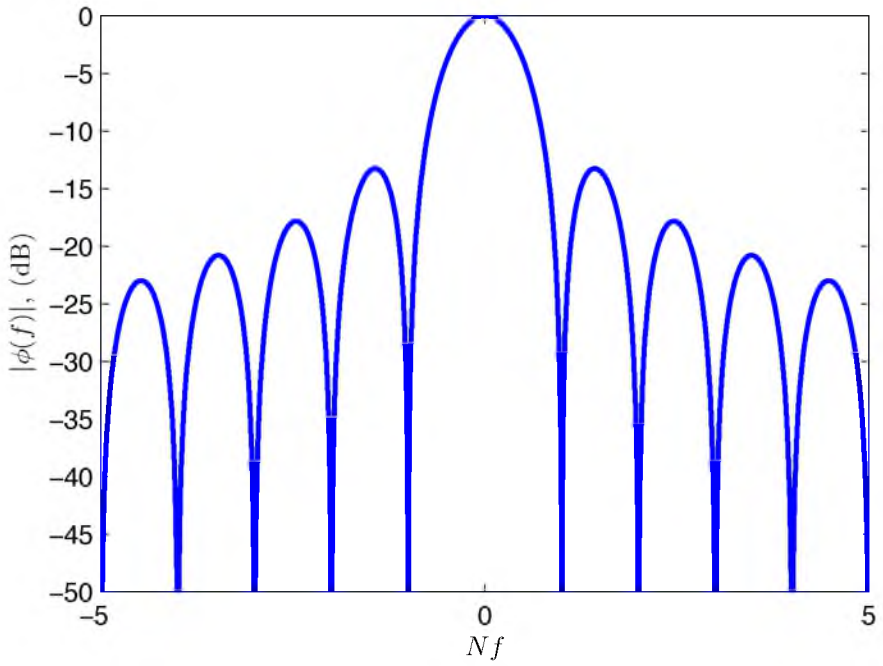


**Figure 1.3**: Power spectral density of a subcarrier in an OFDM system.

that each subcarrier has nulls on the center frequency of the other subcarriers which results in the orthogonality of different subcarriers. However, the side-lobes of each subcarrier are relatively large.

In a cognitive radio setting, in addition to the licensed users which are called primary users (PU), unlicensed users, also known as secondary users (SU) are allowed to communicate over a portion of the spectrum. The SUs should be able to sense the spectrum and use the portions which are not being used by the PUs, *i.e.,* white spaces. The communication of the SUs should not interfere with the PUs. In this setting, OFDM is not the best choice for modulation in the SUs since it has large side-lobes. The large side-lobes of OFDM result in interference among the carriers of different SUs as well as between SUs and PUs.

Moreover, because of the large side-lobes, OFDM is not an appropriate choice for time-varying channels. To elaborate, in a time-varying channel, the variations in the time domain translates to the dispersion in the frequency domain. As a result, in OFDM, the subcarrier nulls that coincide with the center position of other subcarriers and avoid intercarrier interference (ICI) will disappear. Thus, the channel variation

in time may result in a significant level of ICI. The experimental results that are presented in Chapter 6 are a good example of an application where OFDM may be found inefficient.

## 1.2 Filterbank Multicarrier Methods

filterbank multicarrier (FBMC) techniques have a relatively long history. They were introduced even before the introduction of the OFDM in [25]. In 1966, almost two decades before any discussion on OFDM, Chang [24] proposed an FBMC technique. In this technique, pulse amplitude modulated (PAM), *i.e.,* real-valued, symbols were transmitted over a set of (partially) overlapping vestigial side-band (VSB) modulated channels. Fig. 1.4 depicts the general block diagram of FBMC transmitter and receiver systems.

Subsequently, a year later, Saltzberg [23] showed how Chang's method could be modified to transmit quadrature amplitude modulated (QAM), *i.e.,* complex-valued, symbols. It was shown that perfect reconstruction of symbols can be achieved by using a half-symbol space delay between the in-phase and the quadrature components of QAM symbols and by proper choice of transmit and receive pulse shapes. Both methods achieve the maximum bandwidth efficiency, in the sense that a QAM symbol (a pair of PAM symbols, in the case of Chang's method) is transmitted over a bandwidth of 1 Hz within each time period of 1 sec. Polyphase structures for efficient implementation of the Saltzberg's method were later proposed in [29]. Because of the half-symbol space delay between the in-phase and quadrature components, this method has been referred to as offset quadrature amplitude modulation (OQAM) or OFDM-OQAM. We refer to this method as staggered modulated multitone (SMT), which refers to the time staggering between the in-phase and quadrature components of QAM symbols.

Filtered multitone (FMT) is another multicarrier modulation technique that was initially developed for digital subscriber line (DSL) [30–33]. In contrast to SMT and CMT, adjacent subcarriers do not overlap in FMT systems. As a result, FMT can transmit normal QAM symbols which makes it easily generalizable to multiple-input multiple-output (MIMO) systems. On the other hand, not having overlap between

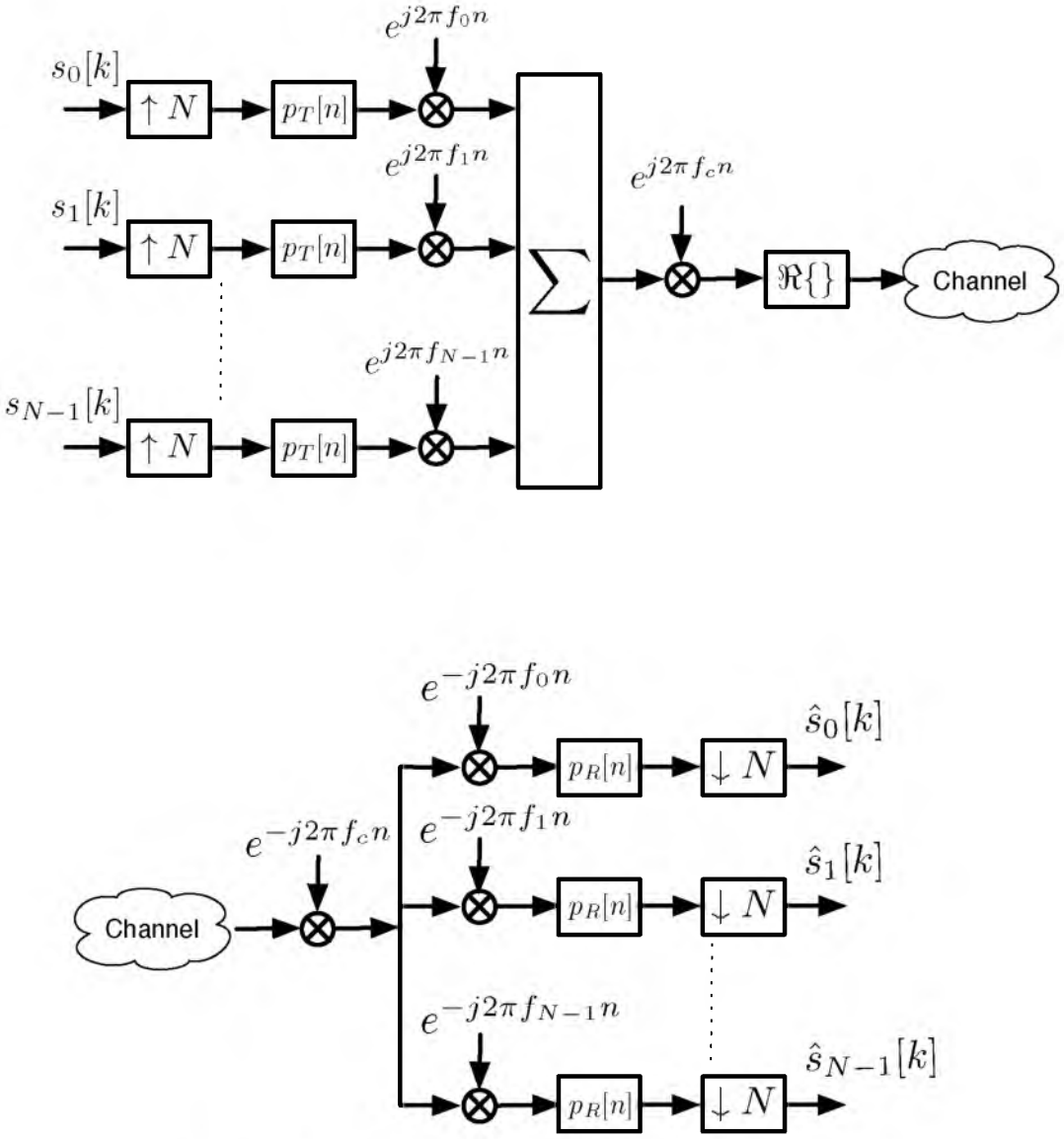


**Figure 1.4**: General structure for filterbank system.

adjacent subcarriers will result in losing some spectral efficiency. Hence, FMT systems can never achieve full spectral efficiency.

### 1.2.1 Cosine-Modulated Multitone

As mentioned previously, the very first proposed filterbank system transmits pulse amplitude modulated (PAM) symbols over a set of vestigial side band (VSB) subcarriers channels [24]. In the 1990s, Sandberg and Tzannes developed a method for digital subscriber line (DSL) called discrete wavelet multitone (DWMT) [34]. In [20], it is shown that DWMT uses cosine-modulated filterbanks (CMFB) for modulation. Hence, in this dissertation, it is referred to as cosine-modulated multitone (CMT). Moreover, it has been shown in [35] that CMT is a reinvention of Chang's method in discrete-time. A simple equalizer design for CMT was proposed in [20].

Fig. 1.5 presents a block diagram of the CMT transceiver. It can be shown that when $p(t)$ is a square-root Nyquist filter in an ideal channel, perfect reconstruction is achieved, *i.e.*, $\hat{s}_k[n] = s_k[n]$ [20].

### 1.2.2 Staggered Modulated Multitone (SMT)

Fig. 1.6 presents a block diagram of the SMT transceiver. In an SMT transmitter, the real and imaginary parts of each QAM symbol are separated and are transmitted with a time offset equal to half of the symbol spacing. Saltzberg showed that if a root-Nyquist filter with symmetric impulse response is used for pulse-shaping at the transmitter and the matched filtering is applied at the receiver, perfect reconstruction of the QAM symbol at the receiver is achieved in an ideal channel.

### 1.2.3 Filtered Multitone (FMT)

FMT was originally proposed as a solution for filtering the narrowband interferences in VDSL channels [30–32]. It has also been considered as a physical layer candidate for wireless communication [33]. Similar to frequency multiplexing, FMT multicarrier systems are designed such that adjacent subcarriers do not overlap. These systems achieve perfect reconstruction by using noncritical sampling [32]. The block diagram of an FMT communication system is shown in Fig. 1.7. An in-depth analysis of FMT systems is presented in Chapter 2

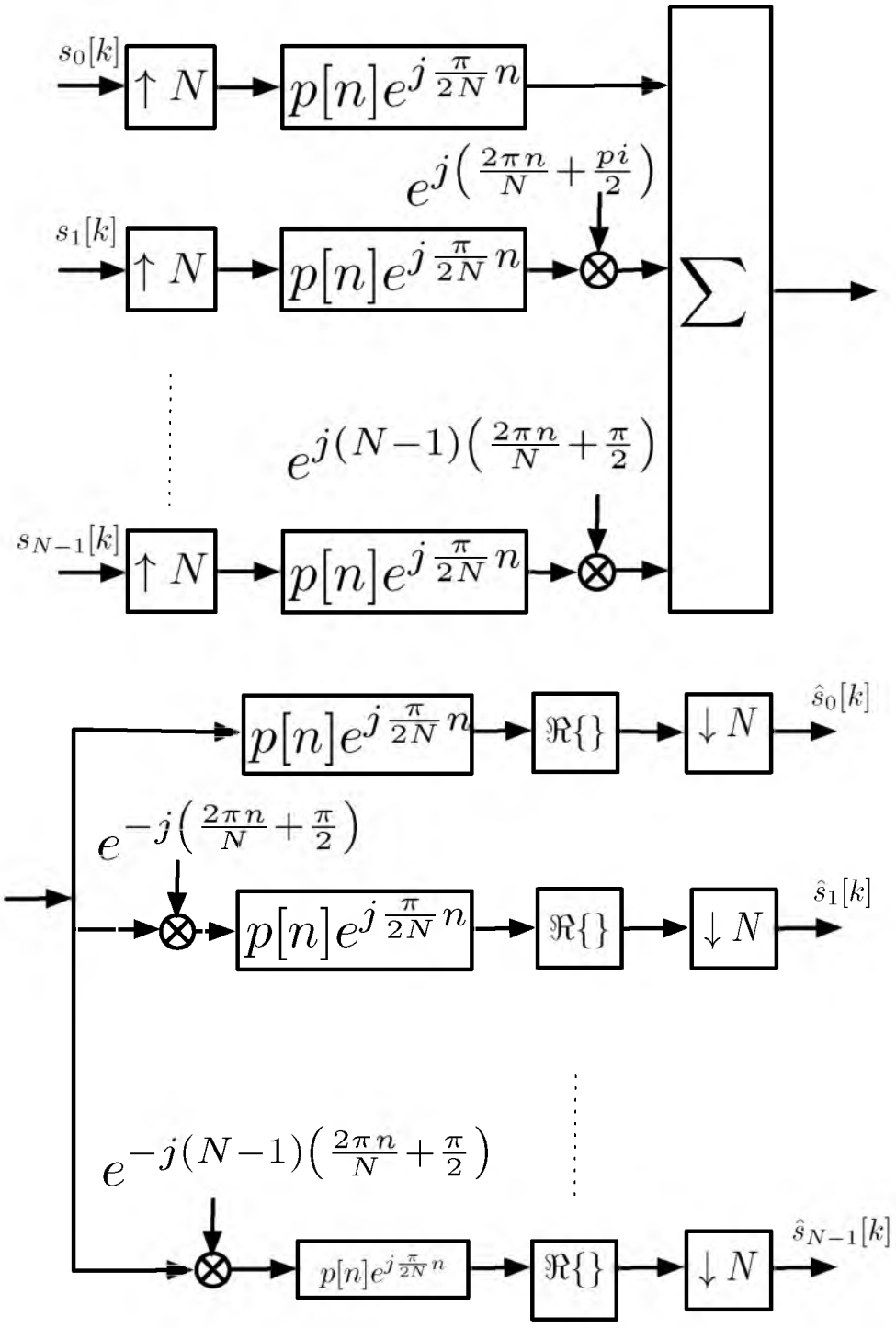


**Figure 1.5**: Block diagram of CMT.

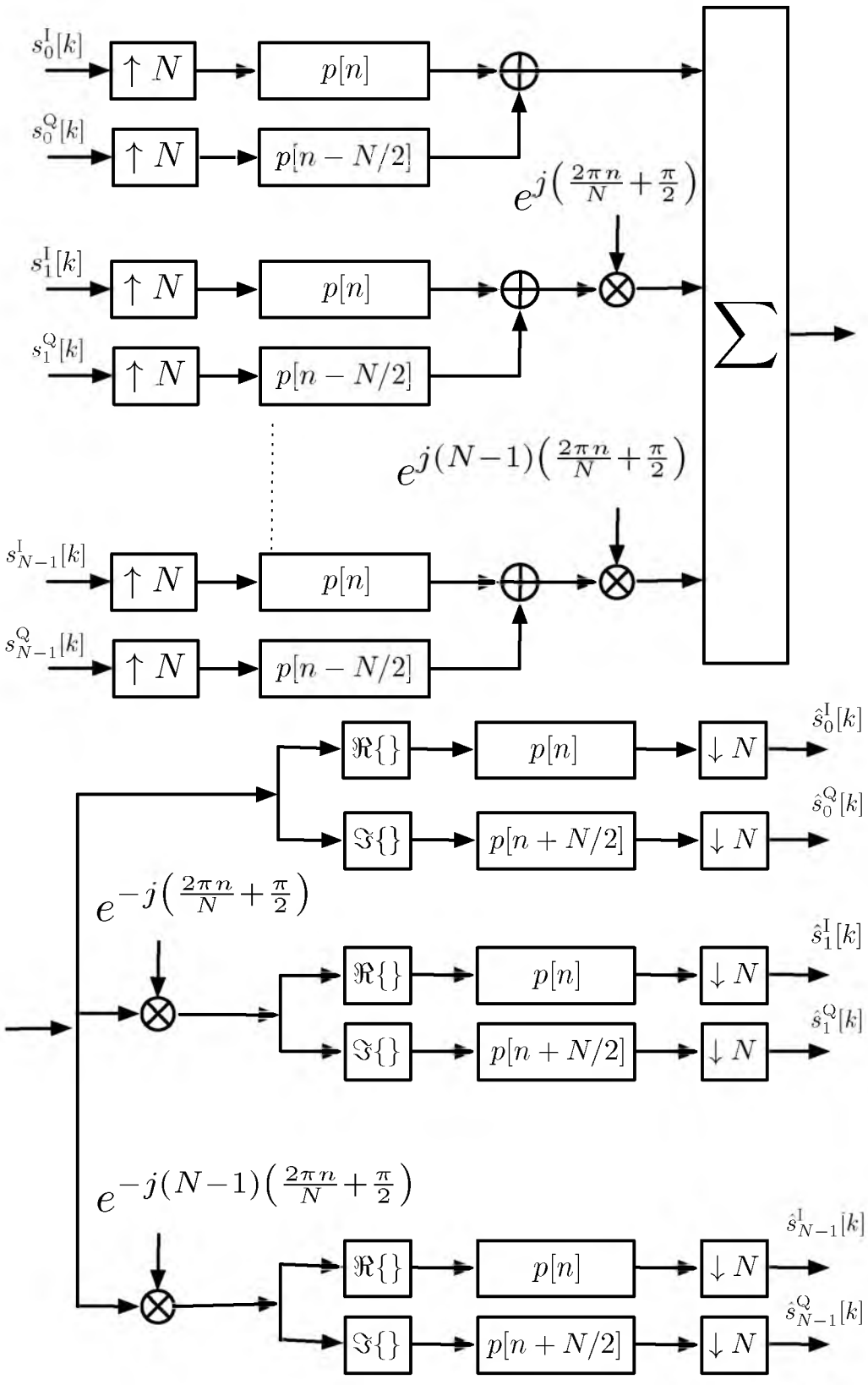


**Figure 1.6**: Block diagram of SMT.

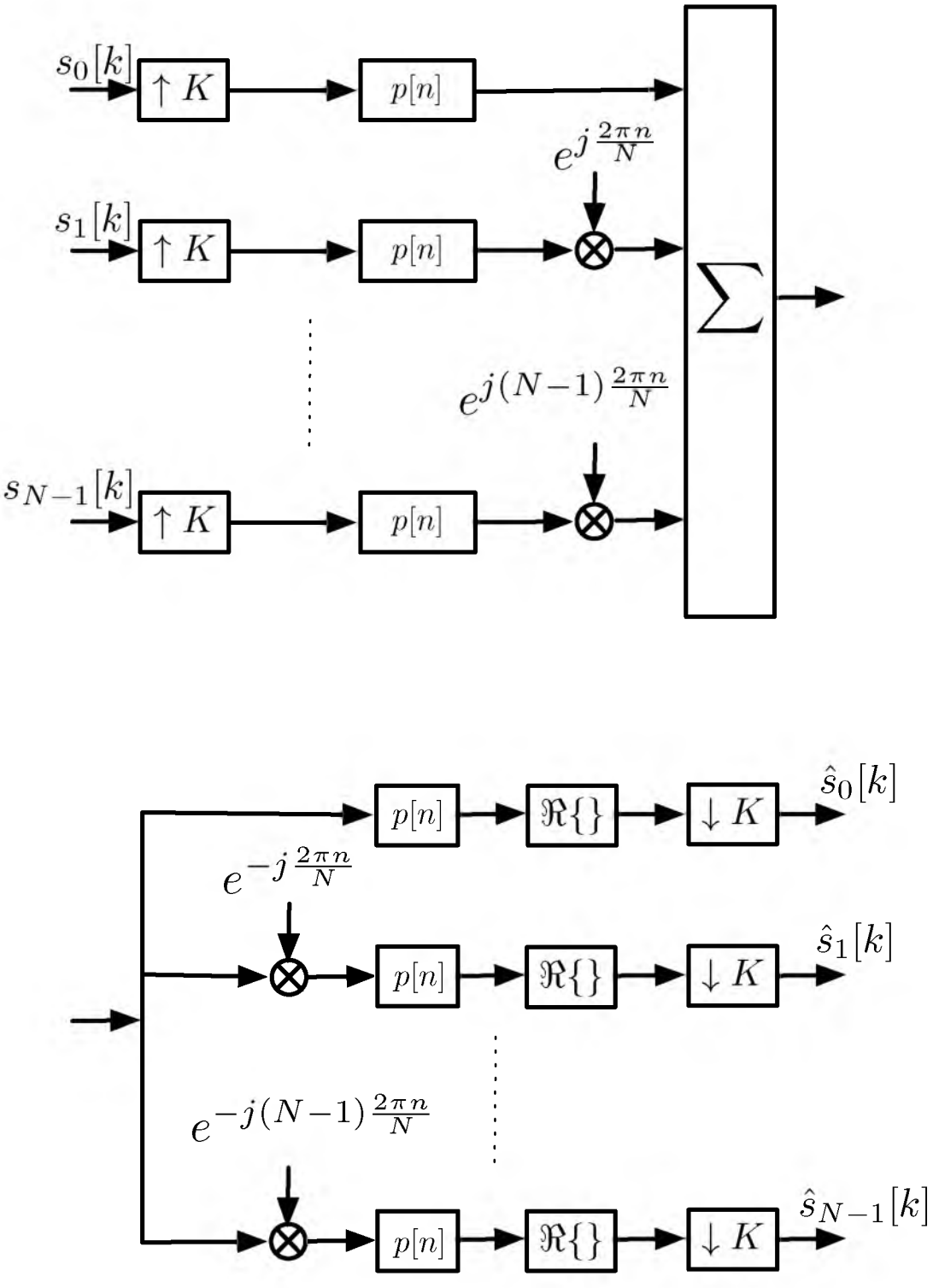


**Figure 1.7**: Block diagram of FMT.

## 1.3 Filtered Multitone for Slow Fading Channels

In a conventional FMT system, subcarrier bands are nonoverlapping. Hence, in a slowly varying channel, ICI is negligible. In this part of the dissertation, slow fading channels, similar to the channels mentioned in [30, 33], are considered. The analysis in [33] is limited to the case where, at the receiver, a single-tap equalizer is used at each subchannel output of FMT. In the first part of this dissertation, we further the analysis of [33] by exploring the FMT performance when a multitap equalizer is used at each subchannel output of FMT. We derive close form solutions for the optimum coefficients of a fractionally spaced equalizer and the signal to intersymbol interference plus noise ratio (SINR) at the equalizer output.

In conventional FMT, under the assumption of slow fading channels, subcarrier channels are nonoverlapping. As a result, each subcarrier channel may be treated independently. In a slowly varying environment, modulation caused by Doppler spread results in some overlap among adjacent subcarrier channels. However, the studies performed in [33] have revealed that compared to other degradations caused by a time-varying channel, the impact of such overlap is negligible. In light of this observation, throughout the first part of this dissertation, we treat each subcarrier channel of an FMT system as an independent single-carrier communication link and thus, our study concentrates on the single-carrier communication.

We note that in a time-invariant environment, to allow a minimum-length (possibly, a single-tap) equalizer, one will set the number of subcarriers in FMT as large as possible. On the other hand, the time span of each symbol within a subchannel increases proportional to the number of subchannels, and in a time-varying environment, one wishes to keep this time span as short as possible. Hence, in a time-varying environment, one should make a decision to strike a balance between system performance and the equalizer complexity. Our analytical results can be used to develop and present a number of design curves for selecting the system parameters in FMT for some standard channel models.

## 1.4 Filtered Multitone for Fast Fading Channels

In the second part of this dissertation, we focus on the channels that exhibit spreading both in time (due to multipath effects) and in frequency (due to time variation of the channel), namely, the doubly dispersive channels. One example of these channels is the UWA channel. Due to the low speed of sound propagation, low carrier frequency, fast changing environment, and multipath effect, the UWA channels are considered highly dispersive both in the time and frequency domain which makes them doubly dispersive channels.

In order to compensate for the time dispersion of UWA channels, the orthogonal frequency division multiplexing (OFDM) has been proposed and widely studied by a number of researchers, *e.g.*, [36–38]. In order to keep the bandwidth efficiency of the transmission sufficiently high, the acceptable norm is to allocate 20% of each OFDM symbol to its cyclic prefix (CP). This is the equivalent of saying the CP length is one quarter of the length of each fast Fourier transform (FFT) block in the OFDM system. Moreover, since the length of CP should be at least equal to the duration of the channel impulse response, and the latter is usually very long in UWA channels, this translates to very long symbols in the OFDM systems adopted for UWA communications. Hence, the channel variation over each OFDM symbol in the very dynamic UWA channels may lead to a significant channel variation over each OFDM symbol, hence, leading to a significant intercarrier interference (ICI) and thus a poor receiver performance.

On the other hand, Le Floch *et al.* [39], noted the significance of FBMC techniques in dealing with doubly dispersive channels. The use of prototype filters that balance between the time and frequency spreading has also been noted in [39]. The isotropic orthogonal transform algorithm (IOTA) of Alard [40] that designs filters that are well localized in both the time domain and the frequency domain was also introduced in [39]. An alternative prototype filter design to IOTA is the method proposed by Haas and Belfiore [1]. In [1], it was noted that the members of a subset of the Hermite functions satisfy the isotropic properties, and it was thus concluded that a class of isotropic filters could be constructed by linearly combining the members of this subset. Haas and Belfiore called filters designed in this way *Hermite designs*. In

this dissertation, we use the term isotropic for both the IOTA design of Alard and the class of filters proposed by Haas and Belfiore.

More detailed studies of the impact of channel variation on the performance of FBMC systems have been preformed and reported in the literature. The most prominent works in this area are [41–46]. Liu et al. [41] studied the impact of channel from an information theoretic point of view. Das and Schniter [42] approached and solved the problem of channel dispersion by considering a prototype filter design that allows a certain level of ISI/ICI and adopt a turbo equalization approach to compensate for the residual ISI/ICI. Tauböck et al. [43] have recently considered the possibility of using compressive sensing for estimating certain doubly dispersive channels. The works presented in [44–46], similar to this dissertation, consider the impact of the channel in the selection of prototype filters for some robust performance.

Furthermore, attempts have been made to adopt the above FBMC methods in multiple-input multiple-output (MIMO) channels. However, although some advancement in this area have been made, *e.g.*, [47–50], a study of these works reveals that the adoption of these FBMC methods to MIMO channels is not as trivial as in the case of OFDM. For instance, to develop FBMC systems that use Alamouti code in their design, the authors in [48] resort to a multicarrier code division multiple access (CDMA) system and in [49], a special block structure is designed. On the other hand, [47] has suggested a method of exploiting the Alamouti diversity gain in the case where there are more antennas at the receiver than at the transmitter. Adoption of FBMC to the cases where independent streams of data are transmitted from different antennas, in order to approach the capacity of MIMO channels, has been recently discussed in [50]. However, the receiver proposed in this paper is either a zero-forcing or a minimum mean square error (MMSE) equalizer-based system. Such receivers are known to suffer from noise enhancement and thus are limited in application. Unfortunately, the more advanced techniques such as those based on sphere decoding [51] or Markov chain Monte Carlo [52] techniques are not applicable.

The second part of this dissertation is motivated by a number of aspects of the above advancements in the area of FBMC techniques as well as some of their shortcomings. First, we note that the isotropic prototype filter design is an excellent

choice for dealing with the doubly dispersive channels in a very effective way. However, in the past, they have been explicitly designed [1, 40] for FBMC systems that follow the principles set in [24] and [23]. Thus, as mentioned above, their adoption to MIMO channels is limited. In this dissertation, we note that FMT, like OFDM, is straightforwardly applicable to MIMO channels. Also, we discuss how isotropic designs can be used to form a new class of FMT systems that are more robust than the FMT systems that have been studied in the past. Moreover, we develop a novel method for designing isotropic filters that are bandwidth efficient and robust against doubly dispersive channels. We note that (as discussed later in this dissertation) the isotropic filter designs which have been reported in [40] and [1], if applied to the FMT system that we propose in this dissertation, achieve a bandwidth efficiency of only 50%. The design method proposed in this dissertation allows one to increase this figure. As an example, a robust design with a bandwidth efficiency of 80% and yet far better performance than an OFDM system with similar bandwidth efficiency is presented in this dissertation.

## 1.5 Contribution of the Dissertation

This dissertation is focused on the application of filtered multitone for fading channels. For slow fading channels, the optimum fractionally spaced equalizer is designed and analyzed. A practical channel estimation-based equalization method has also been proposed. Furthermore, for fast fading channels, a robust filter design is proposed and its performance has been verified through computer simulations. The robust filter design is also applied to single-input multiple-output (SIMO) underwater acoustic communication. In addition, an analysis of possible application of multiple-input multiple-output methods for underwater acoustic communication is also presented and their feasibility in realistic channels are discussed.

The contributions of this dissertation are as follows:

- We study the fractionally spaced equalizers for FMT in slow fading channels. We find closed form equations for the mean square error (MSE) and signal to interference and noise ratio (SINR) of the optimum fractionally spaced equalizers. We show that for normal speeds of vehicles and the state of art parameters

in the current standards, *e.g.*, WiMAX and 3GPP LTE, a single-tap equalizer per subcarrier is sufficient. Our results on this topic have appeared in [53].

- We design a channel estimation-based equalization method for FMT in slow fading channels which takes advantage of the correlation of the channel impulse response in time and frequency domain as well as the limited duration of the channel impulse response. We show that this method performs very close to the optimum single-tap equalizer. Our results on this topic have appeared in [54].

- A cost function to design robust prototype filters for filtered multitone in fast fading channels is proposed. This filter design relaxes on the exact cancellation of ICI and ISI components, in the absence of a channel, in order to reduce the inevitable ICI and ISI in the presence of a doubly dispersive channel. The proposed filter design method is compared with conventional FMT methods as well as OFDM through computer simulations. Our results on this topic have appeared in [55–57].

- We use the designed prototype filter to create FBMC packets for underwater acoustic communications which are tested in an at-sea experiment. The received data from the experiment are decoded and we show that the proposed method significantly outperforms the existing OFDM method for UWA communications. Our results on this topic have appeared in [58].

- The feasibility of implementing a MIMO system for multicarrier UWA communication channels is analyzed. Our study emphasizes the bandwidth efficiency of multicarrier MIMO communication in this application. We find the published results so far have very little gain in the domain of UWA channels.

## 1.6 Organization of the Dissertation

FMT is presented in Chapter 2. The continuous-time structure of an FMT system is presented and its discrete-time counterpart is discussed. The polyphase structure for an efficient implementation of FMT is also derived. Furthermore, Chapter 2 presents the conditions for perfect reconstruction in multicarrier systems, in general.

For a slow fading channel in a conventional FMT system, the amount of intercarrier interference is negligible. Chapter 3 addresses the optimum fractionally spaced equalizer design for slow fading channels. The closed form equations for the minimum mean squared error (MMSE) as well as signal to interference plus noise ratio (SINR) are presented. It is shown through computer simulations that for wireless communication under normal speeds, a single-tap equalizer per subcarrier is sufficient.

In Chapter 4, based on the results of Chapter 3, a practical single-tap equalizer is designed. We derive equations for an MMSE channel estimator. The results of optimum equalizers (when channel is known perfectly) are compared with those of the adaptive equalizers. Our study considers the finite duration of the channel impulse response and used that to improve on the equalizers performance.

Channels that are changing fast in time and frequency domain impose some drawbacks for OFDM as well as conventional FMT systems. In these channels, the assumption of having no ICI no longer holds for both conventional FMT systems and OFDM. In Chapter 5, a novel filter design for doubly dispersive channels is proposed. The proposed filter design is compared with existing methods through computer simulations.

In Chapter 6, we verify the computer simulation results of Chapter 5 for the proposed filter design through an at-sea experiment. Similar packet designs for the proposed method and OFDM are used in order to transmit the data in an at-sea experiment performed off the coast of New-Jersey. The received data are analyzed and the performance of the proposed method is compared with OFDM.

Finally, Chapter 8 presents the concluding remarks and future research. Various areas of research for FMT are identified in Chapter 8.

# CHAPTER 2

# A REVIEW ON FILTERED MULTITONE COMMUNICATION SYSTEMS

Filtered multitone is a member of the class of filterbank multicarrier (FBMC) systems. Conventional FMT systems work similar to frequency division multiplexing methods. There is no overlap between adjacent subcarriers, thus, there is no intercarrier interference (ICI). Intersymbol interference can be avoided by using a square-root Nyquist filter, as in conventional single carrier systems [30–33].

In order to implement FBMC systems, an efficient technique is used that is called polyphase implementation. Polyphase implementation reduces the complexity of FBMC transmitters and receivers by taking advantage of multirate signal processing techniques [33, 59].

In this chapter, we first present the FMT system in Section 5.2. The continuous and discrete-time structure of the transmitter and receiver of an FMT system are presented in Subsections 2.2.1 and 2.2.2, respectively. In Subsection 2.1.3, the perfect reconstruction criterion for FMT systems is presented. The polyphase implementation of FMT systems is discussed in Section 2.2.

## 2.1 Filtered Multitone

### 2.1.1 Transmitter

The structure of an FMT transmitter in continuous time is shown in Fig. 2.1. The input signals $s_1(t)$ through $s_{N-1}(t)$ are continuous-time signals which are obtained from complex-valued data symbols as

$$s_k(t) = \sum_n s_k[n]\delta(t - nT) \tag{2.1}$$

where $s_k[n]$ are complex-valued digital data symbols and $T$ is the symbol duration.

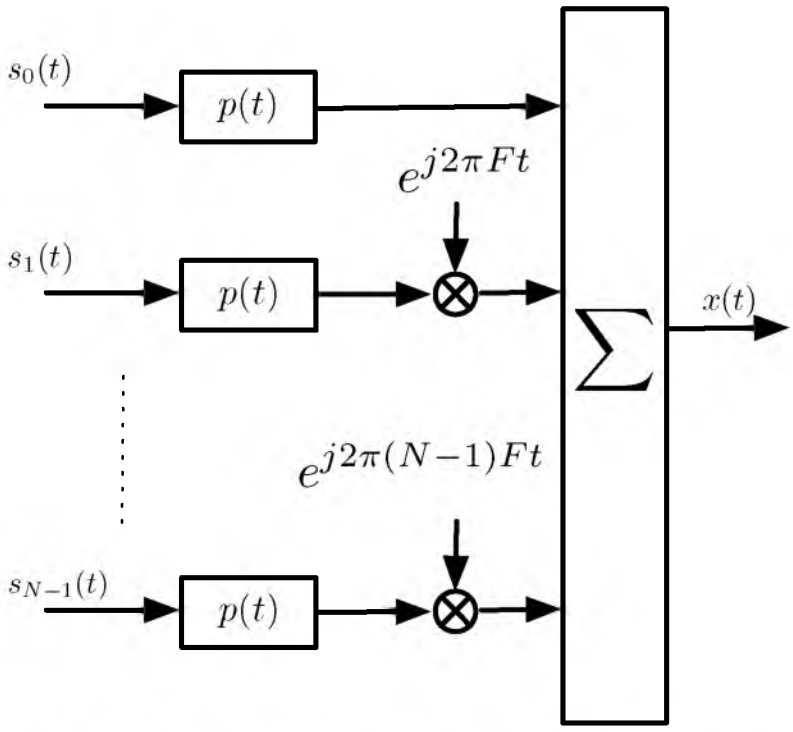


**Figure 2.1**: FMT transmitter in continuous time.

In a CMT or SMT system, the subcarrier spacing, $F$, is equal to the inverse of the symbol duration, $T$. However, in an FMT system, we have

$$F = \frac{1+\alpha}{T} \tag{2.2}$$

where $\alpha$ is called the roll-off factor and determines the excess bandwidth taken by each subcarrier band. Fig. 2.2(a) presents the spectrum of an FMT signal where the frequency is in terms of Hertz. In Fig. 2.2(b), the frequency axis is normalized with respect to a sampling frequency $fs = NF$. $K$ is a constant which is related to $N$ through the following equation

$$K = (1+\alpha)N. \tag{2.3}$$

Hence, we obtain $fs = \frac{K}{T}$, and this, in turn, implies that we have $K$ samples during each symbol period $T$. In order to be able to simplify the discrete-time implementation of FMT, we assume that $K$ is an integer. The discrete-time implementation of an FMT receiver is depicted in Fig. 2.3. The parallel input streams, $s_0[n]$, $s_1[n]$, $\cdots$,

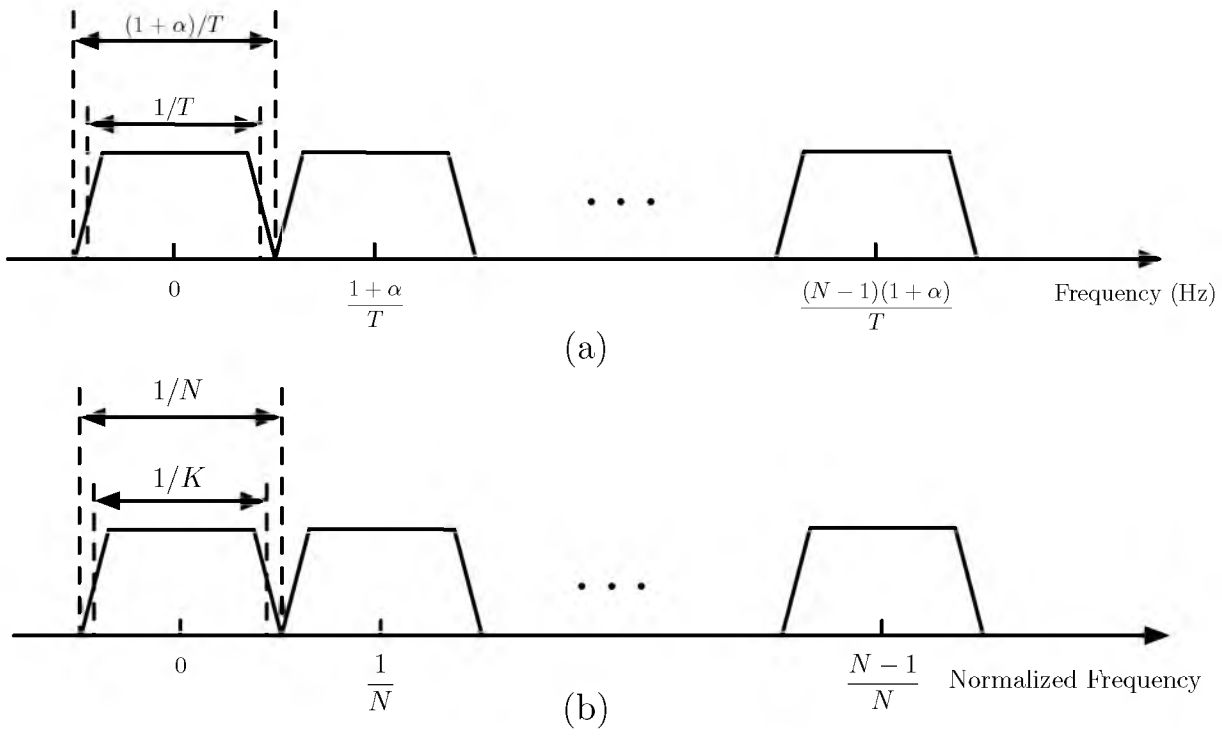


**Figure 2.2**: FMT transmitter in discrete time.

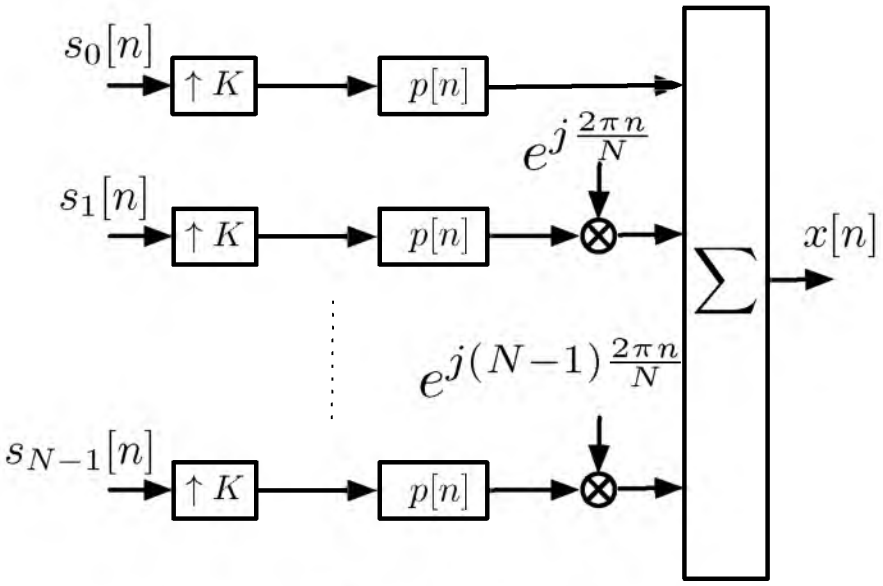


**Figure 2.3**: FMT transmitter in discrete time.

$s_{N-1}[n]$ are zero-interpolated by a factor of $K$ and then passed through the prototype filter and modulated on different subcarrier bands.

### 2.1.2 Receiver

Fig. 2.4 depicts the structure of an FMT receiver in the continuous-time implementation. The received stream $y(t)$ is demodulated using different carriers and passed through the prototype filter and one sample is taken every $T$ seconds. Using the definition of $K$ in (2.3) and similar to the transmitter filterbank, the discrete-time implementation of the receiver is obtained as in Fig. 2.5. In this case, instead of sampling with intervals of $T$, the output of the prototype filter is downsampled by a factor of $K$.

### 2.1.3 Reconstruction

In an FBMC system, the transmit signal is generated as

$$x(t) = \sum_{n} \sum_{k \in \mathcal{K}} s_k[n] p_k(t - nT), \tag{2.4}$$

where

$$p_k(t) = p(t) e^{j2\pi tkF}, \tag{2.5}$$

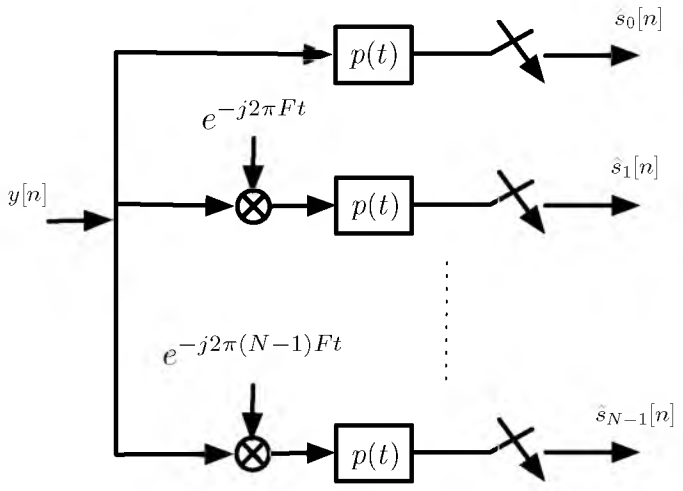


**Figure 2.4**: FMT receiver in continuous time.

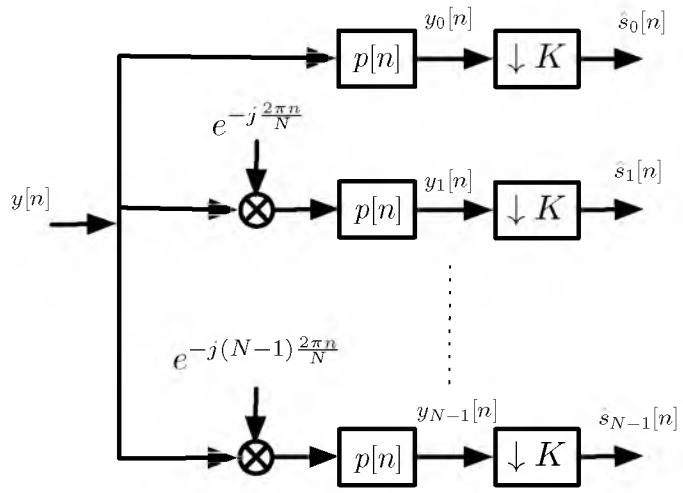


**Figure 2.5**: FMT receiver in discrete time.

$p(t)$ is referred to as the prototype pulse-shaping filter (or, simply, prototype filter), $\mathcal{K}$ is the set of integers that specify the subcarriers in $x(t)$, and $s_k[n]$ are data symbols that are spread across time (represented by the index $n$) and frequency (represented by the carrier index $k$). This concept is depicted in Fig. 2.6. We may also say, $x(t)$ is constructed using the set of basis functions $p_k(t - nT)$. Moreover, we note that in Fig. 2.6, the data *symbol density* in the time-frequency *phase space* is equal to $D = 1/TF$.

Assuming an ideal channel, the received signal $y(t)$ is the same as the transmit signal $x(t)$. In this case, the data symbols $s_k[n]$, for $k \in \mathcal{K}$ and all values of $n$, will be separable, trivially, if the basis functions satisfy

$$\langle p_k(t - mT), p_l(t - nT) \rangle = \delta_{kl}\delta_{mn}, \tag{2.6}$$

where $\delta_{kl}$ is the Kronecker delta function, and we have used the inner product definition

$$\langle p_k(t - mT), p_l(t - nT) \rangle = \int_{-\infty}^{\infty} p_k(t - mT)p_l^*(t - nT)dt. \tag{2.7}$$

The star sign, $*$, denotes complex conjugate. We refer to (2.6) as the orthogonality condition.

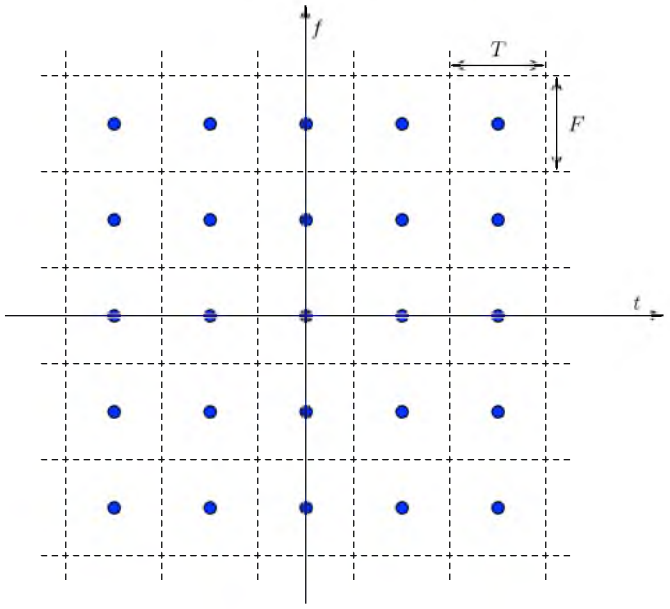


**Figure 2.6**: Spread of data symbols in an FBMC system across time and frequency.

The orthogonality condition (2.6) and further results to be developed in the rest of this dissertation can be best explained through the ambiguity function of $p(t)$, defined as[1]

$$A_p(\tau,\nu) = \int_{-\infty}^{\infty} p(t+\tau/2)p(t-\tau/2)e^{-j2\pi\nu t}dt, \tag{2.8}$$

where $\tau$ is a time delay and $\nu$ is a frequency shift. Using (2.5), one finds that

$$\begin{aligned}\langle p_k(t-mT), p_l(t-nT)\rangle &= \int_{-\infty}^{\infty} p(t-mT)e^{j2\pi kFt}p(t-nT)e^{-j2\pi lFt}dt \\ &\propto A_p((n-m)T,(l-k)F),\end{aligned} \tag{2.9}$$

where $\propto$ denotes proportionate to. The proportionate factor, whose value is irrelevant to the discussions of this dissertation, is a phase shift due to the delays of $mT$ and $nT$. Using (2.9), (2.6) may be written in terms of the ambiguity function as

$$A_p(nT,lF) = \begin{cases} 1, & n=l=0 \\ 0, & \text{otherwise.}\end{cases} \tag{2.10}$$

We refer to (2.10) as the generalized Nyquist criterion.

In conventional FMT systems, the prototype filter is designed as a square-root Nyquist filter with roll-off factor equal to $\alpha$. Taking advantage of the Nyquist criterion, these systems avoid ISI. Furthermore, ICI is avoided because of the fact that the subcarrier bands are nonoverlapping.

## 2.2 Polyphase Implementation of Filtered Multitone Systems

Due to the fact that subcarrier spacing in an FMT system is $\frac{1+\alpha}{T}$ instead of $\frac{1}{T}$, general polyphase structures are not applicable to FMT systems. In this section, we present the polyphase implementations of an FMT transmitter and receiver.

---

[1]The definition (2.8) is for the case where $p(t)$ is a real-valued function of time. In the more general case where $p(t)$ is a complex-valued function, $p(t-\tau/2)$ is replaced by $p^*(t-\tau/2)$.

### 2.2.1 Polyphase Synthesis Filterbank

Following Fig. 2.3, we have

$$\begin{aligned} x[n] &= \sum_{k=0}^{N-1} \sum_{l} s_k[l] p(n - lK) e^{\frac{j2\pi kn}{N}} \\ &= \sum_{l} \left( \sum_{k=0}^{N-1} s_k[l] e^{\frac{j2\pi kn}{N}} \right) p\left[n - lK\right]. \end{aligned} \tag{2.11}$$

To proceed, we write the time index, $n$, as

$$n = \gamma N + \alpha \tag{2.12}$$

where $\gamma$ and $p$ are the quotient and remainder of $n/N$, respectively. Substituting (2.12) in (2.11), we have

$$\begin{aligned} x[\gamma N + \alpha] &= \sum_{l} \left( \sum_{k=0}^{N-1} s_k[l] e^{\frac{j2\pi k\alpha}{N}} \right) p(n - lK) \\ &= \sum_{l} S_\alpha[l] p\left[n - lK\right]. \end{aligned} \tag{2.13}$$

where

$$S_\alpha[l] = \sum_{k=0}^{N-1} s_k[l] e^{\frac{j2\pi k\alpha}{N}} \tag{2.14}$$

is the N-point inverse discrete Fourier transform (IDFT) of input samples $s_0[n]$, $s_1[n]$,$\cdots$, $s_{N-1}[n]$.

In order to further simplify the equation and achieve the polyphase structure, similar to (2.12), $n$ can be rewritten as

$$n = \eta K + \beta \tag{2.15}$$

where $\eta$ and $q$ are the quotient and remainder of $n/K$, respectively. Substituting (2.15) in (2.13), we obtain

$$x[\eta K + \beta] = \sum_{l} S_\alpha[l] p\left[(\eta - l)K + \beta\right]. \tag{2.16}$$

(2.16) can be interpreted as taking the IDFT of the input samples, $s_0[n]$, $s_1[n]$,$\cdots$, $s_{N-1}[n]$ and passing the output samples through the polyphase components of the prototype filter $p[n]$, where the polyphase components are computed with respect

to the decimation factor $K$. Fig. 2.7 shows the polyphase implementation of an FMT transmitter. The commuter at the output of Fig. 2.7 takes $K$ steps after arrival of each set of input symbols. $D_0^{(n)}(z)$, $D_1^{(n)}(z)$, $\cdots$, and $D_{N-1}^{(n)}(z)$ are a set of time-varying filters that are picked up from the set of $K$ polyphase components $E_0(z)$ through $E_{K-1}(z)$ of the prototype filter $P(z) = \sum_n p[n]z^{-n}$. The output at time $n$, $x[n]$ is taken from $D_\alpha^{(n)}(z) = E_\beta(z)$, where $\alpha$ and $\beta$ are defined according to (2.12) and (2.12).

### 2.2.2 Polyphase Analysis Filterbank

Using Fig. 2.5, one can obtain

$$y_k[n] = \sum_l y[l]e^{\left(-j\frac{2\pi kl}{N}\right)}p[n-l]. \tag{2.17}$$

Similar to the transmit side filterbank, $l$ can be written in terms of its quotient and remainder when it is divided to $N$,

$$l = \gamma N + \alpha \tag{2.18}$$

where $\gamma$ and $\alpha$ are the quotient and remainder, respectively. Substituting (2.18) in (2.17), we obtain

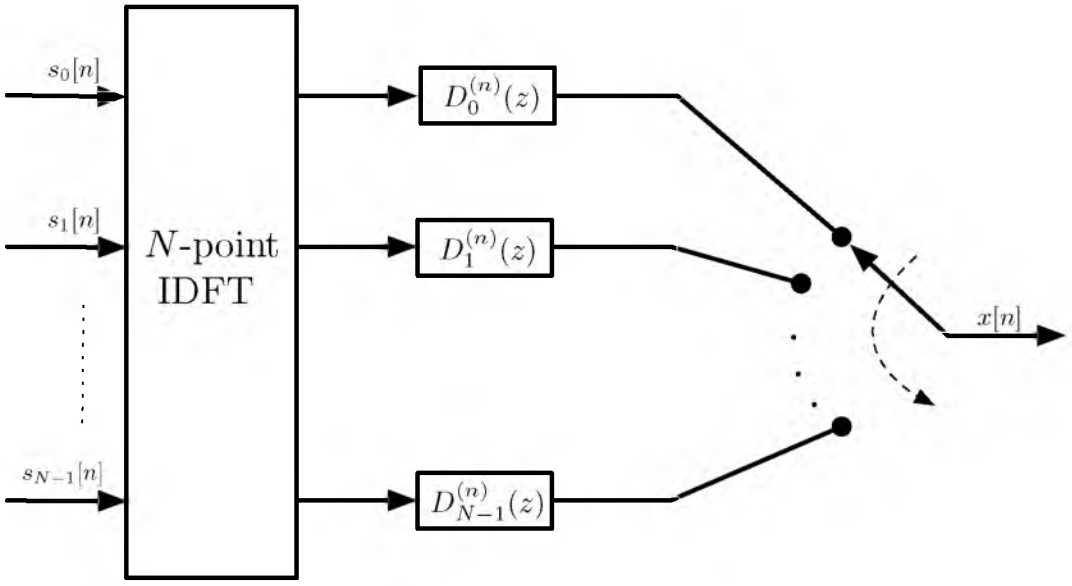


**Figure 2.7**: Polyphase implementation of an FMT transmitter.

$$\begin{aligned} y_k[n] &= \sum_{\gamma}\sum_{p=0}^{N-1} y[\gamma N+\alpha]e^{\left(-j\frac{2\pi k\alpha}{N}\right)}p[n-\gamma N-\alpha] \\ &= \sum_{p=0}^{N-1}\left(\sum_{\gamma} y[\gamma N+\alpha]p[n-\gamma N-\alpha]\right)e^{\left(-j\frac{2\pi k\alpha}{N}\right)}. \end{aligned} \tag{2.19}$$

It is worth noting that the recovered symbol $\hat{s}_k[n]$ is obtained after $K$-fold decimation of $y_k[n]$. To obtain the polyphase structure for computing $y_k[n]$, we write

$$n-\alpha = \kappa N+\beta \tag{2.20}$$

where $\kappa$ and $\beta$ are the quotient and remainder of $(n-\alpha)/N$. Substituting (2.20) in (2.19), we get

$$y_k[n] = \sum_{\alpha=0}^{N-1}\left(\sum_{\gamma} y[\gamma N+\alpha]h[(k-\gamma)N+\beta\right)e^{\left(-j\frac{2\pi k\alpha}{N}\right)}. \tag{2.21}$$

Considering (2.21), a polyphase structure for an FMT receiver can be determined as follows. The commuter feeds samples of the received signal $y[n]$ to the time-varying filters $D_0^{(n)}(z)$ through $D_{N-1}^{(n)}(z)$. $D_0^{(n)}(z)$ through $D_{N-1}^{(n)}(z)$ are picked up from the set of $N$ polyphase components $E_0(z)$ through $E_{N-1}(z)$ of the prototype filter $P(z)$. For any given time $n$, $D_\alpha^{(n)}(z) = E_\beta(z)$, where $\alpha$ and $\beta$ are computed based on (2.18) and (2.20). To obtain $y_k[n]$, the output of these filters is then passed through an $N$-point FFT. This structure is depicted in Fig. 2.8.

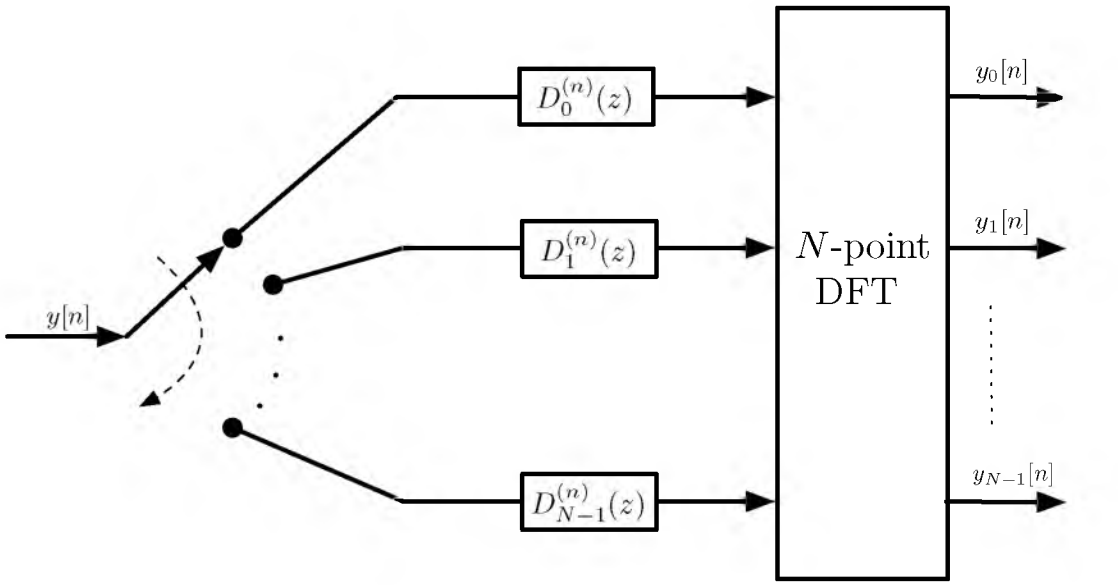


**Figure 2.8**: Polyphase implementation of an FMT receiver.

# CHAPTER 3

# OPTIMUM EQUALIZER DESIGN FOR FILTERED MULTITONE SYSTEMS

Although orthogonal frequency division multiplexing (OFDM) communication systems that use inverse discrete Fourier transform (IDFT) for multicarrier modulation and discrete Fourier transform (DFT) for demodulation are dominantly adopted in the current broadband standards, there have been some reports in recent years that discuss the shortcomings of OFDM in highly mobile and/or multiple access environments. To resolve these problems, a number of authors have proposed a shift from OFDM to filterbank-based multicarrier techniques. This chapter is also along the same line. In this chapter, we present a thorough study of filtered multitone (FMT) in time-varying frequency selective channels. We derive close-form equations for the optimum parameters of per tone fractionally spaced equalizers and also signal to interference plus noise ratio (SINR) and use these to evaluate FMT in typical wireless mobile environments.

Multicarrier modulation techniques that are based on filterbanks have recently been emphasized as an alternative to OFDM, *e.g.*, [20,33,60,61] for wireless communication. Wang *et al.,* [33], particularly, have recently compared FMT with OFDM and concluded that in fading channels, FMT outperforms OFDM.

The analysis in [33] is limited to the case where, at the receiver, a single-tap equalizer is used at each subchannel output of FMT. In this chapter, we further the analysis of [33] by exploring the FMT performance when a multitap equalizer is used at each subchannel output of FMT. We derive close-form solutions for the optimum coefficients of a fractionally spaced equalizer and the signal to intersymbol interference plus noise ratio (SINR) at the equalizer output. We note that in a time-invariant

environment, to allow a minimum-length (possibly, a single-tap) equalizer, one will set the number of subcarriers in FMT as large as possible. On the other hand, the time span of each symbol within a subchannel increases proportional to the number of subchannels, and in a time-varying environment, one wishes to keep this time span as short as possible. Hence, in a time-varying environment, one should make a decision to strike a balance between system performance and the equalizer complexity. Our analytical results can be used to develop and present a number of design curves for selecting the system parameters in FMT for some standard channel models.

## 3.1 Channel Model

In FMT, subcarrier channels are nonoverlapping. As a result, each subcarrier channel may be treated independently. In a time-varying environment, modulation caused by Doppler spread results in some overlap among adjacent subcarrier channels. However, the studies performed in [33] have revealed that compared to other degradations caused by a time-varying channel, the impact of such overlap is negligible. In light of this observation, throughout this chapter, we treat each subcarrier channel of an FMT system as an independent single-carrier communication link and thus, our study concentrates on the single-carrier communication block diagram shown in Fig. 3.1.

The transmit and receive filters are both lowpass filters. Moreover, they are selected such that their combination makes a Nyquist pulse-shape to achieve ISI free transmission when the channel is time-invariant and flat fading. We assume that the transmit and receive filters both have finite impulse responses represented by $\{g_0, g_1, \cdots, g_{N_g-1}\}$ and $\{h_0, h_1, \cdots, h_{N_h-1}\}$, respectively. The input $s(m)$ is the transmit data sequence, and $\hat{s}(m)$ is its estimate at the receiver. $\Delta$ is a delay caused by the sequence of the blocks in the upper branch of Fig. 3.1. The channel is modelled as a multipath channel with the time-varying impulse response $\{c_0(n), c_1(n), \cdots, c_{N_c-1}(n)\}$. The sequence $\nu(n)$ is the channel noise, a white Gaussian complex-valued zero-mean random process with variance of $\sigma_\nu^2$. Note that $m$ is the time index for data symbols and $n$ is the time index after up-sampling to a rate $K$ times faster. The equalizer has an impulse response $\{w_0(m), w_1(m), \cdots, w_{N_w-1}(m)\}$ which is optimized for each

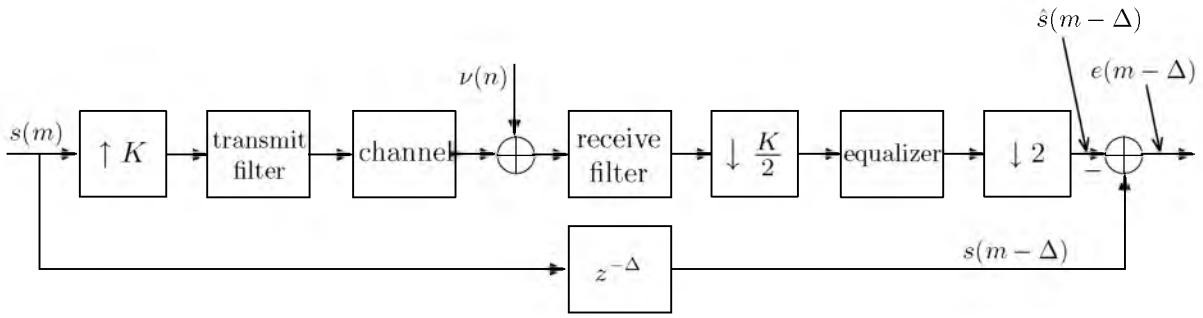


**Figure 3.1**: Block diagram of a single-carrier communication system.

symbol $s(m)$ such that the error $e(m) = s(m) - \hat{s}(m)$ is minimized in the mean square sense.

## 3.2 Equalizer Design and Performance Evaluation

We define the cost function

$$\xi = E[|e(m)|^2] \tag{3.1}$$

where $E[\cdot]$ denotes the ensemble average. Since the channel is time-varying, equalizer setting that minimizes $\xi$ depends on the channel impulse response that each $s(m)$ goes through. To deal with this scenario, we first derive an equation for the optimum setting of the equalizer tap weights $w_k(m)$, for a given $m$ and a sample of the channel $\{c_0(n), c_1(n), \cdots, c_{N_c-1}(n)\}$. We then evaluate $|e(m)|^2$, and perform an ensemble average on it.

We present our derivations in two steps. For clarity of derivations, we first consider a single path channel and derive all the relevant results for this simple case. The results are then extended to multipath channels.

### 3.2.1 The Case of a Single Path Channel

When the channel has a single path, it is characterized by a time-varying scalar gain, say, $c(n)$. We thus obtain equation (3.2)

$$\begin{aligned}
\hat{s}(m-\Delta) &= \sum_{k_2=-\infty}^{\infty}\sum_{k_1=-\infty}^{\infty}\sum_{l=-\infty}^{\infty} s\left(\frac{l}{K}\right) g_{k_1-l}c(k_1)h_{\frac{K}{2}k_2-k_1}w_{2m-k_2}(m) \\
&\qquad + \sum_{k_2=-\infty}^{\infty}\sum_{k_1=-\infty}^{\infty}\left(\nu(k_1)h_{\frac{K}{2}k_2-k_1}w_{2m-k_2}(m)\right) \\
&= \sum_{l=-\infty}^{\infty}\left(s\left(\frac{l}{K}\right)\sum_{k_1=-\infty}^{\infty}\left(c(k_1)g_{k_1-l}\sum_{k_2=-\infty}^{\infty}\left(h_{\frac{K}{2}k_2-k_1}w_{2m-k_2}(m)\right)\right)\right) \\
&\qquad + \sum_{k_1=-\infty}^{\infty}\left(\nu(k_1)\sum_{k_2=-\infty}^{\infty}\left(h_{\frac{K}{2}k_2-k_1}w_{2m-k_2}(m)\right)\right). \qquad (3.2)
\end{aligned}$$

To understand (3.2), the three summations in the first line should be read as follows:

- The summation over $l$ convolves the $K$-fold up-sampled version of $s(m)$ with $g_n$. Here, up-sampling is formulated by replacing $s(m)$ with $s\left(\frac{l}{K}\right)$ and assuming that $s\left(\frac{l}{K}\right) = 0$ when $\frac{l}{K}$ is noninteger.

- The latter convolution is scaled by the channel gain and the result is convolved with $h_n$. This gives the input to the equalizer.

- The equalization is performed through the summation over $k_2$. The result is sampled at even indices of time to take care of the 2-fold decimator that follows the equalizer.

- Following the same line of thoughts, the summation in the second line can be understood similarly.

- The next two lines follow through straightforward manipulations of the summations.

As noted earlier, our goal is to optimize the equalizer coefficients, $w_n(m)$, that minimize the cost function (4.1), for each $m$.

Next, we cast the summations in (3.2) in a matrix formulation. This greatly simplifies our further derivations. We assume that the nonzero elements of $g_n$, $h_n$, and $w_n$ are confined to the intervals $0 \le n \le N_g - 1$, $0 \le n \le N_h - 1$ and $0 \le n \le N_w - 1$,

respectively. Taking these into account and referring to (3.2), one finds that the summation indices are confined to the following intervals:

$$2m - N_w + 1 \leq k_2 \leq 2m$$

$$Km - \frac{K}{2}N_w + \frac{K}{2} - N_h + 1 \leq k_1 \leq Km$$

$$Km - \frac{K}{2}N_w - N_h - N_g + \frac{K}{2} + 2 \leq l \leq Km.$$

Taking note of these ranges, careful examination of (3.2) leads to

$$\hat{s}(m - \Delta) = \mathbf{s}^{\mathrm{T}}(m)\mathbf{G}\mathbf{C}(m)\mathbf{H}\mathbf{w}(m) + \boldsymbol{\nu}^{\mathrm{T}}\mathbf{H}\mathbf{w} \tag{3.3}$$

where $\mathbf{G}$ is obtained by forming a toeplitz matrix whose first row and first column are, respectively, the vectors $\mathbf{g}_{\mathrm{r}}$ and $\mathbf{g}_{\mathrm{c}}$ listed below, and then decimating the formed matrix $K$ fold across its rows, and $\mathbf{H}$ is obtained by forming a toeplitz matrix whose first row and first column are, respectively, the vectors $\mathbf{h}_{\mathrm{r}}$ and $\mathbf{h}_{\mathrm{c}}$, also, listed below, and then decimating the formed matrix $K/2$ fold across its columns.

$$\mathbf{g}_{\mathrm{r}} = \underbrace{\begin{bmatrix} g_{N_g-1} & 0 & 0 & \cdots & 0 \end{bmatrix}}_{\frac{K}{2}N_w+N_h-\frac{K}{2}-1 \text{ elements}}$$

$$\mathbf{g}_{\mathrm{c}} = \underbrace{\begin{bmatrix} g_{N_g-1} & g_{N_g-2} & \cdots & g_0 & 0 & 0 & \cdots & 0 \end{bmatrix}^{\mathrm{T}}}_{\frac{K}{2}N_w+N_h+Ng-\frac{K}{2}-2 \text{ elements}}$$

$$\mathbf{h}_{\mathrm{r}} = \underbrace{\begin{bmatrix} h_{N_h-1} & 0 & 0 & \cdots & 0 \end{bmatrix}}_{\frac{K}{2}N_w-\frac{K}{2} \text{ elements}}$$

$$\mathbf{h}_{\mathrm{c}} = \underbrace{\begin{bmatrix} h_{N_h-1} & h_{N_h-2} & \cdots & h_0 & 0 & 0 & \cdots & 0 \end{bmatrix}^{\mathrm{T}}}_{\frac{K}{2}N_w+N_h-\frac{K}{2}-1 \text{ elements}}$$

$\mathbf{C}(m)$, $\mathbf{s}(m)$, and $\boldsymbol{\nu}(m)$ are listed below equation (3.2)

$$\mathbf{s}(m) = \left[\ s\left(\left\lfloor m - \frac{\frac{K}{2}N_w + N_h + N_g - \frac{K}{2} - 2}{K}\right\rfloor\right),\ \cdots\ , s\,(m-1)\,,\ \ s\,(m)\ \right]$$

$$\boldsymbol{\nu}(m) = \left[\ \nu(Km - \tfrac{K}{2}N_w - N_h + \tfrac{K}{2} + 1),\ \cdots\ , \nu(Km-1), \nu(Km)\ \right]^{\mathrm{T}}$$

$$\mathbf{C}(m) = \begin{bmatrix} 0 & \cdots & 0 & 0 & c(Km) \\ 0 & \vdots & 0 & c(Km-1) & 0 \\ \vdots & \iddots & c(Km-2) & 0 & 0 \\ 0 & \iddots & 0 & 0 & \vdots \\ 0 & & \vdots & \vdots & 0 \\ c(Km - \frac{K}{2}N_w - n_h + \frac{K}{2} + 1) & & 0 & 0 & 0 \end{bmatrix}.$$

We also note that (3.15) can be rearranged as

$$\hat{s}(m-\Delta) = \mathbf{u}^{\mathrm{T}}(m) \begin{bmatrix} \mathbf{GC}(m)\mathbf{H} \\ \mathbf{H} \end{bmatrix} \mathbf{w} \tag{3.4}$$

where

$$\mathbf{u}(m) = \begin{bmatrix} \mathbf{s}(m) \\ \boldsymbol{\nu}(m) \end{bmatrix}.$$

Moreover, for the convenience of the derivations that follow, we note that $s(m-\Delta)$ can be written as

$$s(m-\Delta) = \mathbf{u}^{\mathrm{T}}(m)\mathbf{d}(m) \tag{3.5}$$

where $\mathbf{d}(m)$ is a column vector whose elements are 0 except a 1 at the position that matches $s(m-\Delta)$ in $\mathbf{u}(m)$.

Substituting (3.4) and (3.5) into (4.1), we get

$$\begin{aligned} \xi(m-\Delta) &= E\left[|\hat{s}(m-\Delta) - s(m-\Delta)|^2\right] \\ &= E\left[\left|\mathbf{u}^{\mathrm{T}}(m)\mathbf{q}(m)\right|^2\right] \end{aligned} \tag{3.6}$$

where

$$\mathbf{q}(m) = \begin{bmatrix} \mathbf{GC}(m)\mathbf{H} \\ \mathbf{H} \end{bmatrix} \mathbf{w} - \mathbf{d}(m). \tag{3.7}$$

Equation (3.6) may be rearranged as

$$\begin{aligned} \xi(m-\Delta) &= E\left[\left|\mathbf{q}^{\mathrm{T}}(m)\mathbf{u}(m)\right|^2\right] \\ &= \mathbf{q}^{\mathrm{T}}(m) E\left[\mathbf{u}(m)\mathbf{u}^{\mathrm{H}}(m)\right] \mathbf{q}^{*}(m) \\ &= \mathbf{q}^{\mathrm{T}}(m) \begin{bmatrix} \sigma_s^2\mathbf{I}_s & 0 \\ 0 & \sigma_\nu^2\mathbf{I}_\nu \end{bmatrix} \mathbf{q}^{*}(m) \end{aligned} \tag{3.8}$$

where $\sigma_s^2\mathbf{I}_s$ and $\sigma_\nu^2\mathbf{I}_\nu$ are the correlation matrices of $\mathbf{s}$ and $\boldsymbol{\nu}$ and $\mathbf{I}_s$ and $\mathbf{I}_\nu$ the identity matrices of respective sizes.

Substituting (4.5) into (3.8), it can be rearranged as

$$\begin{aligned}\xi(m-\Delta) &= \sigma_s^2|\mathbf{Q}(m)\mathbf{w}(m)-\mathbf{d}(m)|^2 \\ &= \sigma_s^2(\mathbf{w}^{\mathrm{H}}(m)\mathbf{Q}^{\mathrm{H}}(m)\mathbf{Q}(m)\mathbf{w}(m) \\ &\quad -\mathbf{w}^{\mathrm{H}}(m)\mathbf{Q}^{\mathrm{H}}(m)\mathbf{d}(\mathbf{m}) \\ &\quad -\mathbf{d}^{\mathrm{H}}(m)\mathbf{Q}(m)\mathbf{w}(m)+\mathbf{d}^{\mathrm{H}}(m)\mathbf{d}(m)) \end{aligned} \tag{3.9}$$

where

$$\mathbf{Q}(m) = \begin{bmatrix} \mathbf{GC}(m)\mathbf{H} \\ \frac{\sigma_\nu}{\sigma_s}\mathbf{H} \end{bmatrix} \tag{3.10}$$

Letting $\nabla_{\mathbf{w}}\xi = 0$ and solving for $\mathbf{w}(m)$, the optimum tap-gain vector of the equalizer is obtained as

$$\mathbf{w}_{\mathrm{o}}(m) = \left(\mathbf{Q}^{\mathrm{H}}(m)\mathbf{Q}(m)\right)^{-1}\mathbf{Q}^{\mathrm{H}}(m)\mathbf{d}(m). \tag{3.11}$$

Also, substituting (4.2) into (3.10), and noting that all the underlying processes are stationary, thus, $\xi_{\min}(m-\Delta) = \xi_{\min}(m)$, the minimum value of $\xi$ is obtained as

$$\xi_{\min}(m) = \sigma_s^2\left(1-\mathbf{d}^{\mathrm{H}}(m)\mathbf{Q}(m)\mathbf{w}_{\mathrm{o}}(m)\right). \tag{3.12}$$

The SINR at the equalizer output is thus obtained as

$$\begin{aligned}\mathrm{SINR} &= \frac{E[|s(m)|^2]}{E[\xi_{\min}(m)]} \\ &= \frac{1}{E[1-\mathbf{d}^{\mathrm{H}}(m)\mathbf{Q}(m)\mathbf{w}_{\mathrm{o}}(m)]}\end{aligned} \tag{3.13}$$

### 3.2.2 The Case of a Multipath Channel

For a multipath channel, the channel length, $N_c$, is greater than one. Similar to what we had for the single-tap channel, the expression for the received signal $\hat{s}(m-\Delta)$ can be written in the form presented at the top of the next page.

$$\begin{aligned}\hat{s}(m-\Delta) &= \sum_{k_2=-\infty}^{\infty}\sum_{k_1=-\infty}^{\infty}\sum_{k=0}^{N_c-1}\sum_{l=-\infty}^{\infty} s\left(\frac{l}{K}\right) g_{k_1-k-l}c_k(k_1)h_{\frac{K}{2}k_2-k_1}w_{2m-k_2}(m) \\ &\quad + \sum_{k_2=-\infty}^{\infty}\sum_{k_1=-\infty}^{\infty}\left(\nu(k_1)h_{k_2-k_1}w_{2m-k_2}(m)\right) \\ &= \sum_{l=-\infty}^{\infty}\left(s\left(\frac{l}{K}\right)\sum_{k_1=-\infty}^{\infty}\sum_{k=0}^{N_c-1}\left(c_k(k_1)g_{k_1-k-l}\sum_{k_2=-\infty}^{\infty}\left(h_{\frac{K}{2}k_2-k_1}w_{2m-k_2}(m)\right)\right)\right) \\ &\quad + \sum_{k_1=-\infty}^{\infty}\left(\nu(k_1)\sum_{k_2=-\infty}^{\infty}\left(h_{\frac{K}{2}k_2-k_1}w_{2m-k_2}(m)\right)\right). \end{aligned} \tag{3.14}$$

Using the same approach as the single-tap channel, the optimum coefficients of the equalizer are found and the minimum mean square error is analyzed.

Similar to the single-tap channel case, we assume that the nonzero elements of $g_n$, $h_n$, and $w_n$ are in the intervals $0 \le n \le N_g - 1$, $0 \le n \le N_h - 1$, and $0 \le n \le N_w - 1$, respectively. Hence, the summation indices that contribute nonzero elements to the received signal are in the following ranges

$$2m - N_w + 1 \le k_2 \le 2m$$

$$Km - \frac{K}{2}N_w + \frac{K}{2} - N_h + 1 \le k_1 \le Km$$

$$Km - \frac{K}{2}N_w - N_h - N_g - N_c + \frac{K}{2} + 3 \le l \le Km.$$

Taking these limits into account, (3.14) may be rearranged as

$$\hat{s}(m-\Delta) = \mathbf{s}^{\mathrm{T}}(m)\mathbf{G}\mathbf{C}(m)\mathbf{H}\mathbf{w}(m) + \boldsymbol{\nu}^{\mathrm{T}}(m)\mathbf{H}\mathbf{w}(m) \tag{3.15}$$

where $\mathbf{G}$ is obtained by forming a toeplitz matrix whose first row and first column are, respectively, the vectors $\mathbf{g}_{\mathrm{r}}$ and $\mathbf{g}_{\mathrm{c}}$ listed below, and then decimating the formed matrix $K$ fold across its rows, and $\mathbf{H}$ is obtained by forming a toeplitz matrix whose first row and first column are, respectively, the vectors $\mathbf{h}_{\mathrm{r}}$ and $\mathbf{h}_{\mathrm{c}}$, also, listed below, and then decimating the formed matrix $K/2$ fold across its columns.

$$\mathbf{g}_{\mathrm{r}} = \underbrace{\begin{bmatrix} g_{N_g-1} & 0 & 0 & \cdots & 0 \end{bmatrix}}_{\frac{K}{2}N_w+N_h+N_c-\frac{K}{2}-1 \text{ elements}}$$

$$\mathbf{g}_{\mathrm{c}} = \underbrace{\begin{bmatrix} g_{N_g-1} & g_{N_g-2} & \cdots & g_0 & 0 & 0 & \cdots & 0 \end{bmatrix}^{\mathrm{T}}}_{\frac{K}{2}N_w+N_h+Ng+N_c-\frac{K}{2}-2 \text{ elements}}$$

$$\mathbf{h}_{\mathrm{r}} = \underbrace{\begin{bmatrix} h_{N_h-1} & 0 & 0 & \cdots & 0 \end{bmatrix}}_{\frac{K}{2}N_w - \frac{K}{2} \text{ elements}}$$

$$\mathbf{h}_{\mathrm{c}} = \underbrace{\begin{bmatrix} h_{N_h-1} & h_{N_h-2} & \cdots & h_0 & 0 & 0 & \cdots & 0 \end{bmatrix}}_{\frac{K}{2}N_w + N_h - \frac{K}{2} - 1 \text{ elements}}^{\mathrm{T}}.$$

Other vectors and matrices in (3.15) are listed on the next page. Moreover, using the definition (4.5), one finds that (4.2), (4.3), and (4.4) are also applicable here.

## 3.3 Numerical Results

In this section, we use the analytical equations of the previous section to evaluate the performance of the FMT under different channel conditions and for different equalizer lengths.

We consider transmission through a 20 MHz wide channel at the carrier frequency 5 GHz. The sampling rate at the channel (the equivalent baseband) is set equal to $1/(20\text{ MHz}) = 0.05\ \mu$s. The rural area COST 207 model [62] is used to calculate the mean power of each tap of the channel and the Doppler spectrum of each channel tap is considered to be the Jakes' spectrum.

The mobile unit is assumed to move at different velocities and the maximum Doppler frequency is calculated as

$$f_{\mathrm{d,max}} = \frac{v}{c} f_c \tag{3.16}$$

where $f_c$ is the carrier frequency, $c$ is the speed of light, and $v$ is the speed of the mobile unit. For the simulations presented here, the averaged signal-to-noise ratio (SNR) is set equal to 30 dB.

Fig. 3.2 presents SINR when the mobile station is moving at a speed 70 miles/h (= 112 km/h) and the upsampling rate $K$ varies between 5 and 128. We note that $K$ is also directly related to the number of subcarrier bands within the 20 MHz bandwidth. So, by increasing $K$, the width of each subcarrier band reduces and as a result, the channel for each subcarrier may be approximated by a flat fading gain. This expected phenomenon is seen in Fig. 3.2, where we find that as $K$ increases, an equalizer with a single-tap performs as good as multitap equalizers.

In WiMAX where the COST 207 model is applicable, the number of subcarrier bands in 20 MHz is 2048. Extrapolating the curves in Fig. 3.2, it is obvious that all

$$\mathbf{s}(m) = \left[ \begin{array}{cccc} s\left(\lfloor m - \frac{\frac{K}{2}N_w + N_h + N_g + N_c - \frac{K}{2} - 3}{K} \rfloor\right) & \cdots & s\,(m-1) & s\,(m) \end{array} \right]^{\mathrm{T}}$$

$$\boldsymbol{\nu}(m) = \left[ \begin{array}{cccc} \nu(Km - \frac{K}{2}N_w - N_h + \frac{K}{2} + 1), & \cdots & , \nu(Km-1) & , \nu(Km) \end{array} \right]^{\mathrm{T}}$$

$$C = \left[ \begin{array}{ccccc} 0 & \cdots & 0 & 0 & c_0(Km) \\ 0 & \cdots & 0 & c_0(Km-1) & c_1(Km) \\ \vdots & \iddots & c_0(Km-2) & c_1(Km-1) & \vdots \\ 0 & \cdots & c_1(Km-2) & \vdots & c_{N_c-1}(Km) \\ 0 & \iddots & \vdots & c_{N_c-1}(Km-1) & 0 \\ c_0(Km - \frac{K}{2}N_w - N_h + \frac{K}{2} + 1) & \iddots & c_{N_c-1}(Km-2) & 0 & 0 \\ c_1(Km - \frac{K}{2}N_w - N_h + \frac{K}{2} + 1) & \vdots & 0 & 0 & \vdots \\ \vdots & \iddots & \vdots & \vdots & \\ c_{N_c-1}(Km - \frac{K}{2}N_w - N_h + \frac{K}{2} + 1) & & 0 & 0 & 0 \end{array} \right]$$

$$\mathbf{w}(m) = \left[ \begin{array}{cccc} w_{N_w-1}(m) & w_{N_w-2}(m) & \ldots & w_0(m) \end{array} \right]^{\mathrm{T}}.$$

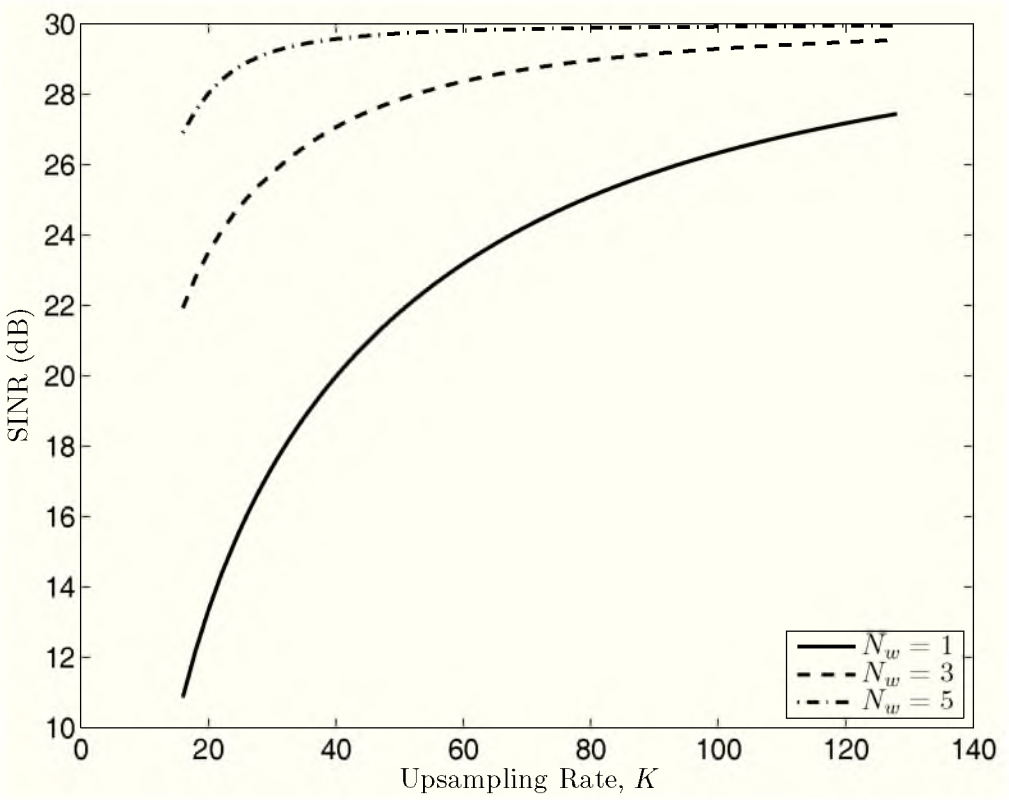


**Figure 3.2**: SINR graphs of the system under different equalizer lengths

the three curves merge to the SNR value 30 dB and thus, a single-tap equalizer works as good as a multitap equalizer. However, as demonstrated below, some loss may incur at higher speed of the mobile station and, thus, the use of multitap equalizers can be helpful.

Fig. 3.3 shows how SINR changes as the speed of the mobile station is varied between 0 and 500 km/h. The case considered is that of a WiMAX setup, where each subcarrier channel has the bandwidth of 20 MHz/2048 = 9765 Hz. As seen, at a typical car speed up to 150 km/h, there is no significant difference between single-tap and multitap equalizers. However, at higher speeds (say, in a high-speed train) noticeable differences are observed.

## 3.4 Summary

In this chapter, we derived equations that allow evaluation of filtered multitone (FMT) when applied to mobile wireless communication systems. We considered using per tone channel equalizers with different taps. The numerical results showed that when the number of subcarrier bands in a 20 MHz bandwidth is small (equivalent to saying each subcarrier band has a relatively wideband), fractionally spaced equalizers with 3 taps per tone or more may be required to avoid any significant loss. However, as the number of subcarrier band increases to typical numbers seen in current standards, *e.g.*, WiMAX/IEEE 802.16, single-tap equalizers suffice.

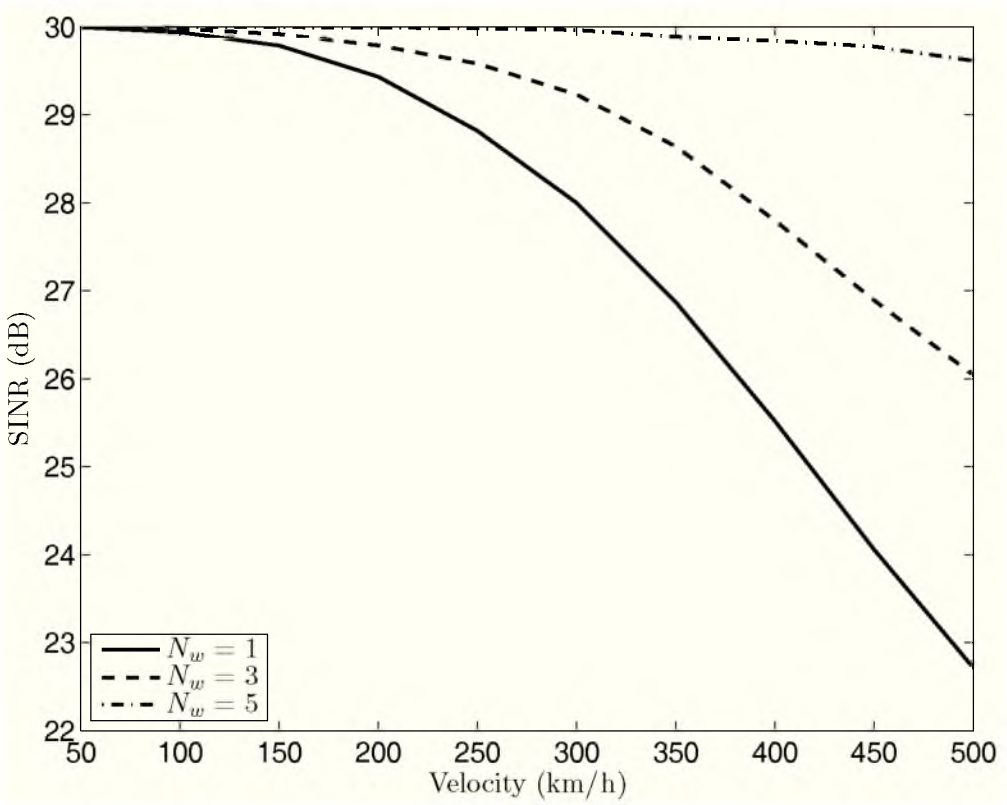


**Figure 3.3**: SINR graphs of the system under different equalizer lengths

# CHAPTER 4

# CHANNEL ESTIMATION FOR FILTERED MULTITONE SYSTEMS

In Chapter 3, we presented a thorough study of filtered multitone (FMT), a class of FBMC systems, in time-varying frequency selective channels. We derived close-form equations for the optimum parameters of per tone fractionally spaced equalizers and also signal to interference plus noise ratio (SINR) and used these to evaluate FMT in typical wireless mobile environments. These results provide an upper limit to the performance of this class of FBMC systems.

In this chapter, we study the performance of an adaptive channel estimation algorithm that attempts to reach this upper limit. To further improve the channel estimate, the proposed method uses a minimum mean square error (MMSE) channel estimator and considers the fact that the channel impulse response is limited in time.

To resolve the problems associated with adaptation of equalizers in FMT, when applied to time-varying channels, we propose the following solution. We note that according to our earlier studies in Chapter 3, for typical wireless mobile channels, single-tap equalizers per subcarrier are sufficient. In such cases, the optimum equalizer setting is (almost) independent of the channel noise and is equal to the inverse of the channel gain at each subcarrier. We thus take an indirect approach to setting the equalizers. We first identify the channel using the commonly known techniques from the OFDM literature, [63]. We also make use of the prior knowledge that the impulse responses of channels of interest are limited in time to make the channel frequency responses smooth. We show through numerical simulations that this method has excellent performance in typical mobile wireless channels of interest.

The rest of this chapter is organized as follows. In Section 4.1, a review of the optimum equalizer design is presented. Section 4.2 presents the proposed channel estimation method. In Section 4.3, we present the numerical results and compare the proposed equalizer with the optimum equalizer. Finally, a summary of this chapter is presented in Section 4.4.

## 4.1 Equalizer Design and Performance Evaluation

In FMT, the interference caused by ICI in time-varying channels is much lower than the interference from ISI. As a result, each subcarrier can be treated independently [33]. Hence, we can treat each subcarrier of FMT as an independent single-carrier communication system and for designing the optimum equalizer, we use the block diagram of single-carrier communication system as shown in Fig. 3.1.

In Chapter 3, we defined the cost function

$$\xi = E[|e(m)|^2]. \tag{4.1}$$

To deal with this scenario, we first derive an equation for the optimum setting of the equalizer tap weights $w(m)$, for a given $m$ and a sample of the channel, $\{c_0(n), c_1(n), \cdots, c_{N_c-1}(n)\}$. We then evaluate $|e(m)|^2$, and perform an ensemble average on it.

It has been shown that the optimum equalizer coefficients, the minimum squared error, and the signal to interference and noise ratio can be calculated using (4.2), (4.3), and (4.4), respectively

$$\mathbf{w}_{\mathrm{o}}(m) = \left(\mathbf{Q}^{\mathrm{H}}(m)\mathbf{Q}(m)\right)^{-1}\mathbf{Q}^{\mathrm{H}}(m)\mathbf{d}(m) \tag{4.2}$$

$$\xi_{\min}(m) = \sigma_s^2\left(1 - \mathbf{d}^{\mathrm{H}}(m)\mathbf{Q}(m)\mathbf{w}_{\mathrm{o}}(m)\right) \tag{4.3}$$

$$\begin{aligned} \mathrm{SINR} &= \frac{E[|s(m)|^2]}{E[\xi_{\min}(m)]} \\ &= \frac{1}{E[1 - \mathbf{d}^{\mathrm{H}}(m)\mathbf{Q}(m)\mathbf{w}_{\mathrm{o}}(m)]} \end{aligned} \tag{4.4}$$

where

$$\mathbf{Q}(m) = \begin{bmatrix} \mathbf{GC}(m)\mathbf{H} \\ \mathbf{H} \end{bmatrix} \mathbf{w} - \mathbf{d}(m) \tag{4.5}$$

and $\mathbf{G}$ is obtained by forming a toeplitz matrix whose first row and first column are, respectively, the vectors $\mathbf{g}_{\mathrm{r}}$ and $\mathbf{g}_{\mathrm{c}}$ listed below, and then decimating the formed matrix $K$ fold across its rows, and $\mathbf{H}$ is obtained by forming a toeplitz matrix whose first row and first column are, respectively, the vectors $\mathbf{h}_{\mathrm{r}}$ and $\mathbf{h}_{\mathrm{c}}$, also, listed below, and then decimating the formed matrix $K/2$ fold across its columns. $\mathbf{h}_{\mathrm{r}}$, $\mathbf{h}_{\mathrm{c}}$ are listed below and $\mathbf{C}$ is presented in the next page.

$$\mathbf{g}_{\mathrm{r}} = \underbrace{\begin{bmatrix} g_{N_g-1} & 0 & 0 & \cdots & 0 \end{bmatrix}}_{\frac{K}{2}N_w+N_h+N_c-\frac{K}{2}-1 \text{ elements}}$$

$$\mathbf{g}_{\mathrm{c}} = \underbrace{\begin{bmatrix} g_{N_g-1} & g_{N_g-2} & \cdots & g_0 & 0 & 0 & \cdots & 0 \end{bmatrix}^{\mathrm{T}}}_{\frac{K}{2}N_w+N_h+Ng+N_c-\frac{K}{2}-2 \text{ elements}}$$

$$\mathbf{h}_{\mathrm{r}} = \underbrace{\begin{bmatrix} h_{N_h-1} & 0 & 0 & \cdots & 0 \end{bmatrix}}_{\frac{K}{2}N_w-\frac{K}{2} \text{ elements}}$$

$$\mathbf{h}_{\mathrm{c}} = \underbrace{\begin{bmatrix} h_{N_h-1} & h_{N_h-2} & \cdots & h_0 & 0 & 0 & \cdots & 0 \end{bmatrix}^{\mathrm{T}}}_{\frac{K}{2}N_w+N_h-\frac{K}{2}-1 \text{ elements}}.$$

## 4.2 Channel Estimation

Based on the numerical results presented in Chapter 3, an optimum single-tap equalizer has almost the same mean square error as the optimum multiple-tap equalizer. Knowing this result and considering the fact that the design and adaptation of a single parameter is much simpler than the design and adaptation of multiple parameters, we choose to further our research to design of single-tap equalizers, for FMT communication systems that are based on channel estimation. If we use a single-tap equalizer, the fractionally-spaced equalizer will be replaced by a single-tap symbol-spaced equalizer. Fig. 4.1 presents the structure of the proposed receiver. In each subcarrier channel, the output of the symbol-spaced downsampler, $\hat{s}_k[n]$, is multiplied by the respective equalizer gain, $w_k[n]$.

$$\mathbf{C} = \begin{bmatrix} 0 & \cdots \\ 0 & \cdots \\ \vdots & \ddots \\ 0 & \cdots \\ 0 & \ddots \\ c_0(Km - \frac{K}{2}N_w - N_h + \frac{K}{2} + 1) & \ddots \\ c_1(Km - \frac{K}{2}N_w - N_h + \frac{K}{2} + 1) & \vdots \\ \vdots & \ddots \\ c_{N_c-1}(Km - \frac{K}{2}N_w - N_h + \frac{K}{2} + 1) & \end{bmatrix}$$

$$\begin{bmatrix} 0 & 0 & c_0(Km) \\ 0 & c_0(Km-1) & c_1(Km) \\ c_0(Km-2) & c_1(Km-1) & \vdots \\ c_1(Km-2) & \vdots & c_{N_c-1}(Km) \\ \vdots & c_{N_c-1}(Km-1) & 0 \\ c_{N_c-1}(Km-2) & 0 & 0 \\ 0 & 0 & \vdots \\ \vdots & \vdots & \\ 0 & 0 & 0 \end{bmatrix}$$

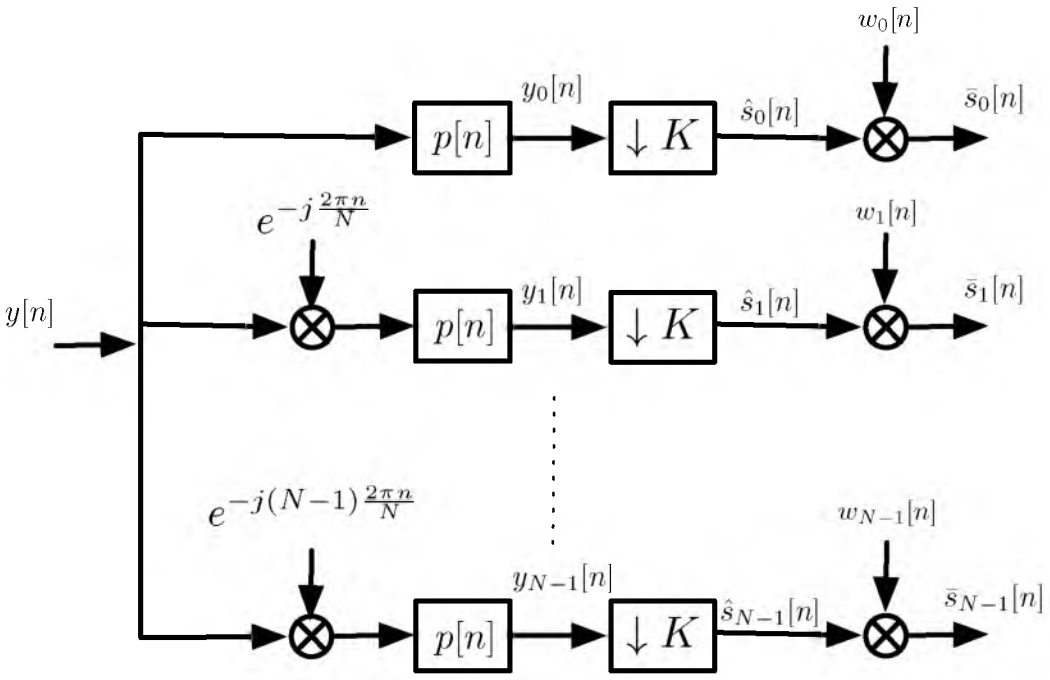


**Figure 4.1**: The proposed FMT receiver structure.

For the purpose of channel estimation, we assume that the input-output relationship of a subcarrier follows Fig. 4.2 and has the following form

$$\hat{s}_k[n] = s_k[n]c_k[n] + \nu_k[n] \tag{4.6}$$

where $c_k[n]$ is the channel gain on the $k$th subcarrier at time index $n$ and $\nu_k[n]$ is the noise added to the $k$th subcarrier at time index $n$. In other words, the received signal before equalization is considered to be equal to the transmitted signal passed through a time-varying flat-fading channel with additive white Gaussian noise. An initial channel estimate can be calculated as

$$\check{c}_k[n] = \frac{\hat{s}_k[n]}{s_k[n]} = c_k[n] + \frac{\nu_k[n]}{s_k[n]}. \tag{4.7}$$

It has been shown in [63] that for a wide-sense stationary uncorrelated scattering (WSSUS) channel, coefficients at different times and different subcarriers are correlated in the following way

$$E\{c_{k+k_1}[n+n_1]c_k^*[n]\} = r_f[k_1]r_t[n_1] \tag{4.8}$$

where $r_f[k_1]$ and $r_t[m_1]$ represent the correlation in time and frequency, respectively. For a channel which follows the Jakes Doppler model, these parameters can be calculated as

$$\begin{aligned} r_f[k_1] &= \sum_{k=0}^{N_c-1} \sigma_k^2 e^{-j\frac{2\pi k_1 k}{N}} \\ r_t[n_1] &= J_0(2\pi n_1 T_s f_d). \end{aligned} \tag{4.9}$$

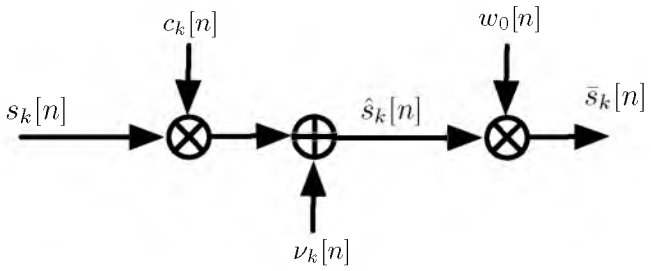


**Figure 4.2**: Block diagram of a single subcarrier.

We take advantage of these correlations in time and frequency domain to create an MMSE channel estimate using a window of the first order estimates in time and frequency. Viz.,

$$\overline{c}_k[n] = \sum_{k_1=-L_f}^{L_f} \sum_{n_1=-L_t}^{0} f_{k_1}[n_1]\check{c}_{k-k_1}[n-n_1] \tag{4.10}$$

where $f_{k_1}[n_1]$ is designed in order to minimize $E(|\overline{c}_k[n] - c_k[n]|^2)$. In order to find the optimum channel estimator coefficients, we follow the Wiener-Hopf equation principles. The autocorrelation of the first order channel estimates can be derived as

$$E\left\{\check{c}_l k+k_1][n+n_1]\check{c}_k^*[n]\right\} = r_f[k_1]r_t(n_1) + \sigma_\nu^2\delta[n_1,k_1] \tag{4.11}$$

where

$$\delta[n_1,k_1] = \begin{cases} 1 & n_1 = k_1 = 0 \\ 0 & \text{otherwise} \end{cases} . \tag{4.12}$$

Similarly, the cross correlation between the channel estimates and the channel coefficient values can be calculated as

$$E\left\{\check{c}_{k+k_1}[n+n_1]c_k^*[n]\right\} = r_f[k_1]r_t(n_1). \tag{4.13}$$

Using the Wiener equation for an MMSE design, we get

$$\mathbf{f} = \mathbf{R}^{-1}\mathbf{p} \tag{4.14}$$

where $\mathbf{f}$ and $\mathbf{p}$ are defined as

$$\begin{aligned} \mathbf{f} &= \left[f_{L_f}[0], f_{L_f-1}[0], \cdots, f_{-L_f}[-L_t]\right] \\ \mathbf{p} &= \left[r_f[L_f]r_t[0], r_f[L_f-1]r_t[0], \cdots, r_f[-L_f]r_t[-L_t]\right] \end{aligned}$$

and $\mathbf{R}$ is given in (4.15).

$$\mathbf{R} = \begin{bmatrix} r_f[0]r_t[0] & r_f[1]r_t[0] & \cdots & r_f[2*L_f]r_t[L_t] \\ r_f[-1]r_t[0] & r_f[0]r_t[0] & \cdots & r_f[2*L_f-1]r_t[L_t] \\ \vdots & \vdots & \vdots & \\ r_f[-2L_f]r_t[0] & r_f[-2L_f+1]r_t[0] & \cdots & r_f[0]r_t[L_t] \\ r_f[0]r_t[-1] & r_f[1]r_t[-1] & \cdots & r_f[2*L_f]r_t[L_t-1] \\ \vdots & \vdots & \vdots & \\ r_f[-2L_f]r_t[-L_t] & r_f[-2L_f+1]r_t[-L_t] & \cdots & r_f[0]r_t[0] \end{bmatrix} + \sigma_\nu^2 * I. \tag{4.15}$$

Moreover, considering the fact that the channel impulse response is time-limited, we can further improve the channel estimate. In order to take advantage of this

observation, the IDFT of the channel estimates is taken and the first $L_c$ samples of the result are preserved and the other $M - L_c$ samples are set equal to zero. The DFT of the constructed samples will provide the final channel estimates.

The single-tap equalizer at each subcarrier at each time sample, $w_k[n]$, is then calculated as the inverse of the channel estimate.

## 4.3 Numerical Results

In this section, we evaluate the performance of the designed FMT equalizer under different channel signal-to-noise ratio (SNR) and for different Doppler frequencies.

We consider transmission through a 20 MHz wide channel at the carrier frequency of 5 GHz. The transmit and receive filters are square-root Nyquist filters with upsampling rate of 320 which are designed using the method described in [64]. The roll-off factor is 0.25 in order to have the same spectral efficiency as the OFDM method used in [18]. The type 2 propagation model of IEEE 802.16 is used to calculate the mean power of each tap of the channel and the Doppler spectrum of each channel tap is considered to be the Jakes' spectrum.

The mobile unit is assumed to move at different velocities and the maximum Doppler frequency is calculated as

$$f_{\mathrm{d,max}} = \frac{v}{c} f_c \tag{4.16}$$

where $f_c$ is the carrier frequency, $c$ is the speed of light, and $v$ is the speed of the mobile unit.

Fig. 4.3 presents SINR when the mobile station is moving at a speed 30 miles/h (= 48 km/h) and the signal-to-noise ration varies between 10 dB and 40 dB.

Fig. 4.4 shows how SINR changes as the speed of the mobile station is varied between 0 and 80 mph. The case considered is that of a WiMAX setup, where each subcarrier channel has the bandwidth of 20 MHz/256 = 78125 Hz. For the simulations presented here, the averaged signal-to-noise ratio (SNR) is set equal to 30 dB.

It can be seen that the proposed equalizer method has a loss of approximately 1dB in SINR compared to the optimum single-tap equalizer.

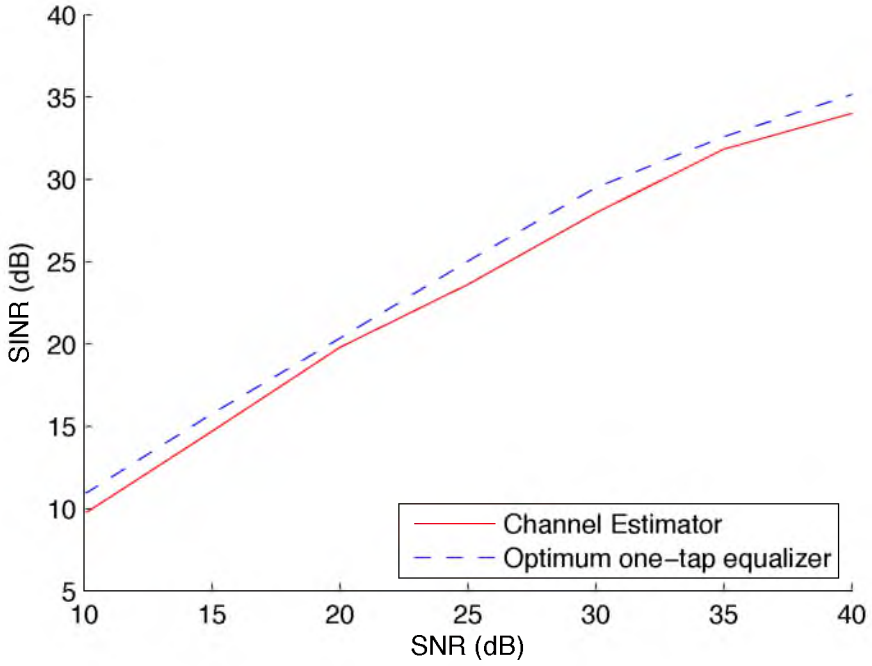


**Figure 4.3**: SINR graphs of the system under different input signal-to-noise ratios

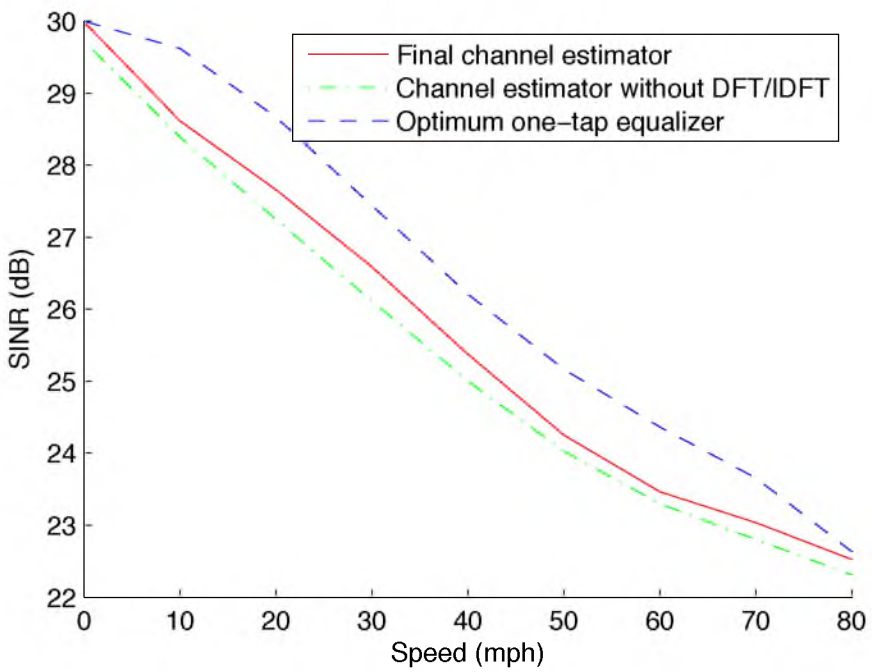


**Figure 4.4**: SINR graphs of the system under different velocities

## 4.4 Summary

In the previous chapter, assuming that channel was known perfectly, we derived equations for evaluation of an FMT system when per tone fractionally spaced equalizers are adopted in a mobile wireless channel. It was found that at typical max car speeds of up to 150 km/h, when the number of subcarriers channels is in the order specified in WiMAX, single-tap equalizers suffice.

In this chapter, we furthered our study by introducing adaptive single-tap equalizers based on channel estimation. We derived equations for an MMSE channel estimator. The results of optimum equalizers (when channel is known perfectly) were compared with those of the adaptive equalizers, and we found that a loss of 1 dB incurs. Our study considered the finite duration of the channel impulse response and used that to improve on the equalizers performance.

# CHAPTER 5

# FILTERED MULTITONE FOR FAST FADING CHANNELS

The work presented in this chapter is motivated by the needs in the doubly dispersive communication channels. We propose and develop the use of filterbank multicarrier (FBMC) technique for communications in doubly dispersive channels. A novel cost function for optimization of the filterbank prototype filter, to achieve a robust performance in doubly dispersive channels, is proposed. A design algorithm that optimizes the proposed cost function is then developed.

This chapter is organized as follows. A literature review is presented in Section 5.1. A new class of FMT systems is introduced in Section 5.2. A brief review of the isotropic filter designs of [40] and [1] is presented in Section 5.4. The impact of the channel on the ambiguity function is developed in Section 5.5. This paves the way for development of our design procedure in Section 5.6. Numerical results are presented in Section 5.7. The concluding remarks are made in Section 5.8.

## 5.1 Background

Le Floch *et al.* [39] noted the significance of FBMC techniques in dealing with the channels that exhibit spreading both in time (due to multipath effects) and in frequency (due to time variation of the channel), namely, the doubly dispersive channels. The use of prototype filters that balance between the time and frequency spreading has also been noted in [39]. The isotropic orthogonal transform algorithm (IOTA) of Alard [40], which designs filters that are well localized in both time and frequency domain, was also introduced in [39]. An alternative prototype filter design to IOTA is the method proposed by Haas and Belfiore [1]. In [1], it was noted that the members of a subset of the Hermite functions (defined in Section 5.4) satisfy the

isotropic properties, and thus it was concluded a class of isotropic filters could be constructed by linearly combining the members of this subset. Haas and Belfiore called the filters designed in this way *Hermite designs*. In this chapter, we use the term isotropic for both the IOTA design of Alard and the class of filters proposed by Haas and Belfiore.

The FMT system proposed in this chapter is based on an alternative design to those of [44], [46] and [65]. However, the differences exist. The designs presented in both [44] and [46] are for the *symbol density* $D = 0.5$ (see Subsection 2.1.3 for the definition of the symbol density). In this chapter, we emphasize the symbol densities in the range of $0.5 \leq D < 1$ and emphasize mostly a comparison of FMT and OFDM. The design in [65] (as well as [66]) has more similarity to the design presented in this paper in the sense that it also uses the Hermite pulse shapes to overcome the doubly dispersive effect of the channel. However, unfortunately, this work does not provide sufficient detail of the proposed design procedure for us to reproduce their results for comparison with our designs.

## 5.2 Doubly Dispersive Filtered Multitone (FMT)

In the case of conventional FMT, the constraints (2.10) for $l \neq 0$ and $\forall n$ are conventionally satisfied by designing $p(t)$ to be a square-root Nyquist filter with a roll-off factor $\alpha$ and subcarriers are spaced at $F = \frac{1+\alpha}{T}$. This leads to subcarriers that belong to nonoverlapping bands and thus, by virtue of filtering, they do not interfere with one another. However, to allow a good bandwidth efficiency, $\alpha$ has to be a small value. This, in turn, translates to a narrow transition band for the prototype filter $p(t)$, and as will be shown through numerical results later, this leads to a poor performance in doubly dispersive channels.

This chapter proposes the isotropic designs as prototype filters that may be designed for robust behavior in doubly dispersive channels. Such designs relaxes on the transition band of $p(t)$, but make sure that (2.10) is satisfied (accurately or approximately). Moreover, as is discussed in the subsequent sections, we design $p(t)$ such that the impact of channel in disturbing the null points of the ambiguity function $A_p(\tau, \nu)$ is minimized; see Chapter 2 for the definition of the ambiguity function,

$A_p(\tau, \nu)$. To differentiate the FMT designs that have been proposed in the past, [30], with the FMT designs of this chapter, we refer to the former as FMT-c (conventional FMT) and to the latter as FMT-dd (FMT for doubly dispersive channels).

## 5.3 Time-Frequency Localized Pulses

Le Floch *et al.* [39] have argued that an FBMC system that addresses both time and frequency dispersions should be constructed using a prototype filter $p(t)$ whose time and frequency dispersions match those of the channel. For this purpose, one may define the dispersion of $p(t)$ and $P(f)$, respectively, as

$$\sigma_t = \sqrt{\int_{-\infty}^{\infty} t^2 |p(t)|^2 dt} \tag{5.1}$$

and

$$\sigma_f = \sqrt{\int_{-\infty}^{\infty} f^2 |P(f)|^2 df}. \tag{5.2}$$

We also note that $p(t)$ is commonly designed to be an even function and thus, the same prototype filter is used at both the transmitter and receiver (as a matched pair).

On the other hand, the channel time and frequency dispersion are respectively quantified by $\Delta\tau$ (a measure of duration of the channel impulse response) and $\Delta\nu$ (a measure of the channel Doppler spread). To match the prototype filter with these loosely defined quantities, it is intuitively sound to choose $p(t)$ such that the following identity holds [39]:

$$\frac{\sigma_t}{\Delta\tau} = \frac{\sigma_f}{\Delta\nu}. \tag{5.3}$$

Moreover, it has been noted that since time and frequency may be thought as a pair of dual variables, a reasonable choice of $p(t)$ is the one with the following property:

$$P(f) = p(\ell f), \quad \text{for a constant scaling factor } \ell, \tag{5.4}$$

*i.e.,* a function that has the same form in both the time and frequency domains.

To avoid ISI, $p(t)$ should be designed so that $p(t) \star p(t)$ (where $\star$ denotes convolution) be a Nyquist pulse – say, with zero-crossings at an interval $T$. In that case, we say $p(t)$ is a root-Nyquist filter, in time. Using the symmetry constraint (5.4), $P(f)$

is also a root-Nyquist filter, in frequency, with zero-crossings at an interval $F = T/\ell$. This clearly avoids ICI, if data symbols are spread in a set of grid points as in Fig. 2.6. We may also note that in such an FBMC setup, the transmitted data symbols are spread over a grid of points with the density $D = \frac{1}{TF}$. Furthermore, (5.3) may be written as

$$\frac{T}{\Delta\tau} = \frac{F}{\Delta\nu} \tag{5.5}$$

or

$$\frac{T}{F} = \frac{\Delta\tau}{\Delta\nu} = \frac{\sigma_t}{\sigma_f} = \ell. \tag{5.6}$$

Accordingly, it is intuitively understood that to maximize the symbol density $D$, one should concentrate on designs that minimize the time-delay spread product $\sigma_t\sigma_f$. On the other hand, the Heisenberg-Gabor uncertainty principle [67] states that when $\int_{-\infty}^{\infty} |p(t)|^2 dt = 1$,

$$\sigma_t\sigma_f \geq \frac{1}{4\pi} \tag{5.7}$$

where the equality holds only when $p(t)$ is equal to the Gaussian pulse

$$g(t) = e^{-\pi t^2}. \tag{5.8}$$

Also, the Gaussian pulse $g(t)$ has the interesting property that $G(f) = g(f)$, *i.e.,* it satisfies (5.4), with $\ell = 1$. However, $p(t) = g(t)$ does not satisfy the root-Nyquist condition, necessary for ISI and ICI free transmission.

Next, we present two methods that have been proposed in the past to design filters that satisfy the generalized Nyquist criterion (2.10) and at the same time have good time-frequency localization. This will pave the way for development of our robust design method that will be introduced in the subsequent sections.

## 5.4 Isotropic Prototype Filter Design Methods

The term *isotropic*, in the context of filter design, refers to the class of filters whose time and frequency responses are the same within a scaling factor. Mathematically, this may be formulated as in equation (5.4). In addition, as was noted earlier, to avoid ISI and ICI, $p(t)$ must be constrained to satisfy (2.10).

The IOTA design/algorithm that was first introduced by Alard [40] starts with the Gaussian pulse $g(t) = e^{-\pi t^2}$ and converts it to the orthogonalized pulse

$$p(t) = \boldsymbol{\mathcal{F}}^{-1}\boldsymbol{\mathcal{O}}_T\boldsymbol{\mathcal{F}}\boldsymbol{\mathcal{O}}_F g(t) \tag{5.9}$$

where $\boldsymbol{\mathcal{F}}$ and $\boldsymbol{\mathcal{F}}^{-1}$, respectively, denote the Fourier and inverse Fourier transforms, and $\boldsymbol{\mathcal{O}}_a$ is an orthogonalization operator defined as

$$y(u) = \frac{x(u)}{\sqrt{\frac{1}{a}\sum_{k=-\infty}^{\infty} |x(u - k/a)|^2}}. \tag{5.10}$$

The orthogonalization step $\boldsymbol{\mathcal{O}}_T$ constrains the design to a root-Nyquist filter with the zero-crossing parameter $T$ along the time axis. Similarly, the orthogonalization step $\boldsymbol{\mathcal{O}}_F$ constrains the design to a root-Nyquist filter with the zero-crossing parameter $F$ along the frequency axis.

The design procedure proposed by Haas and Belfiore [1], on the other hand, constructs an isotropic filter according to the equation

$$p(t) = \sum_{k=0}^{L} a_k h_{4k}(t) \tag{5.11}$$

where $h_n(t)$ are the set of Hermite functions defined as

$$h_n(t) = \frac{1}{(2\pi)^{n/2}} e^{\pi t^2} \frac{d^n}{dt^n} e^{-2\pi t^2}. \tag{5.12}$$

Note that $h_0(t) = g(t)$ and, thus, it is an isotropic function, with parameter $\ell = 1$. Moreover, it can be shown that the set of functions $h_n(t)$ for $n = 4k$, $k = 1, 2, \cdots$ are also isotropic, with the same parameter. This implies that the construction (5.11) for any set of coefficients $a_k$ leads to an isotropic function. In [1], the coefficients $a_k$ have been calculated to construct a filter $p(t)$ that satisfies the set of constraints (2.10) exactly, and hence results in ISI and ICI free transmission when used as prototype filter in an FBMC system. However, as discussed below, the presence of a channel results in dispersion of transmit pulses, and thus render ISI/ICI free transmission impossible.

## 5.5 Channel Impact

The general input-output relationship for a linear time-varying channel may mathematically be expressed as, [28],

$$y(t) = \int_{-\infty}^{\infty} c(\tau, t)x(t-\tau)dt \tag{5.13}$$

where $c(\tau, t)$ denotes the equivalent baseband channel impulse response at delay $\tau$ and at time instant $t$. Assuming the channel is wide sense stationary (WSS), the autocorrelation function of the channel impulse response is defined as

$$\phi_c(\tau_1, \tau_2; \Delta t) = \mathrm{E}\left[c^*(\tau_1; t)c(\tau_2; t+\Delta t)\right]. \tag{5.14}$$

Under an additional assumption that the channel has the uncorrelated scattering property, (5.14) is simplified to

$$\phi_c(\tau_1, \tau_2; \Delta t) = \phi_c(\tau_1; \Delta t)\delta(\tau_1 - \tau_2). \tag{5.15}$$

In order to quantify the average power output of the channel at different time delays and Doppler frequencies, the scattering function is defined as the Fourier transform of the channel correlation function, *viz.,*

$$S(\tau, \lambda) = \int_{-\infty}^{\infty} \phi_c(\tau; \Delta t)e^{-j2\pi\lambda\Delta t}d\Delta t. \tag{5.16}$$

For detailed derivations and the related definitions that lead to the results in (5.13) through (5.16), the reader may refer to [28].

The ambiguity function $A_p(\tau, \nu)$ that was defined in (2.8) provides a measure of ISI and ICI in the absence of the channel. When $p(t)$ is designed to satisfy (2.10), there is no ISI and ICI. However, the dispersion introduced by the channel, along the time and frequency axes, will result in some distortion in the transmitted pulses $p_k(t - nT)$ and this, in turn, leads to a stochastic ambiguity function that no longer satisfies the generalized Nyquist criterion (2.10). To add the effect of the channel in the ambiguity function $A_p(\tau, \nu)$, we proceed as follows.

We note that adding the channel effect, the ISI/ICI are characterized by the disturbed ambiguity function

$$A_p^{\mathrm{d}}(\tau,\nu) = \int_{-\infty}^{\infty} p(t+\frac{\tau}{2})p'^{*}(t-\frac{\tau}{2})e^{-j2\pi\nu t}dt \tag{5.17}$$

where

$$p'(t) = \int_{-\infty}^{\infty} c(\tau,t)p(t-\tau)dt, \tag{5.18}$$

*i.e.,* the pulse shape obtained after passing $p(t)$ through the channel. Substituting (5.18) in (5.17), we obtain

$$A_p^{\mathrm{d}}(\tau,\nu) = \int_{-\infty}^{\infty}\int_{-\infty}^{\infty} p(t+\frac{\tau}{2})p(t-\frac{\tau}{2}-\rho)c^{*}(\rho,t)e^{-j2\pi\nu t}d\rho dt. \tag{5.19}$$

Note that in (5.19) and the subsequent equations, in this section, we have dropped the conjugate sign $(*)$ from $p(\cdot)$ as it is a real-valued function of time. Since the channel response $c(\tau,t)$ is stochastic, $A_p^{\mathrm{d}}(\tau,\nu)$ is also stochastic. However, the ISI and ICI power can be determined by averaging $|A_p^{\mathrm{d}}(\tau,\nu)|^2$.

Using (5.19), (5.14), and (5.15), one finds that

$$\begin{aligned}
\mathrm{E}[|A_p^{\mathrm{d}}(\tau,\nu)|^2] &= \int_{-\infty}^{\infty}\int_{-\infty}^{\infty}\int_{-\infty}^{\infty}\int_{-\infty}^{\infty} \mathrm{E}[c^{*}(\rho,t)c(\rho',t')]p(t+\frac{\tau}{2})p(t-\frac{\tau}{2}-\rho) \\
&\qquad \times p(t'+\frac{\tau}{2})p(t'-\frac{\tau}{2}-\rho')e^{-j2\pi\nu(t-t')}d\rho' dt' d\rho dt \\
&= \int_{-\infty}^{\infty}\int_{-\infty}^{\infty}\int_{-\infty}^{\infty} \phi_c(\rho;t'-t)p(t+\frac{\tau}{2})p(t-\frac{\tau}{2}-\rho)p(t'+\frac{\tau}{2}) \\
&\qquad \times p(t'-\frac{\tau}{2}-s_1)e^{-j2\pi\nu(t-t')}dt d\rho dt'.
\end{aligned} \tag{5.20}$$

Recalling that the channel impulse response is the inverse Fourier transform of the scattering function, we have

$$\phi_c(\rho;t'-t) = \int_{-\infty}^{\infty} S(\rho;\lambda)e^{j2\pi\lambda(t'-t)}d\lambda. \tag{5.21}$$

Substituting (5.21) in (5.20), we obtain

$$\begin{aligned}\mathrm{E}[|A_p^{\mathrm{d}}(\tau,\nu)|^2] &= \int_{-\infty}^{\infty}\int_{-\infty}^{\infty}\int_{-\infty}^{\infty}\int_{-\infty}^{\infty} S(\rho;\lambda)p(t+\frac{\tau}{2})p(t-\frac{\tau}{2}-\rho)p(t'+\frac{\tau}{2}) \\ &\quad \times p(t'-\frac{\tau}{2}-\rho)e^{-j2\pi t(\nu+\lambda)}e^{j2\pi t'(\nu+\lambda)}dtdt'd\rho d\lambda. \quad (5.22)\end{aligned}$$

Defining $\theta = t - \frac{\rho}{2}$ and $\theta' = t' - \frac{\rho}{2}$, (5.22) may be rearranged as

$$\begin{aligned}\mathrm{E}[|A_p^{\mathrm{d}}(\tau,\nu)|^2] &= \int_{-\infty}^{\infty}\int_{-\infty}^{\infty}\int_{-\infty}^{\infty}\int_{-\infty}^{\infty} S(\rho;\lambda)p(\theta+\frac{\tau+s_1}{2})p(\theta-\frac{\tau+s_1}{2}) \\ &\quad \times p(\theta'+\frac{\tau+\rho}{2})p(\theta'-\frac{\tau+\rho}{2}) \\ &\quad \times e^{-j2\pi\theta(\nu+\lambda)}e^{j2\pi t_2'(\nu+\lambda)}d\theta d\theta' d\rho d\lambda \\ &= \int_{-\infty}^{\infty}\int_{-\infty}^{\infty} S(\rho;\lambda)\left|A_p(\tau+\rho;\nu+\lambda)\right|^2 d\rho d\lambda. \quad (5.23)\end{aligned}$$

The above results may be explained as follows. The channel time-frequency dispersion directly carries over the ambiguity function. The disturbed ambiguity function $A_p^{\mathrm{d}}(\tau,\nu)$ is obtained by adding many (infinite) replicas of time and frequency shifted and scaled versions of $A_p(\tau,\nu)$. This leads to the final result (5.23) that may be interpreted as passing $|A_p(\tau,\nu)|^2$ through a two-dimensional (lowpass) filter with the impulse response $S(-\tau,-\nu)$. As a result, the null points (2.10) of $A_p(\tau,\nu)$ that would guarantee ISI and ICI free transmission over an ideal channel will disappear in $A_p^{\mathrm{d}}(\tau,\nu)$. Hence, we conclude, ISI and ICI free transmission over a dispersive channel is not possible and thus argue it makes more sense to design $p(t)$ with the goal of minimizing ISI and ICI power while including the channel scattering as part of a wisely selected cost function. We follow such a design strategy in the following section.

## 5.6 Design Procedure

Substituting (5.11) in (2.8), we obtain

$$\begin{aligned}A_p(\tau,\nu) &= \int_{-\infty}^{\infty}\sum_{n=0}^{L}\sum_{l=0}^{L} a_n a_l h_{4n}(t+\frac{\tau}{2})h_{4l}(t-\frac{\tau}{2})e^{-j2\pi\nu t}dt \\ &= \sum_{n=0}^{L}\sum_{l=0}^{L} a_n a_l A_{n,l}(\tau,\nu) \quad (5.24)\end{aligned}$$

where

$$A_{n,l}(\tau,\nu)=\int_{-\infty}^{\infty}h_{4n}(t+\frac{\tau}{2})h_{4l}(t-\frac{\tau}{2})e^{-j2\pi\nu t}dt. \tag{5.25}$$

Defining

$$\mathbf{a}=\begin{bmatrix} a_0 & a_1 & \cdots & a_L \end{bmatrix}^{\mathrm{T}} \tag{5.26}$$

and

$$\mathbf{A}(\tau,\nu)=\begin{bmatrix} A_{0,0}(\tau,\nu) & A_{0,1}(\tau,\nu) & \cdots & A_{0,L}(\tau,\nu) \\ A_{1,0}(\tau,\nu) & A_{1,1}(\tau,\nu) & \cdots & A_{1,L}(\tau,\nu) \\ \vdots & \vdots & \ddots & \vdots \\ A_{L,0}(\tau,\nu) & A_{L,1}(\tau,\nu) & \cdots & A_{L,L}(\tau,\nu) \end{bmatrix} \tag{5.27}$$

(5.24) may be rearranged as

$$A_p(\tau,\nu)=\mathbf{a}^{\mathrm{T}}\mathbf{A}(\tau,\nu)\mathbf{a}. \tag{5.28}$$

### 5.6.1 Haas and Belfiore Design

In [1], it was proposed that the coefficients $a_0$ through $a_L$ can be determined by substituting (5.28) in (2.10) for $(n,l)=(0,0)$ and $L$ other significant choices of $(n,l)$, and solving the resulting system of equations. It was, numerically, demonstrated that this leads to very good designs. To further clarify this procedure and pave the way for the new developments in the sequel, we discuss the method of [1] in the context of a specific design. Fig. 5.1 presents the grid of all choices of $(n,l)$. Here, it is assumed that the constraints (2.10) are applied at the origin and the 12 nearest grid points to it. In this figure, three different sets of grid points are identified.

(a) The significant points at which the constraints (2.10) should be imposed. There are four such points and these are indicated as solid circles with an additional circle around each of them.

(b) Once the desired constraints are imposed at the latter points, it follows from the even symmetry and isotropic property of $p(t)$ that the same constraints will automatically be imposed at the rest of the points indicated by solid circles.

(c) The remaining grid points, indicated by empty circles, will satisfy the constraints (2.10), within a good approximation, thanks to the exponential decay of the designed pulse $p(t)$ as $t$ increases.

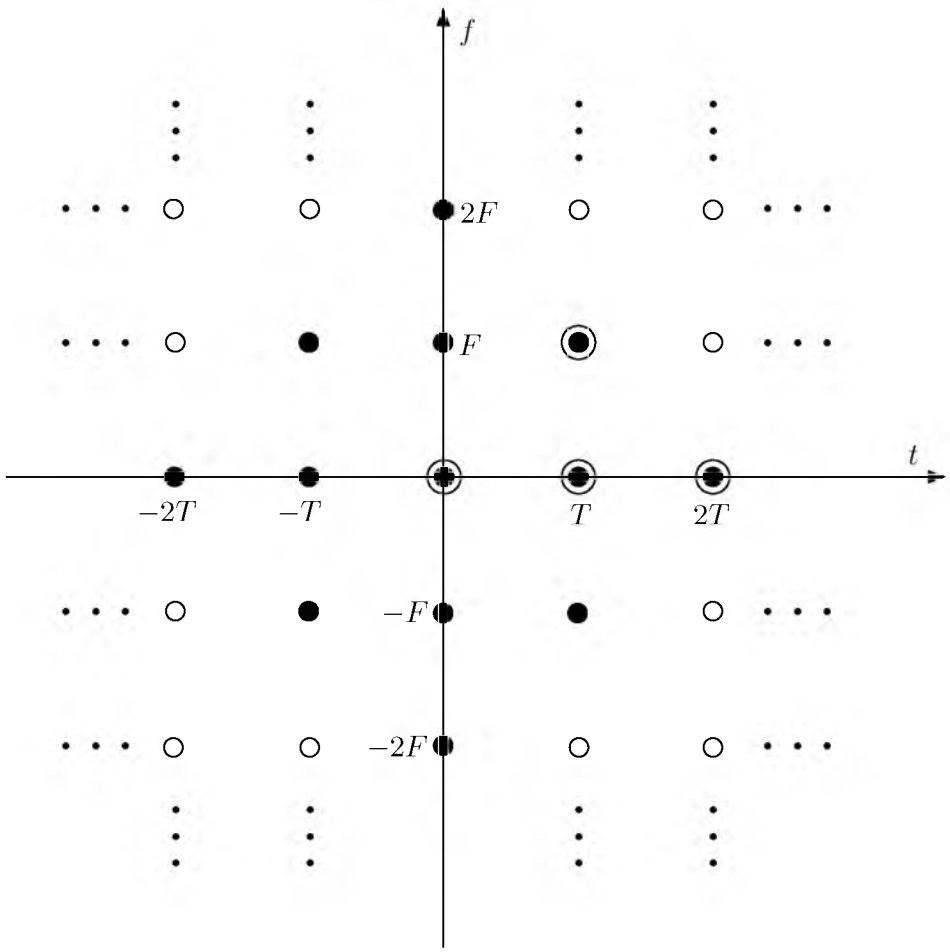


**Figure 5.1**: Grid of $(n, l)$ points at which the constraints (2.10) should be imposed. The solid circles (with or without additional circles around them) indicate the points at which the constraints (2.10) are strictly imposed. The rest of the points, by design, satisfy the constraints within a good approximation.

We note that to satisfy the constraints (2.10) at the origin and the 12 nearest grid points to it, it is sufficient to apply constraints to only 3 of the latter points. A unique design is thus obtained if the design is made based on $h_0(t)$, $h_4(t)$, $h_8(t)$, and $h_{12}(t)$, *i.e.,* the choice of $L = 3$ in (5.24) through (5.28).

It should be also noted that since, here, the designed filter is isotropic, with the parameter $\ell = 1$, the identity $T = F$ should hold. Hence, given a desired density $D = 1/TF$, the design must be for the parameters $T = F = 1/\sqrt{D}$. Once $p(t)$ is obtained based on these parameters, applying a time scaling factor, one can set $T$ to any desired value. This will set $F$ equal to $1/TD$.

### 5.6.2 Robust Design

As discussed in Section 5.5, the presence of a channel will result in a disturbed ambiguity function, $A_p^{\mathrm{d}}(\tau,\nu)$, in which the null points of $A_p(\tau,\nu)$ are smeared out, as a result of the filtering/smoothing effect caused by the channel scattering function $S(\tau,\lambda)$. Noting this, one may obtain a better system by relaxing on the zeros of $A_p(\tau,\nu)$ because of reasons mentioned below.

Consider a filter with a perfect or an approximate null point '$a$' as in the plots presented in Fig. 5.2(a). Note that, although $A_p(\tau,\nu)$ is a function of two variables $\tau$ and $\nu$, for convenience and clarity of presentations, here, the plots are drawn as the function of a single variable. Design 1 shows the case where $A_p(\tau,\nu)$ has a perfect null. This is presented on the left side of Fig. 5.2(a). The plot presented on the left side of Fig. 5.2(b) symbolizes the result after $A_p(\tau,\nu)$ is convolved with $S(\tau,\nu)$. The plots showing the case where $A_p(\tau,\nu)$ has an approximate, but wider null, are presented under the column identified as Design 2. As seen, after considering the channel effect, Design 2, indeed, may lead to a better/more robust performance.

Considering the above observation, we argue that to design a robust prototype filter for an FBMC system, the constraints on the nulls of the ambiguity function $A_p(\tau,\nu)$ may be relaxed. Each null point is replaced by a region in the $(\tau,\nu)$-plane. This we call it the *null region* and attempt to design $p(t)$ such that the average of $|A_p(\tau,\nu)|^2$ over each null region is minimized. To this end, we define and minimize the cost function

$$\zeta = \gamma_0 \int_{\mathcal{A}_0} |A_p(\tau,\nu) - 1|^2 \, d\tau d\nu + \sum_{k=1}^{L} \gamma_k \int_{\mathcal{A}_k} |A_p(\tau,\nu)|^2 \, d\tau d\nu \tag{5.29}$$

where $\gamma_k$s are a set of positive weighting factors, $\mathcal{A}_0$ is the region around $(\tau,\nu)=(0,0)$ over which the peak of $A_p(\tau,\nu)$ retains approximately equal to one, and $\mathcal{A}_k$, for $k=1,2,\cdots,L$, are a set of null regions. Using (5.28), (5.29) may be rearranged as

$$\zeta = \gamma_0 \int_{\mathcal{A}_0} \left|\mathbf{a}^{\mathrm{T}}\mathbf{A}(\tau,\nu)\mathbf{a} - 1\right|^2 d\tau d\nu + \sum_{k=1}^{L} \gamma_k \int_{\mathcal{A}_k} \left|\mathbf{a}^{\mathrm{T}}\mathbf{A}(\tau,\nu)\mathbf{a}\right|^2 d\tau d\nu. \tag{5.30}$$

To develop a numerical method for the minimization of $\zeta$, we sample the ambiguity function along the time axis $\tau$ and the frequency axis $\nu$. This converts (5.30) to

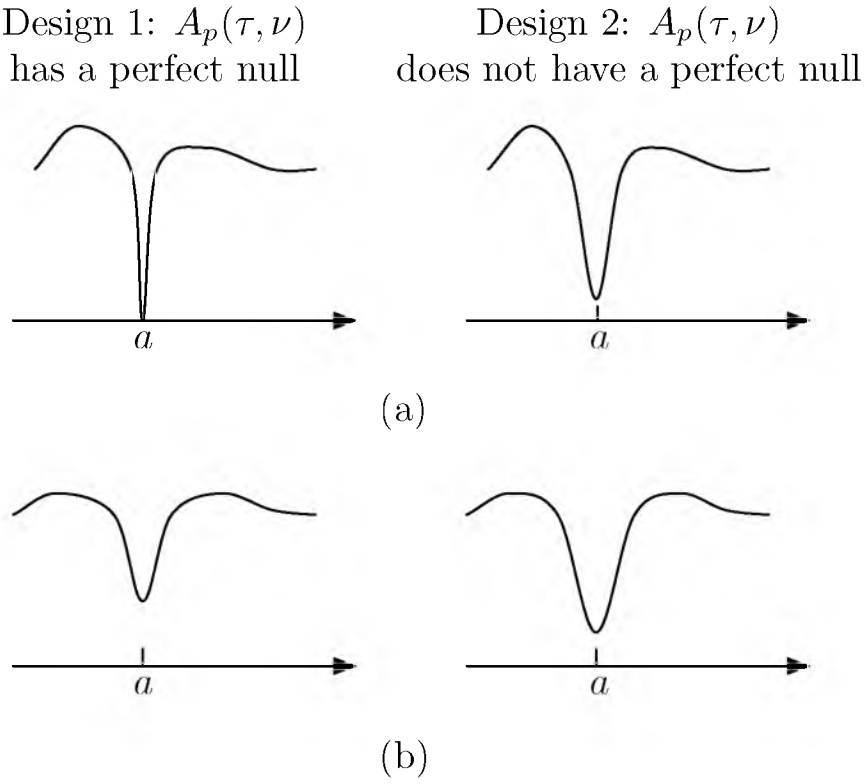


**Figure 5.2**: A set of plots symbolizing a null point or an approximate null point of $A_p(\tau, \nu)$ and the result after smearing caused by the scattering effect of a channel. (a) The plots before smearing. (b) The plots after smearing.

$$\zeta = T_s F_s \left( \sum_{k=0}^{L} \sum_{(mT_s, nF_s) \in \mathcal{A}_k} \gamma_k \left| \mathbf{a}^{\mathrm{T}} \mathbf{A}(mT_s, nF_s) \mathbf{a} - u_k \right|^2 \right) \tag{5.31}$$

where $T_s$ and $F_s$ are the sampling periods along the time axis and frequency axis, respectively, and

$$u_k = \begin{cases} 1, & k = 0 \\ 0, & k \neq 0. \end{cases} \tag{5.32}$$

We note that since $\zeta$ is a fourth order function of the vector $\mathbf{a}$, it is likely to be a multimodal function, *i.e.*, it may have a number of maxima and minima points. Therefore, the task of finding the value of $\mathbf{a}$ that minimizes $\zeta$ globally may not be trivial. However, fortunately, some prior work [64] on designing Nyquist filters has led to a similar cost function, and thus, the algorithm developed there may also be adopted here.

The method proposed in [64], when applied to the problem here, starts with defining the error vector

$$\mathbf{e} = \mathbf{B}\mathbf{a} - \mathbf{u} \tag{5.33}$$

where $\mathbf{B}$ is a tall matrix whose rows are $\mathbf{a}^{\mathrm{T}} \mathbf{A}(mT_s, nF_s)$, for all values of $m$ and $n$ where $(mT_s, nF_s) \in \mathcal{A}_k$, $k = 0, 1, 2, \cdots, L$, and $\mathbf{u}$ is a column vector whose elements are 1 when $(mT_s, nF_s) \in \mathcal{A}_0$, and 0 otherwise. Using (5.33), one finds that

$$\zeta = \mathbf{e}^{\mathrm{T}} \mathbf{\Gamma} \mathbf{e} \tag{5.34}$$

where $\mathbf{\Gamma}$ is a diagonal matrix whose diagonal elements are the weight factors $\gamma_k$ and are chosen to match the elements of $\mathbf{e}$. Now, minimizing $\zeta$ may be thought as a weighted least squares problem in which the error vector is $\mathbf{e}$ and $\mathbf{\Gamma}$ carries the weight factors. However, this is different from the standard least squares problem where the error vector $\mathbf{e}$ is a first order function of the unknown parameters. Here, $\mathbf{e}$ is a quadratic function of the parameter vector $\mathbf{a}$. Hence, the minimizer of $\zeta$ may best be found by adopting an iterative method. According to [64], an effective iterative algorithm that finds a good solution to the problem (possibly the global minimum of $\zeta$) can be implemented by taking the following steps:

1. Find an initial estimate of $\mathbf{a}$ that is close to the global minimum point of $\zeta(\mathbf{a})$. Call this $\mathbf{a}_0$. Also, let $i = 0$.

2. Find the vector $\mathbf{a}$ that minimizes $\zeta_i = \mathbf{e}_i^{\mathrm{T}} \boldsymbol{\Gamma} \mathbf{e}_i$, where $\mathbf{e}_i = \mathbf{B}_i \mathbf{a} - \mathbf{u}$ and $\mathbf{B}_i$ is obtained by substituting $\mathbf{a} = \mathbf{a}_i$ for the computation of $\mathbf{B}$. The solution to this minimization problem is

$$\hat{\mathbf{a}} = \left(\mathbf{B}^{\mathrm{T}} \boldsymbol{\Gamma} \mathbf{B}\right)^{-1} \mathbf{B}^{\mathrm{T}} \boldsymbol{\Gamma} \mathbf{u}. \tag{5.35}$$

3. Let

$$\mathbf{a}_{i+1} = \frac{\mathbf{a}_i + \hat{\mathbf{a}}}{2}. \tag{5.36}$$

4. Increment $i$ by one, and repeat Steps 2, 3, and 4 until the algorithm converges.

In the above algorithm, a proper initial choice for $\mathbf{a}_0$ that we found numerically leads to good solutions is the vector whose first element is 1 and the rest of its elements are 0. That is, we start with the Gaussian pulse as a first guess and add the higher order Hermite functions in the subsequent iterations. Moreover, through numerical experiments, we noted that a more stable algorithm is obtained if one starts the design by selecting $L = 1$ and increasing it to 2, 3, and 4 after every few iterations.

Step 3, in the above algorithm, sets $\mathbf{a}_{i+1}$ equal to the average of the solution from the previous iteration, $\mathbf{a}_i$, and the least square solution obtained in Step 2. In [68] and [64], this step was found necessary to guarantee the convergence and stability of the algorithm. The equal weights given to $\mathbf{a}_i$ and $\hat{\mathbf{a}}$ may be substituted with an average using different weights, if necessary, to guarantee a more stable operation of the algorithm or a faster convergence of the algorithm. The choice of equal weights is just by convenience and has been found to work well in most cases. Moreover, since in any case, each design takes only a few seconds, a designer may examine different choices of the weights and choose the set that works the best for the case in hand.

### 5.6.3 Hexagonal versus Rectangular Lattice

The spread of data symbols in Fig. 2.6 follow an orientation that is referred to as rectangular lattice. In [69], it is argued that better designs may be obtained by adopting the hexagonal orientation depicted in Fig. 5.3. The argument in [69] follows the fact that he hexagonal orientation allows maximum separation of points for a given symbol density. We refer an interested reader to the detailed discussions in [69].

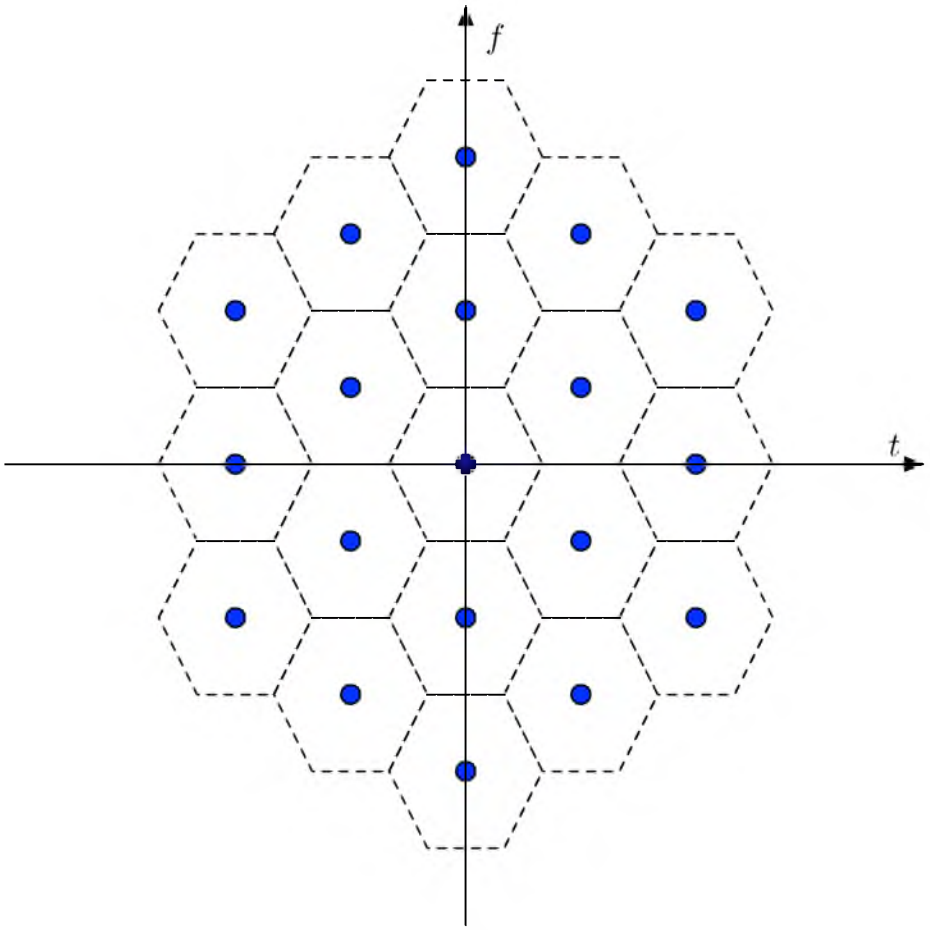


**Figure 5.3**: Spread of data symbols in a hexagonal time-frequency lattice/grid.

In this chapter, to design prototype filters for an orientation that follows the hexagonal lattice, we choose the constrained points according to those depicted in Fig. 5.4. We also set $T = 2F$ and note that for this choice, enforcing design constraints at the points indicated by solid circles with an additional circle around each of them is sufficient. As in the case of a rectangular lattice, once the constraints are applied to these points, similar constraints will be automatically imposed to the rest of solid circles, following the isotropic property of the designs. Moreover, the remaining grid points, indicated by empty circles, will satisfy the constraints (7), within a good approximation, thanks to the exponential decay of the designed pulse $p(t)$ as $t$ increases. Finally, a time scaling can be applied to $p(t)$ to set $T$ to any desired value.

## 5.7 Numerical Results

To demonstrate the effectiveness of the proposed design procedure, we present a few numerical examples. We consider a channel model whose impulse response spans over an interval $(-\frac{\Delta\tau}{2}, \frac{\Delta\tau}{2})$ and consists of a number of independent paths that are uniformly distributed in this interval and all have the same power, *i.e.,* a constant delay power profile is assumed. Each path is assumed to be subject to an independent Doppler shift according to the Jakes' model [70] with a maximum Doppler shift $f_d = \frac{\Delta\nu}{2}$. This is equivalent to saying there is a frequency spreading in the interval $(-\frac{\Delta\nu}{2}, \frac{\Delta\nu}{2})$ with a distribution that follows that of the Jakes' model. We use the time-delay product $\Delta\tau\Delta\nu$ to quantify the channel spreading in both time and frequency. We also note that for a given $\Delta\tau\Delta\nu$, our channel model may be thought as a worst case scenario, since a realistic channel with a typical exponential delay power profile and with a time span $\Delta\tau$ is characterized by a much smaller effective time spread when compared to the assumed uniform power profile. Similarly, in a practical channel, not all the paths may suffer from the same maximum Doppler shift.

First, we use our algorithm to obtain the design presented in [1]. This assures us that we have an algorithm which delivers similar designs to those of the previous reports.[1] Moreover, this design will allow us to evaluate and highlight its poor

[1] [1] does not given any detail of how the presented numerical results have been obtained.

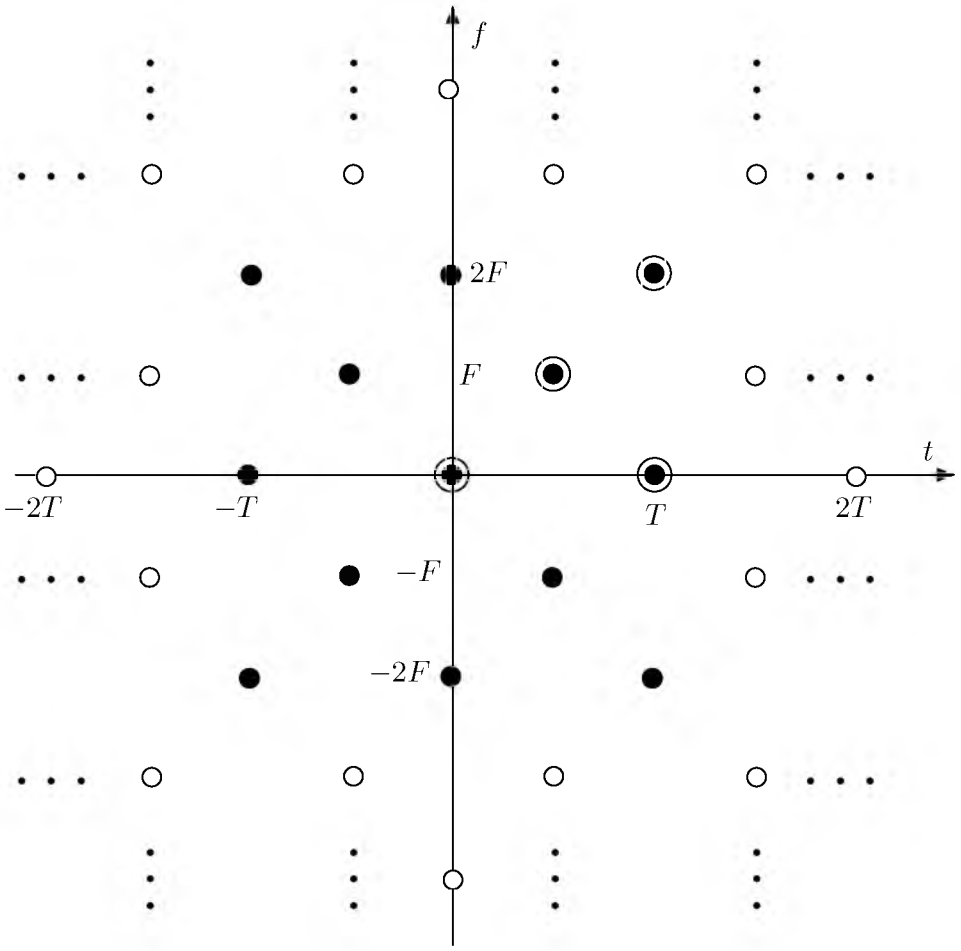


**Figure 5.4**: Grid of points at which the constraints should be imposed for the hexagonal design. The solid circles (with or without additional circles around them) indicate the points at which the constraints are strictly or approximately imposed. The rest of the points, by design, satisfy the constraints within a good approximation.

performance in doubly dispersive channels, when compared with the robust designs that are proposed in this chapter. The design presented in [1] assumes a density $D = 1/TF = 0.5$. We make the same assumption here. Moreover, to run our design procedure, we set $\Delta\tau = \Delta\nu = 0$ and assume a rectangular lattice as in Fig. 2.6, with $T = F = \sqrt{2}$. The results of this design with and without the channel effect are presented in Fig. 5.5.

Fig. 5.6 and Fig. 5.7 present the results of the robust isotropic designs for the cases of rectangular and hexagonal lattices, respectively. These designs are obtained for the channel model that was introduced above and for the choice of the parameters $\Delta\tau = 0.2T$ and $\Delta\nu = 0.2F$. Also, as in the case of Fig. 5.5, the designs are for the density $D = 0.5$. More specifically, the designs are obtained by setting $T = F = \sqrt{2}$

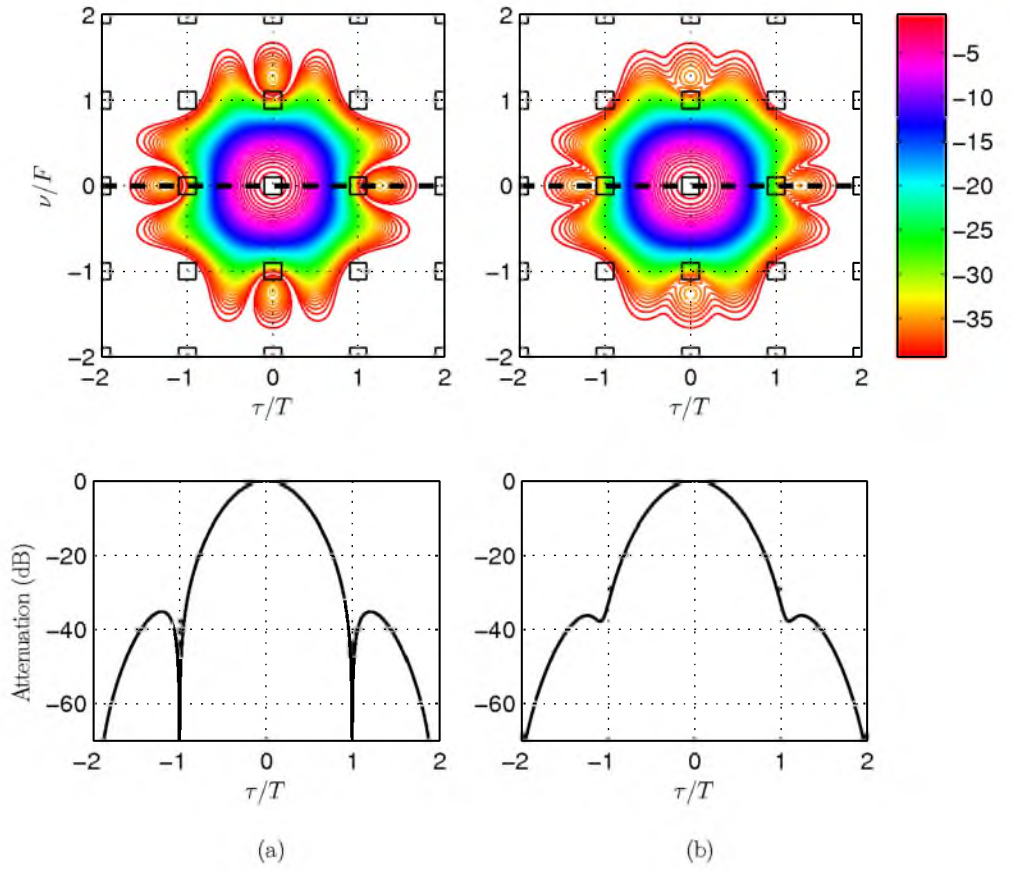


**Figure 5.5**: Results of a design based on the method of [1]. (a) Mesh plot of the ambiguity function $A_p(\tau, \nu)$ and its cross section along the indicated line. (b) The disturbed plots after adding the channel effect.

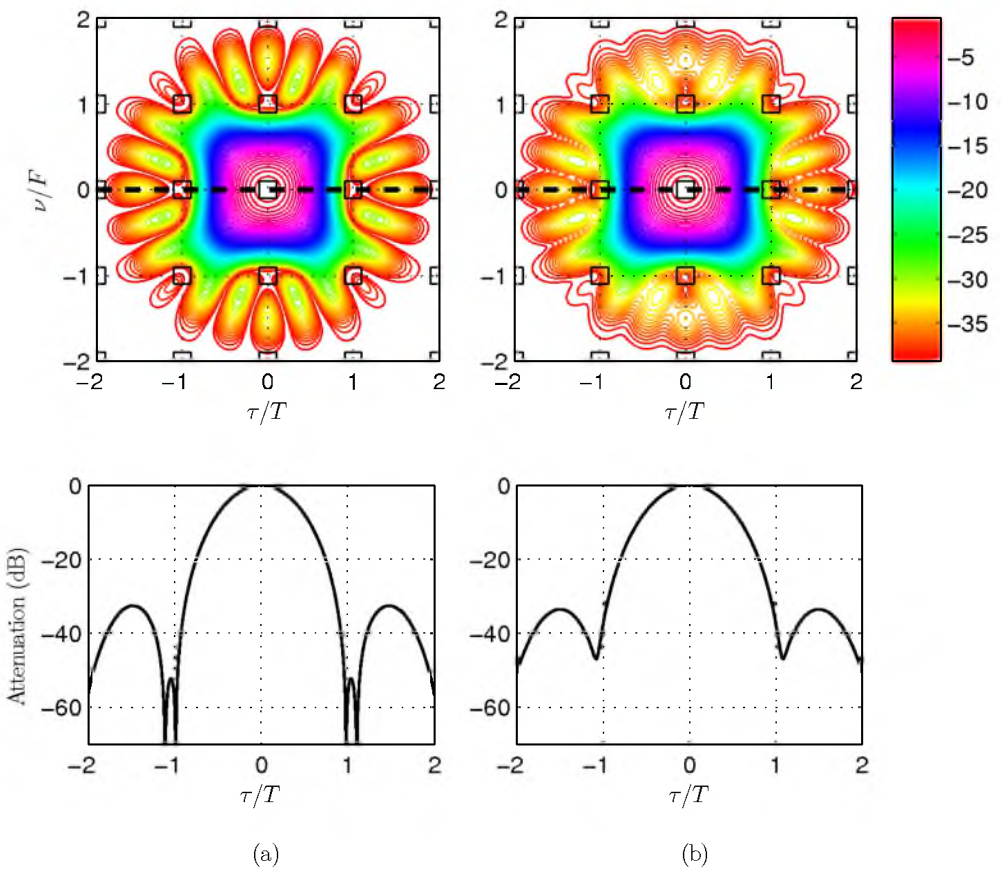


**Figure 5.6**: Results of a design based on the method of this chapter and a rectangular lattice. (a) Mesh plot of the ambiguity function $A_p(\tau, \nu)$ and its cross section along the indicated line. (b) The disturbed plots after adding the channel effect.

and thus, $\Delta\tau = \Delta\nu = 0.2\sqrt{2}$ and running the procedure discussed in Section 5.6. The results clearly show the desired performance of the designs. As seen, wide nulls appear in the ambiguity function $A_p(\tau, \nu)$ and this clearly leads to robust performance in the presence of a channel; compare Figs. 5.6(b) and 5.7(b) with Fig. 5.5(b). Moreover, as one would expect, the superior performance of the design when the grid points are set in a hexagonal lattice instead of a rectangular lattice is clearly observed.

Fig. 5.8 presents a set of results that compare the signal-to-interference ratio (SIR) of the robust isotropic designs (*i.e.*, FMT-dd) with OFDM and FMT-c (the conventional FMT) systems. Three sets of results, corresponding to the density values $D = \frac{1}{TF} = \frac{1}{2}$, $\frac{2}{3}$, and $\frac{4}{5}$, are presented. The robust isotropic designs are obtained for the channel model introduced above and the parameters $\Delta\tau = 0.2T$ and $\Delta\nu =$

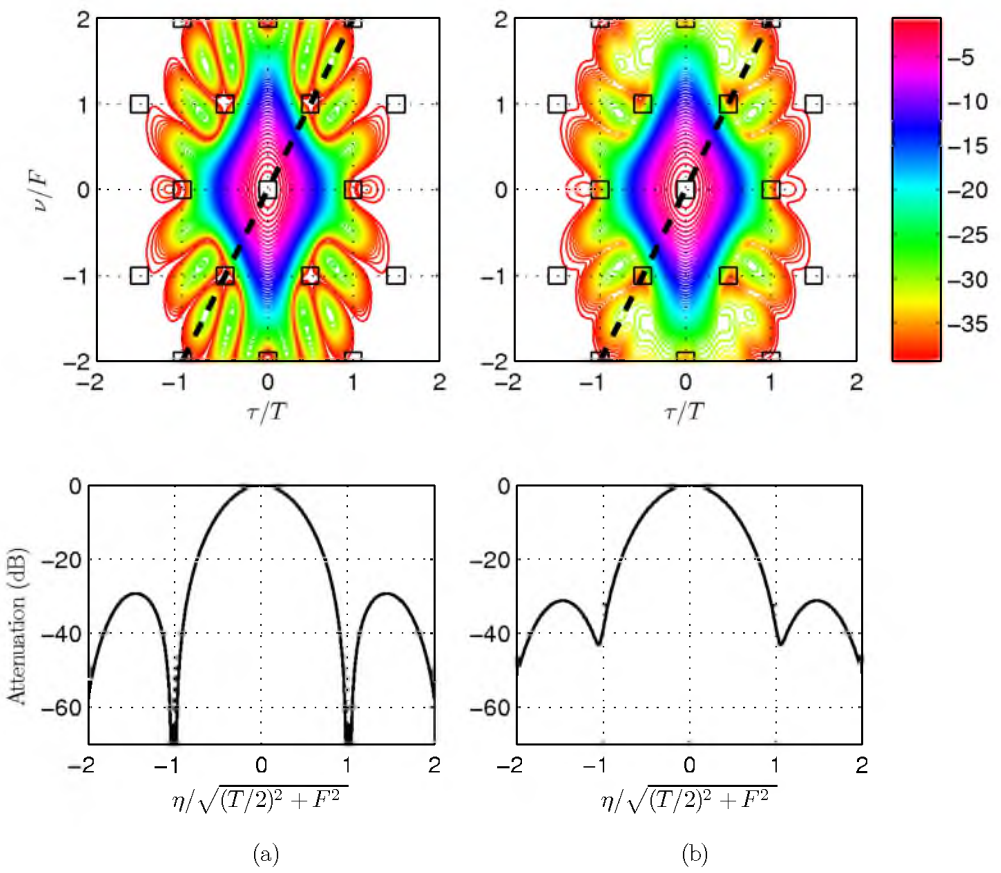


**Figure 5.7**: Results of a design based on the method of this chapter and a rectangular lattice. (a) Mesh plot of the ambiguity function $A_p(\tau, \nu)$ and its cross section along the indicated line, denoted by the variable $\eta$. (b) The disturbed plots after adding the channel effect.

$0.2F$. These designs are then examined for values of $\Delta\tau\Delta\nu$ in the range of 0 to 0.1. For FMT-c, the prototype filter is designed in each of the three cases with the aim of achieving a stopband attenuation of 60 dB or better. Also, following the basic principle of FMT-c, the roll-off factors of the prototype filters for the density values $D = \frac{1}{2}$, $\frac{2}{3}$, and $\frac{4}{5}$, are set equal to 1, 0.5, and 0.25, respectively. For OFDM, the density $D = \frac{1}{TF}$ is set by adjusting the ratio of cyclic prefix length, $T_{\text{CP}}$, over the length of FFT, $T_{\text{FFT}}$. More particularly, we note that since in OFDM $F = \frac{1}{T_{\text{FFT}}}$ and $T = T_{\text{CP}} + T_{\text{FFT}}$, $D = \frac{T_{\text{FFT}}}{T_{\text{CP}}+T_{\text{FFT}}}$ and, thus, $\frac{T_{\text{CP}}}{T_{\text{FFT}}} = \frac{1}{D} - 1$.

The results presented in Fig. 5.8 lead to the following observations:

- In high mobility environments, FMT-dd designs significantly outperform OFDM

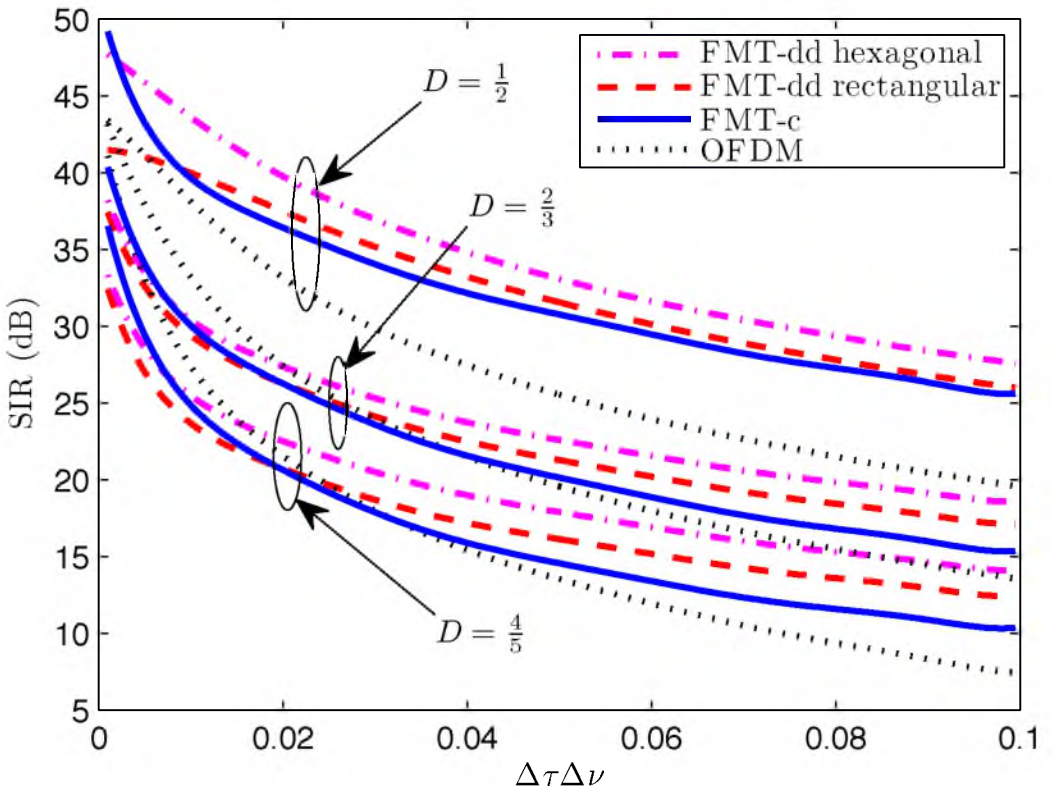


**Figure 5.8**: The ambiguity function of the prototype filter $p(t)$ designed using the method of this chapter. The design is for the density $\frac{1}{TF} = \frac{1}{2}$.

and FMT-c.

- FMT-c outperforms OFDM. This is in line with a few recent reports that have compared FMT-c and OFDM in mobile environments [33, 53].

- The isotropic designs that are based on the hexagonal lattice consistently perform around 2 dB better than their rectangular lattice counterparts. This shows 1 dB improvement over the earlier results in [69].

- As density $D$ decreases, the performance of FMT-c approaches that of the FMT-dd with rectangular lattice.

## 5.8 Summary

We introduced a new form of filtered multitone (FMT) which is specially designed to handle doubly dispersive channels. We coined the name FMT for doubly dispersive

(FMT-dd) and developed a prototype filter design method for robust performance of FMT-dd systems. The proposed method was applied to two common methods of data symbol orientation in the time-frequency space; namely, rectangular and hexagonal lattices. We found that our design led to multicarrier systems that outperform both OFDM and the conventional FMT systems significantly. In particular, a gain of 5 to 8 dB improvement over OFDM was observed. Moreover, our numerical results confirmed the previous predictions of the literature that the hexagonal orientation of data symbols in the time-frequency space should outperform its rectangular counterpart. However, we observed a gain of 2 dB in our design examples which was 1 dB better than what was already reported in [69].

# CHAPTER 6

# SINGLE-INPUT MULTIPLE-OUTPUT UNDERWATER COMMUNICATION

The increasing need for high speed communication in underwater acoustic (UWA) channels has led to many recent research publications. UWA links are known to be among the most challenging communication channels in use today [71, 72]. The relatively slow propagation velocity of acoustic waves, combined with multipath propagation that can include multiple water surface and seabed interactions, results in channel impulse responses that spread over many tens or even many hundreds of transmitted symbols, even at modest data rates. Moreover, the presence of surface and internal waves combined with the movement of communicating vehicles introduces Doppler and fading effects that may be an order of magnitude greater than those experienced in wireless electromagnetic channels. Hence, UWA links fall under the class of doubly dispersive channels with large dispersion both in time and frequency.

In this chapter, we propose the application of FMT-dd developed in Chapter 5 to underwater acoustic communications. The theoretical results derived in Chapter 5 are validated and confirmed to be applicable to UWA communications, by examining real data from an at-sea experiment (ACOMM10).

In order to compensate for the time dispersion of UWA channels, the orthogonal frequency division multiplexing (OFDM) has been proposed and widely studied by a number of researchers, *e.g.*, [36–38]. OFDM removes intersymbol interference (ISI) perfectly through use of a cyclic prefix (CP) whose length should be at least equal to the duration of the channel impulse response. On the other hand, in order to keep the bandwidth efficiency of the transmission sufficiently high, the acceptable norm is to allocate not more than 20% of each OFDM symbol to CP. This is the equivalent

of saying the CP length is one quarter of the length of each fast Fourier transform (FFT) block in the OFDM system. Moreover, since the length of CP should be at least equal to the duration of the channel impulse response, and the latter is usually very long in UWA channels, this translates to a very long symbol duration in any OFDM system that may be adopted for UWA communications. However, the use of long symbols may result in a significant degradation of the receiver performance since UWA channels also introduce a significant dispersion along the frequency axis. This leads to a significant level of intercarrier interference (ICI).

We acknowledge that other researchers have also made attempts to apply FBMC techniques to UWA communications. Gomes and Stojanovic [73], in particular, have also applied FMT to UWA channels. However, significant differences between their methods and what is presented in this dissertation exist. They propose to use an FMT system with relatively wideband subcarriers. Thus, their design requires a multitap equalizer per subcarrier band. We extend the number of subcarriers to a sufficiently large number so that each subcarrier can be equalized using a single-tap equalizer. Moreover, the method proposed in [73] follows the conventional FMT (FMT-c) approach, *i.e.*, keeps the subcarrier band spectra nonoverlapping. We, on the other hand, allow some overlapping of the subcarrier bands; however we design the underlying prototype filter to satisfy the Nyquist criterion both in time and frequency, and thus, minimize ISI and ICI, simultaneously. Hwang and Schniter [74] have also studied the use of FBMC in UWA channels. They have proposed a coded pulse-shaped multicarrier scheme that converts a doubly dispersive channel into an ICI channel with small ICI spread. Subsequently, they have developed a soft equalizer for detection. This approach, clearly, results in a complex receiver structure and thus renders its applicability limited.

To summarize, the approach that we have taken in this dissertation is to develop a multicarrier signalling technique that offers a low complexity, yet leads to an effective receiver with a significant improvement over its peers. We are particularly interested in comparing the proposed multicarrier system with an OFDM system with a comparable complexity. As our experimental results in Section 6.3 show, the multicarrier signalling that is proposed in this chapter outperforms OFDM (filtered-OFDM, to

be exact) with a significant margin. We acknowledge that the comparisons made in this chapter do not address many recent advancements in the applications of OFDM to UWA channels [72], [75–93], which all involve very high complexity channel estimation algorithms, *e.g.*, matching pursuit or basis pursuit, [72, 76–81], advanced channel coding techniques, *e.g.*, turbo codes [90], or low-density parity check (LDPC) codes [87,88], and usually a turbo "channel estimation and data detection" loop. The latter, in particular, increases the complexity of the receiver by at least an order of magnitude. There is no doubt that these advancements are of great value and future studies should concentrate on their further developments and extensions to FBMC signalling of this chapter, which should also enjoy the same level of improvement as OFDM. Such a study is beyond the scope of this thesis and thus is left for future studies.

A point that should be mentioned here is that the FBMC transmitter and receiver are slightly more complex than their OFDM counterpart. The multicarrier synthesis at the transmitter and analysis at the receiver in an OFDM system are performed through an inverse fast Fourier transform (IFFT) and an FFT, respectively. In the case of FBMC, these should be replaced by synthesis and analysis filter banks, which, when implemented in polyphase structures, in addition to IFFT/FFT, require implementation of the polyphase components filters as well [94]. This, depending on the size of IFFT/FFT, constitutes a 30 to 50% increase in complexity of the synthesis/analysis part of the system. Noting that there are more processing blocks in the system, some, like channel decoder, significantly more complex and common to both FBMC and OFDM, we argue that this is a very low price for the level of improvement that the results in this chapter demonstrate.

This chapter is organized as follows. The transmitter and receiver structures are presented in Sections 6.1 and 6.2, respectively. Analysis of the results from an at-sea experiment (ACOMM10) are presented in Section 6.3. The concluding remarks are made in Section 6.4.

## 6.1 Transmitter

The general packet structure that we have adopted for both OFDM and FBMC is presented in Fig. 6.1. Each OFDM or FBMC packet starts with a short preamble consisting of 10 cycles of a periodic signal, each of length 25% of the FFT length in our OFDM symbols. This preamble was selected in prediction of possibly using it when the received signal was subject to some time scaling; thus, the subcarrier frequency would undergo some frequency shift. For the experiments reported in this section, there is no time scaling; thus, the short preamble has no use here.

Following the short preamble, a long preamble is transmitted. The long preamble differs for OFDM and FBMC. For OFDM, the long preamble consists of two OFDM symbols transmitted back-to-back preceded by a CP which is twice as long as the normal CP, similar to the long preamble proposed by Schmidl and Cox [95] and the one commonly used in wireless channels, *e.g.*, in IEEE 802.11a,g. Moreover, to reduce intercarrier interference in OFDM, each OFDM symbol is pulse-shaped using a rectangular window with raised-cosine edges; *e.g.*, see [22] for details. The raised-cosine roll-off factor is set equal to 5%.

For FBMC, on the other hand, the long preamble consists of one FBMC symbol which is partially overlapped with the short preamble and payload. It is similar to the long preamble proposed by Peiman Amini and Farhang-Boroujeny [96]. The short preamble and long preamble symbols are designed (through a random search) to minimize the peak-to-average power ratio (PAPR) of the transmitted signal.

The carrier frequency is 20 kHz. The data bits are encoded using a rate 1/2 recursive symmetric convolutional code (RSC) encoder with the the generator polynomials (23, 35). The modulation schemes examined in this experiment are QPSK, 8PSK, and 16QAM. The subcarrier spacing for both OFDM and FBMC is 12.2 Hz, and a

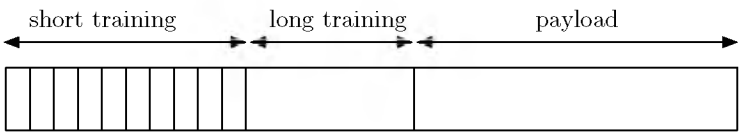


**Figure 6.1**: Packet structure.

total of 399 ($= 19 \times 21$) subcarriers are transmitted. From these, 19 subcarriers are null subcarriers and 96 subcarriers are pilot subcarriers. The remaining subcarriers are used to transmit the modulated data. Fig. 6.2 presents the null, pilot, and data subcarriers placements. The per subcarrier symbol rate is also the same for OFDM and FBMC and is equal to 9.765 symbol/sec. Each packet consists of 7 codewords. Each codeword spans over 8 consecutive OFDM/FBMC symbols. Accordingly, each codeword consists of 4560 symbols (coded). A long preamble symbol is inserted between each pair of consecutive code words. These, as explained below, are used to resynchronize the receiver to each incoming code word.

## 6.2 Receiver Structure

### 6.2.1 Timing Recovery

For each receive hydrophone, timing recovery and channel estimation is performed independently. The results from all hydrophones are then combined using a maximum ratio combiner. We tried different methods to find the best method of finding a correct timing phase for processing of both OFDM and FBMC signals. For FBMC, we found that an acceptable timing phase is obtained by correlating the incoming signal with the transmitted long preamble and choosing the highest peak as the midpoint of the received data symbols.

For OFDM, we examined the method of Schmidl and Cox [95] as well as correlating one cycle of the IFFT output of the transmitted signal of the long preamble with the received signal and choosing the peak of the correlator output as the timing phase. Direct application of any of these methods did not result in a successful timing phase. Further examination of the received signals revealed that an improved

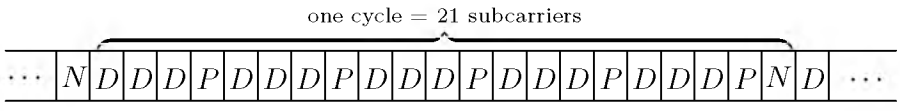


$D$: data
$P$: pilot
$N$: null

**Figure 6.2**: Subcarrier placement. 19 cycles of the placement are repeated across the transmission band.

timing phase estimation could be obtained by taking the following additional steps. Starting with the coarse timing phase obtained from the correlator, the extracted frame of the received long preamble is compared with its transmit counterpart to obtain an estimate of the channel. Any timing phase error at this stage can be detected by noting that the identified channel will be cyclically rotated by the same amount. Hence, the residual timing phase error is estimated and accordingly, a more accurate estimate of the timing phase is selected for the subsequent data frames.

We examined the above method also when the coarse timing phase estimate was obtained using the method of Schmidl and Cox [95]. Our experiments showed that the correlator method provides a more accurate estimate and, thus, the reported results below are obtained using the correlator method followed by our proposed timing phase fine-tuning method.

### 6.2.2 Channel Estimation

Our preliminary data analysis experiments revealed that because of fast variation of the UWA channels, the channel estimation should be made separately for each frame of OFDM/FBMC. We thus use the pilot symbols within each frame to obtain the channel estimate and accordingly equalize the output signals from the data subcarriers. The channel is assumed to be flat fading over each subcarrier. Hence, the channel at each subcarrier is estimated as a complex-valued gain. Accordingly, we model the demodulated signal at the output of each subcarrier channel and each receiver as

$$\hat{s}_{ki}[n] = H_{ki}[n]s_k[n] + \nu_{ki}[n], \tag{6.1}$$

where $s_k[n]$ is the data transmitted on the $k$-th subcarrier during the $n$-th symbol interval, $H_{ki}[n]$ is the complex-valued channel gain at the $k$-th subcarrier between the transmitter and the $i$-th receive hydrophone, and $\hat{s}_{ki}[n]$ is the corresponding received signal at the $i$-th receive hydrophone. The channel noise is denoted by $\nu_{ki}[n]$. Using the channel model (6.1), a least squares procedure can be readily developed for channel estimation. The details of such estimator can be found in [58]. The result is a set of channel gains $\begin{bmatrix} \hat{H}_{0,i}[n] & \hat{H}_{1,i}[n] & \cdots & \hat{H}_{N-1,i}[n] \end{bmatrix}^{\mathrm{T}}$, in the frequency domain, that will be used for equalizing the analyzed subcarrier signals.

### 6.2.3 Noise Variance Estimation

An estimate of noise variance for each receive hydrophone is needed in order to combine the received signals from various hydrophones and also in order to decode the combined signals. In order to compute the noise variance, we assume that at the pilot subcarrier, $\hat{H}_{ki}[n] = H_{ki}[n]$ within a acceptable approximation and thus,

$$\nu_{ki}[n] = \hat{s}_{ki}[n] - s_{ki}[n]\hat{H}_{ki}[n]. \tag{6.2}$$

Moreover, assuming that the channel noise is white, the noise variance will be the same over all the subcarriers. Accordingly, we estimate the noise variance by finding the average of the squared magnitude values of $\nu_{ki}[n]$ over all pilot subcarriers as

$$\hat{\sigma}^2_{\nu}[n] = \frac{1}{N_p}\sum_{k} |\nu_{ki}[n]|^2 \tag{6.3}$$

where $N_p$ is the number of the pilot subcarriers.

### 6.2.4 Maximum Ratio Combining

We assume that over each subcarrier, the channel can be approximated by a flat-fading gain. Under this assumption, the optimum receiver would be the maximum ratio combining (MRC) [97], where the improved estimate of the received signal is calculated as

$$\tilde{s}_k[n] = \frac{\sum_{i=1}^{N_r} \frac{\hat{s}_{ki}[n]}{\sigma^2_{\nu,i}[n]} \hat{H}^*_{ki}[n]}{\sum_{i=1}^{N_r} \frac{|\hat{H}_{ki}[n]|^2}{\sigma^2_{\nu,i}[n]}}, \tag{6.4}$$

where $i$ is the hydrophone index and $N_r$ is the number of receive hydrophones. The variance of the noise contained in $\tilde{s}_k[n]$ is given by

$$\tilde{\sigma}^2_{\nu}[n] = \left( \sum_{i=1}^{N_r} \frac{\left|\hat{H}_{ki}[n]\right|^2}{\sigma^2_{\nu,i}[n]} \right)^{-1}. \tag{6.5}$$

### 6.2.5 Decoding

The data are decoded using a maximum *a posteriori* (MAP) decoder. In order to compute the *a posterior* log-likelihood ratio (LLR) values, we assume that after equalization, the channel is modelled as an additive white Gaussian noise (AWGN) channel. For this type of channel, the *a posteriori* LLR values can be easily calculated, given the noise variance for each subcarrier at each receiver hydrophone, [98].

## 6.3 Data Analysis Results

We transmitted codewords for both OFDM and FBMC. QPSK, 8PSK, and 16QAM constellations were examined. For each constellation, we transmitted 49 codewords. The receiver was an array of 8 hydrophones. For each hydrophone, the correct timing offset is found and the channel is estimated for each OFDM/FBMC symbol block. The synchronized samples for the hydrophones are then combined using the MRC and the results are passed to the MAP decoder.

Figs. 6.3, 6.4, and 6.5 show the histograms of BER values of OFDM and FBMC systems. The results show that FBMC outperforms OFDM with a large margin. For instance, by combining signals from all 8 hydrophones, FBMC successfully detects all codewords correctly, *i.e.*, with BER of zero, for QPSK and 8PSK constellations. For 16QAM constellation, it detects 92% of the codewords (45 out of 49) correctly. Two codewords are detected with BER values of better than 0.01, and only one codeword has a BER of greater than 0.01, but less than 0.1. In comparison, OFDM fails to correctly detect one codeword for QPSK constellation, 18 of the codewords for 8PSK constellation, and 48 (out of 49) codewords for 16QAM constellation. In the latter case, OFDM fails to detect almost 50% of the codewords with a BER of worse than 0.1.

In order to develop further insight into the performance difference between FBMC and OFDM, we also study the SINR of the two systems at the receiver output. The SINR values are calculated as follows. We assume that the channel estimate obtained using the pilot symbols is perfect, and use it to equalize the signals for each subcarrier accordingly. The difference between each equalized signal and the actual transmitted symbol is considered as the interference-plus-noise component. The ratio of the magnitude-squared of each transmitted symbol over the magnitude-squared of the corresponding interference-plus-noise component is then calculated, converted to decibel, and recorded for all OFDM/FBMC symbols. Fig. 6.6 presents the histograms of these results for QPSK constellation. The results are presented for three cases, for using 1, 2, or 8 receive hydrophones, respectively. The histograms are consistent with the BER results presented above. It is interesting to note that for the case of one receive hydrophone, the difference between FMT-dd and OFDM is around 5 dB and

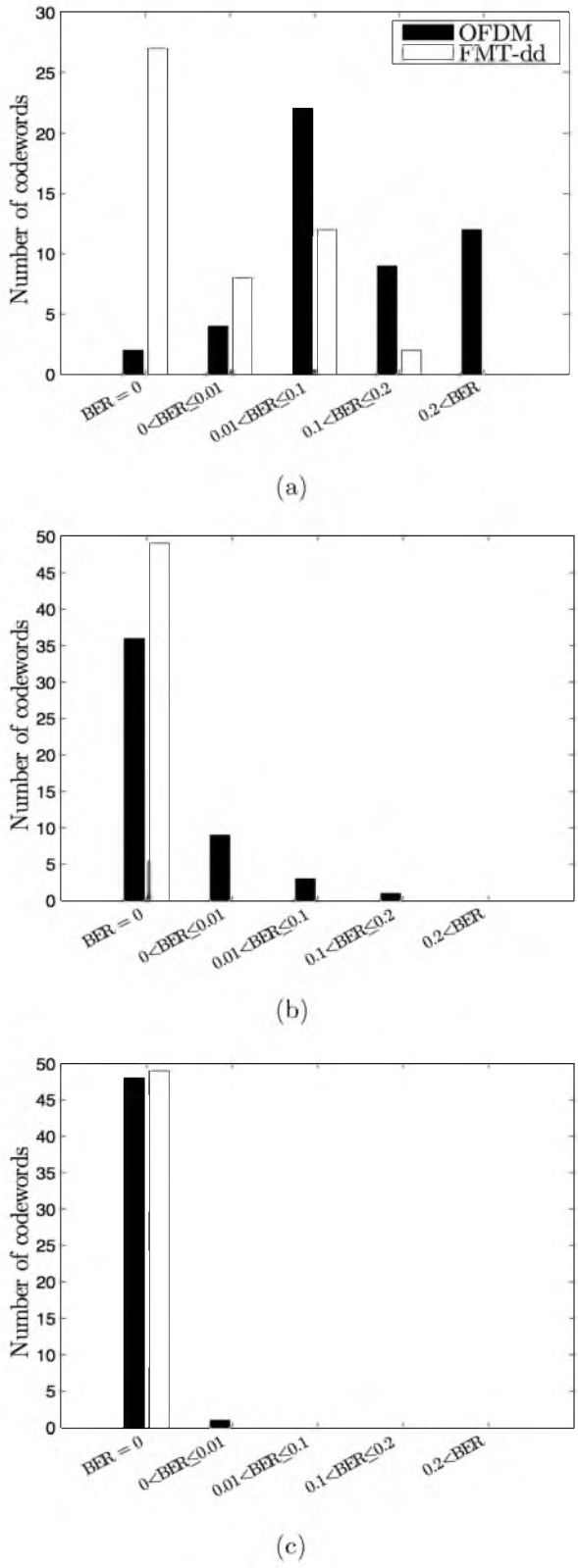


**Figure 6.3**: BER histogram for QPSK constellation. (a) 1 receive hydrophone (b) 4 receive hydrophones (c) 8 receive hydrophones

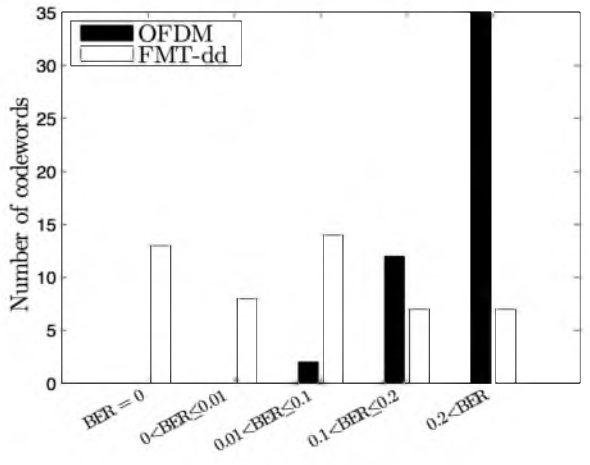


(a)

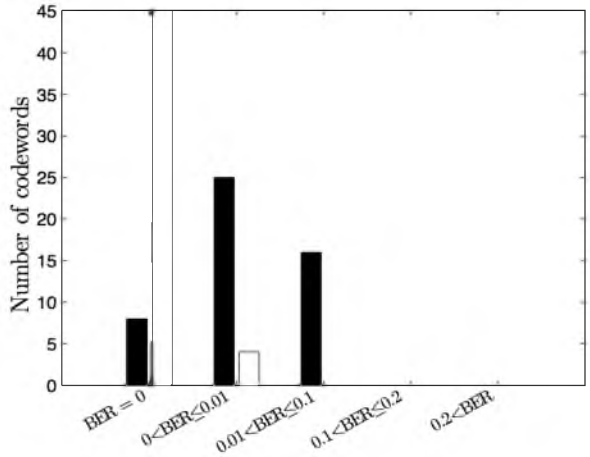


(b)

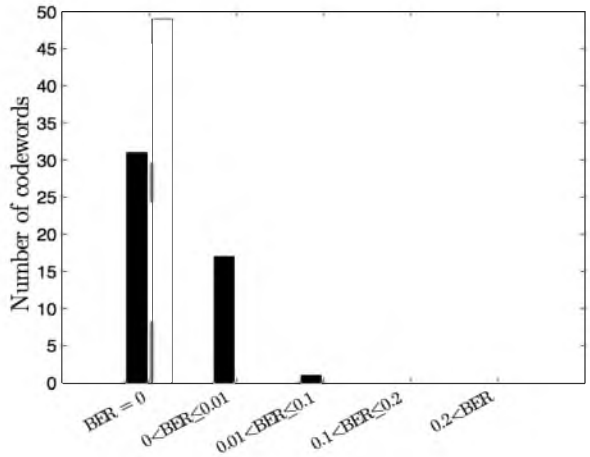


(c)

**Figure 6.4**: BER histogram for 8PSK constellation. (a) 1 receive hydrophone (b) 4 receive hydrophones (c) 8 receive hydrophones

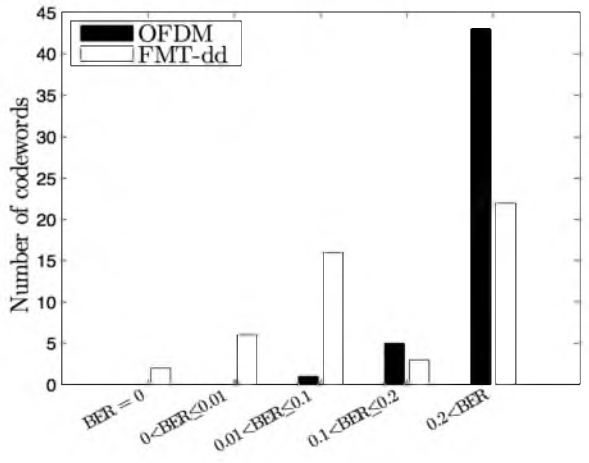


(a)

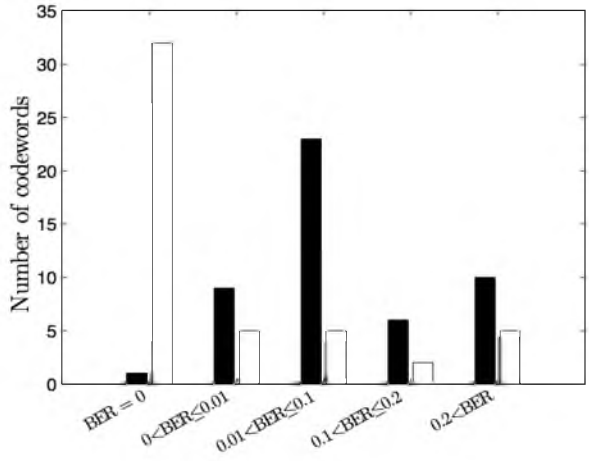


(b)

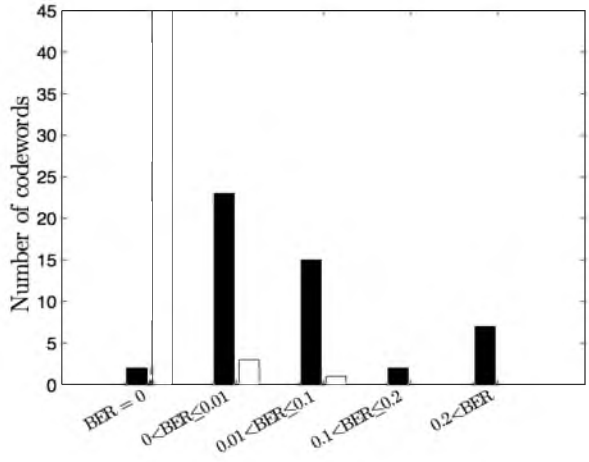


(c)

**Figure 6.5**: BER histogram for 16QAM constellation. (a) 1 receive hydrophone (b) 4 receive hydrophones (c) 8 receive hydrophones

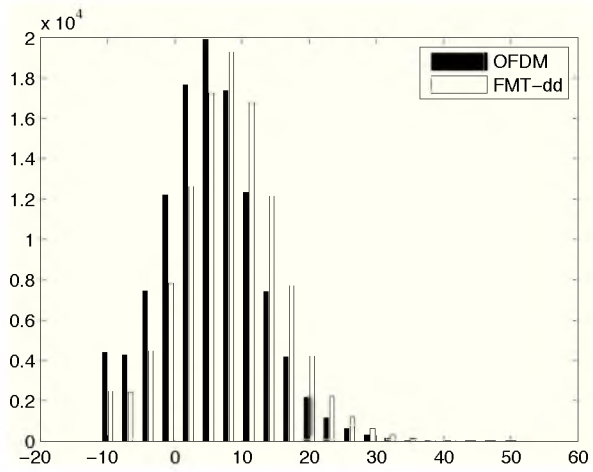


(a)

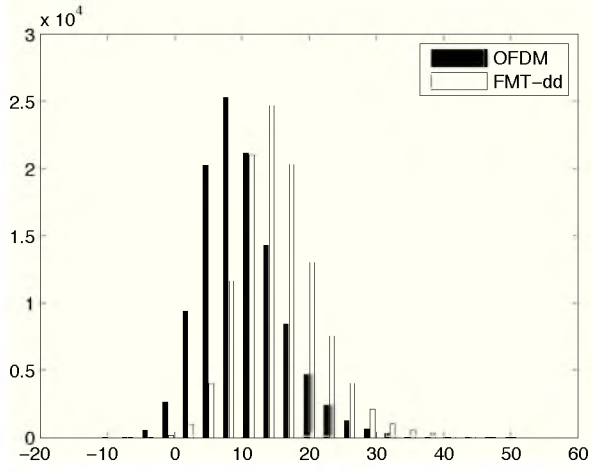


(b)

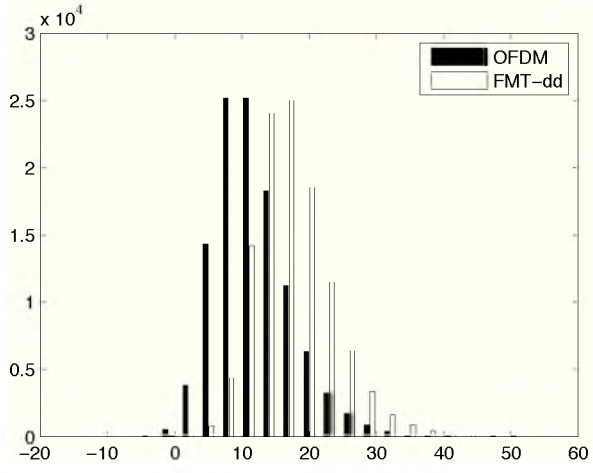


(c)

**Figure 6.6**: SINR histogram for QPSK constellation. (a) 1 receive hydrophone (b) 4 receive hydrophones (c) 8 receive hydrophones

this value is a close match to the SIR comparisons presented in Fig. 5.8. For the cases of 4 and 8 hydrophones, FMT-dd outperforms OFDM by as much as 10 dB. Similar results are observed for 8PSK, in Fig. 6.7 and 16QAM, in Fig. 6.8.

## 6.4 Summary

In this chapter, a novel UWA communication method using a class of FBMC systems using the filter design from Chapter 5 was studied. Among the various FBMC systems in the literature, we found FMT to be an excellent choice for UWA communications. The experimental results demonstrated that this new design provided a significant gain over OFDM. This finding was confirmed by testing our design in an at-sea experiment (ACOMM10).

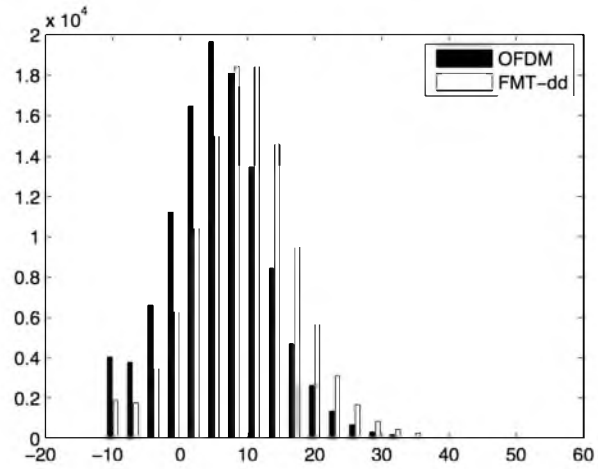


(a)

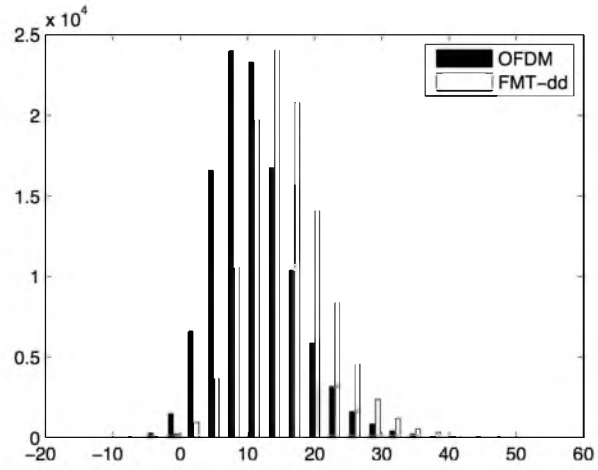


(b)

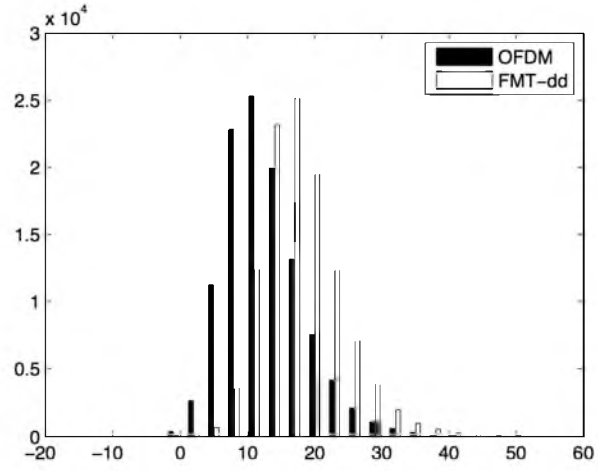


(c)

**Figure 6.7**: SINR histogram for 8PSK constellation. (a) 1 receive hydrophone (b) 4 receive hydrophones (c) 8 receive hydrophones

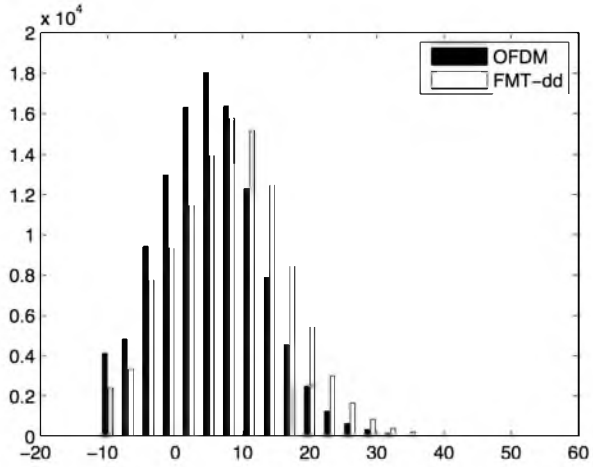


(a)

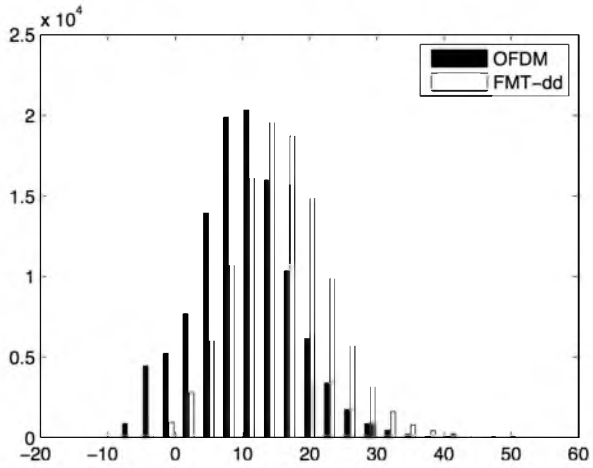


(b)

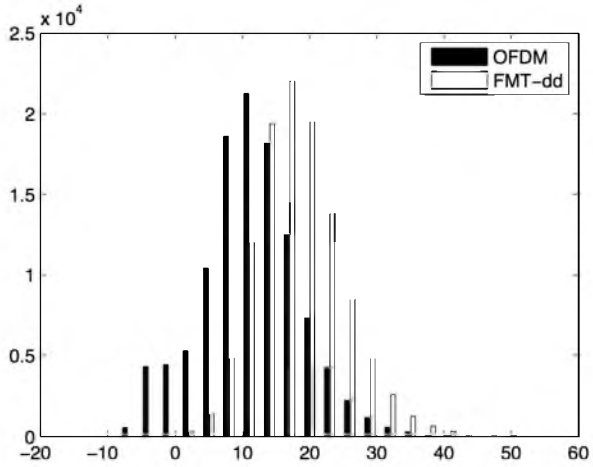


(c)

**Figure 6.8**: SINR histogram for 16QAM constellation. (a) 1 receive hydrophone (b) 4 receive hydrophones (c) 8 receive hydrophones

# CHAPTER 7

# MULTIPLE-INPUT MULTIPLE-OUTPUT UNDERWATER ACOUSTIC COMMUNICATIONS

Multiple-input multiple-output (MIMO) systems are widely used in wireless communications in order to obtain faster and more reliable communication systems. In Chapter 6, we considered using a single transmitter with multiple receivers to increase the reliability of our UWA communication system. In this chapter, we consider the feasibility of transmitting multiple streams simultaneously on multiple transmit antennas to gain a higher rate for multicarrier underwater communications.

Communication systems that use multiple antennas at both transmitter and receiver could offer a significant gain in throughput [95]. They have been proposed in the latest wireless communication standards, such as 3GPP-LTE, IEEE 802.11n, and IEEE 802.11m.

Researchers have studied the application of MIMO for UWA communications for single carrier systems [99–105]. It has been shown that applying a joint channel estimation and data detection methods based on Markov Chain Monte Carlo (MCMC) improves the BER significantly [106]. MCMC detectors are good choices for doubly dispersive channels because they have low computational complexity compared to the optimum MAP detectors and offer a comparable performance.

Applying MIMO to multicarrier UWA communications has also been studied. For instance, [72, 87] have proposed and studied MIMO-OFDM systems. They have studied MIMO-OFDM with up to 4 transmit antennas and up to 12 receive antennas.

The main challenge in the application of multicarrier MIMO to UWA communications is channel estimation. Assuming a flat fading channel over each subcarrier,

at each receive antenna, one has to estimate as many channel gains as the number of transmit antennas. On the other hand, because of the fast fading environment, these channel gains change significantly from one multicarrier symbol to the next multicarrier symbol, and therefore, a large number of pilot symbols have to be devoted for channel estimation. This, as demonstrated in this chapter, limits the applicability of MIMO techniques to UWA channels. The contribution made in this chapter is to reveal the limitations of MIMO techniques in the challenging UWA channels.

The rest of this chapter is organized as follows. In Section 7.1, the task of channel estimation in multicarrier MIMO channels for UWA communication systems is laid out. Simulation results of the performance of a MIMO communication system in doubly dispersive channels are presented in Section 7.2. Finally, Section 7.3 presents a summary of our findings of this chapter.

## 7.1 Multicarrier MIMO Channel Estimation

In the previous chapters, we developed a packet structure for UWA communication systems and used it for an at-sea experiment. In our packet, to be sure of the system ability to correctly estimate the channel and track its fast variation, one out of every four subcarriers was a pilot (see Fig. 6.1) . Extending the same packet structure for a MIMO system with two transmit antennas results in the pilot data structure shown in Fig. 7.1. Note that at the points where pilots are inserted for each of the antennas, a null is inserted at the other antennas, to allow direct estimation of the respective channel gains. As seen, with this arrangement, half of the subcarriers are allocated to pilots/nulls and thus, only one half of the channel resources will be available to transmit data. The situation becomes worse if one attempts to transmit from three antennas. This scenario that is presented in Fig. 7.2 leads to a situation where only one quarter of channel resources will be available for data.

Elaborating more on the scenarios presented in Figs. 7.1 and 7.2, and also the packet structure when there is only one transmit antenna (presented in Chapter 6), one will make the following observations. The number of effective data symbols per subcarrier for the case of one transmit antenna only is $3/4 = 0.75$. This increases to $2\times1/2 = 1$, when the number of transmit antennas increases to two. For the case

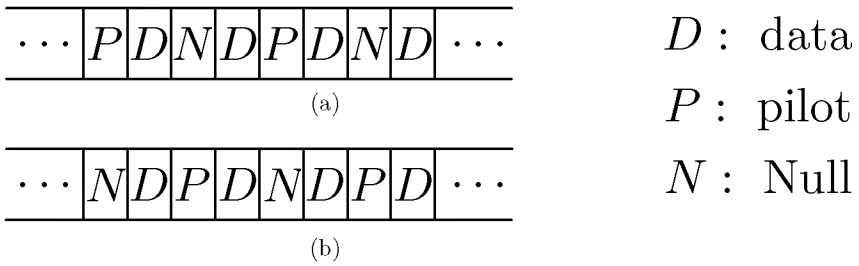


**Figure 7.1**: Subcarrier placement for a 2 transmitter MIMO underwater communication system. (a) Subcarrier placement for the first transmitter. (b)Subcarrier placement for the second transmitter.

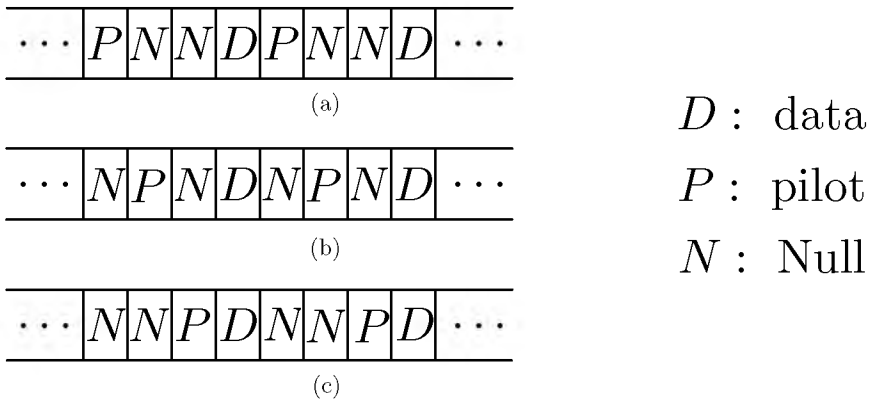


**Figure 7.2**: Subcarrier placement for a 3 transmitter MIMO underwater communication system. (a) Subcarrier placement for the first transmitter. (b)Subcarrier placement for the second transmitter. (b)subcarrier placement for the third transmitter.

of three transmit antennas, the number of effective data symbols per subcarrier is equal to $3\times1/4 = 0.75$. That is, one gains nothing in terms of the effective data symbols if the number of transmit antennas is increased from one to three. This rather disappointing observation will be even worse when one takes into account the unavoidable channel estimation errors. This point will become more clear later when we present our numerical results.

Next, we consider the more general scenarios where for the case of a single transmit

antenna, one out of every $L$ subcarriers is a pilot. In that case, the number of transmit antennas may be varied between one and $L-1$ before we reach a point where there will be no resources for transmission of data. If we denote the number of transmit antennas by $S$, following the same line of thoughts that led to the above results, here, the number of effective symbols per subcarriers is obtained as

$$r(S) = \frac{S(L-S)}{L-1}. \tag{7.1}$$

We also define the MIMO gain

$$\mathcal{G}(S) = \frac{r(S)}{r(1)}. \tag{7.2}$$

Using (7.1) in (7.2), we obtain

$$\mathcal{G}(S) = \frac{S(L-S)}{L-1}. \tag{7.3}$$

Fig. 7.3 presents a set of plots of $\mathcal{G}(S)$ for different choices of the parameter $L$. The observation made here is that as $L$ increases, the maximum MIMO gain also increases, albeit at a rather slow pace. To make this observation more explicit, Fig. 7.4 presents the maximum value of the MIMO gain, $\mathcal{G}(S)$, as $L$ is varied between 4 and 16. We note that for UWA channels, the choices of $L$ beyond 6 or 7 are probably unrealistic, because both fast variation of channel in time and frequency impose the need for a significant number of pilots. The experimental results reported in the literature use values of $L$ in the range 4 to 16 [81]. Therefore, realistically, according to the plots in Figs. 7.3 and 7.4, a MIMO gain of more than 2 may not be possible. This gain is achieved when the number of transmit antennas is around 4. We note that this is different from what has been reported for wireless electromagnetic channels where the MIMO gain is equal to the number of transmit antennas [97].

## 7.2 Simulation Results

Similar to the packet format in Section 6.1, here also, we consider a packet format with 400 subcarriers. Subcarrier spacing is equal to 12.5 Hz. The transmit data are coded using a rate 1/2 convolutional encoder similar to the one used in the previous chapter. The transmitted data are passed through a channel with a sparse tapped delay line model. The channel has 4 taps at delays of 0, 6, 14, and 20

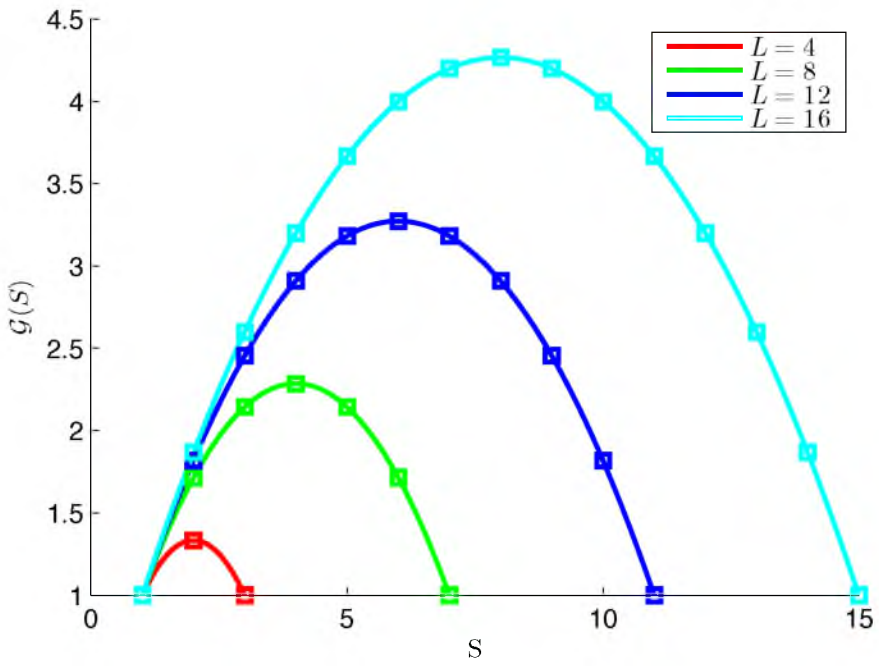


**Figure 7.3**: $\mathcal{G}(S)$ for different choices of the parameter $L$.

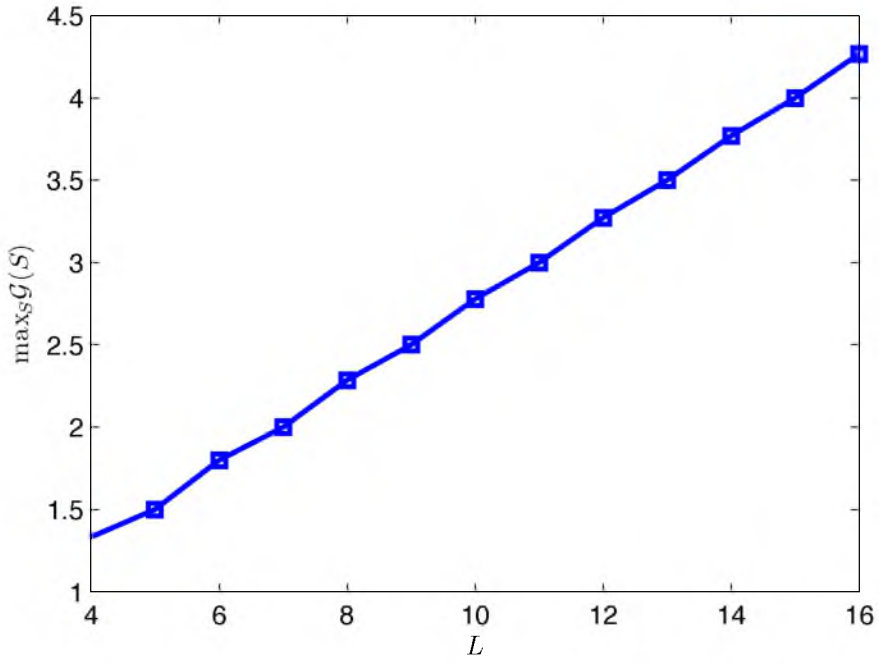


**Figure 7.4**: Maximum value of the MIMO gain, $\mathcal{G}(S)$, as $L$ is varied between 4 and 16.

samples. The mean powers of the taps are 1, 0.5, 0.2, and 0.05, respectively. Each tap has a Jakes' Doppler spread where the maximum Doppler frequency is 2 Hz. We assume channel noise is absent and examine the received data symbols that are extracted using a minimum mean square error (MMSE) equalizer. To shed light on the receiver performance under different conditions, we examine signal-to-interference (SIR) of the extracted symbols. These results are given for two cases: (i) when the channel is estimated according to the channel estimation algorithm that was presented in the previous chapter; and (ii) when the channel estimate is obtained averaging the true channel over the current symbol. The latter provides us with an idea of how far one possibly can go (in the limit) if he takes advantage of advanced channel estimation algorithms and turbo joint channel estimation and data detection techniques [107, 108].

Table 7.1, Table 7.2, and Table 7.3 show the output SIR when $L$ is equal to 4, 6, and 8, respectively. The results clearly show the SIR performance starts degrading as the number of transmit antennas is increased. It can be seen that the difference between the performance of a single transmitter system and multiple transmitter system starts increasing when the pilot subcarrier spacing, $L$, is increased. For the case of $L = 8$, we lose around 5 dB in SIR when 4 transmitters are used instead of 1. This decrease in SIR could significantly degrade the overall performance of the system.

Figs. 7.5, 7.6, and 7.7 present the eye pattern of the output samples of the receiver for QPSK, 16QAM, and 64QAM constellations when $L = 8$. As the number of transmitters increases, the eye patterns become more distorted. Due to this distortion, the constellation points are not visible for higher order constellations and a higher number of transmitters.

**Table 7.1**: SIR in dB for different constellations and number of transmitters when $L = 4$.

| $S$ | QPSK | 16QAM | 64QAM |
|---|---|---|---|
| 1 | 21.6 | 21.6 | 21.6 |
| 2 | 20.2 | 20.1 | 20.2 |
| 3 | 19.6 | 19.5 | 19.5 |

**Table 7.2**: SIR in dB for different constellations and number of transmitters when $L = 6$.

| $S$ | QPSK | 16QAM | 64QAM |
|---|---|---|---|
| 1 | 19.5 | 19.4 | 19.4 |
| 2 | 17.4 | 17.2 | 17.3 |
| 3 | 15.6 | 15.6 | 15.5 |

**Table 7.3**: SIR in dB for different constellations and number of transmitters when $L = 8$.

| $S$ | QPSK | 16QAM | 64QAM |
|---|---|---|---|
| 1 | 19.7 | 19.6 | 19.8 |
| 2 | 17.1 | 17.0 | 17.0 |
| 3 | 15.6 | 15.6 | 15.6 |
| 4 | 14.0 | 13.9 | 13.9 |

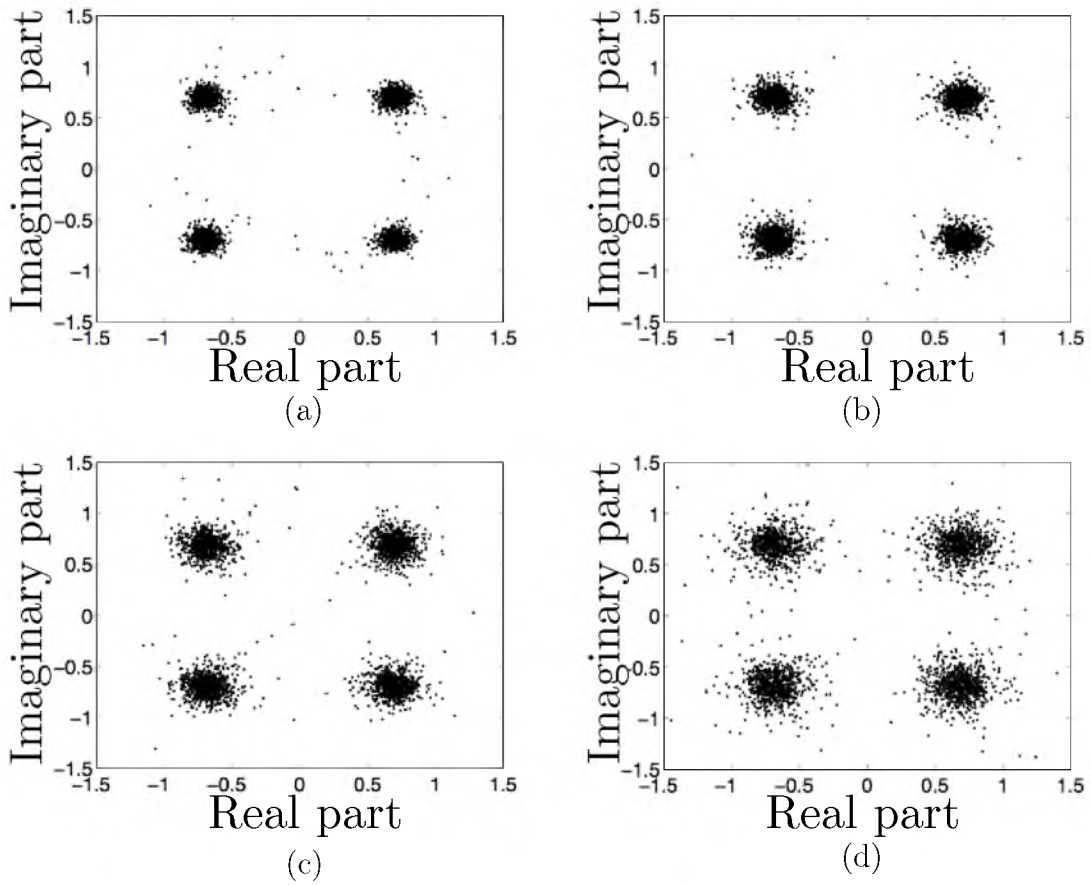


**Figure 7.5**: Eye diagram for QPSK constellation. (a) 1 transmit hydrophone (b) 2 transmit hydrophone (c) 3 transmit hydrophone (d) 4 transmit hydrophone

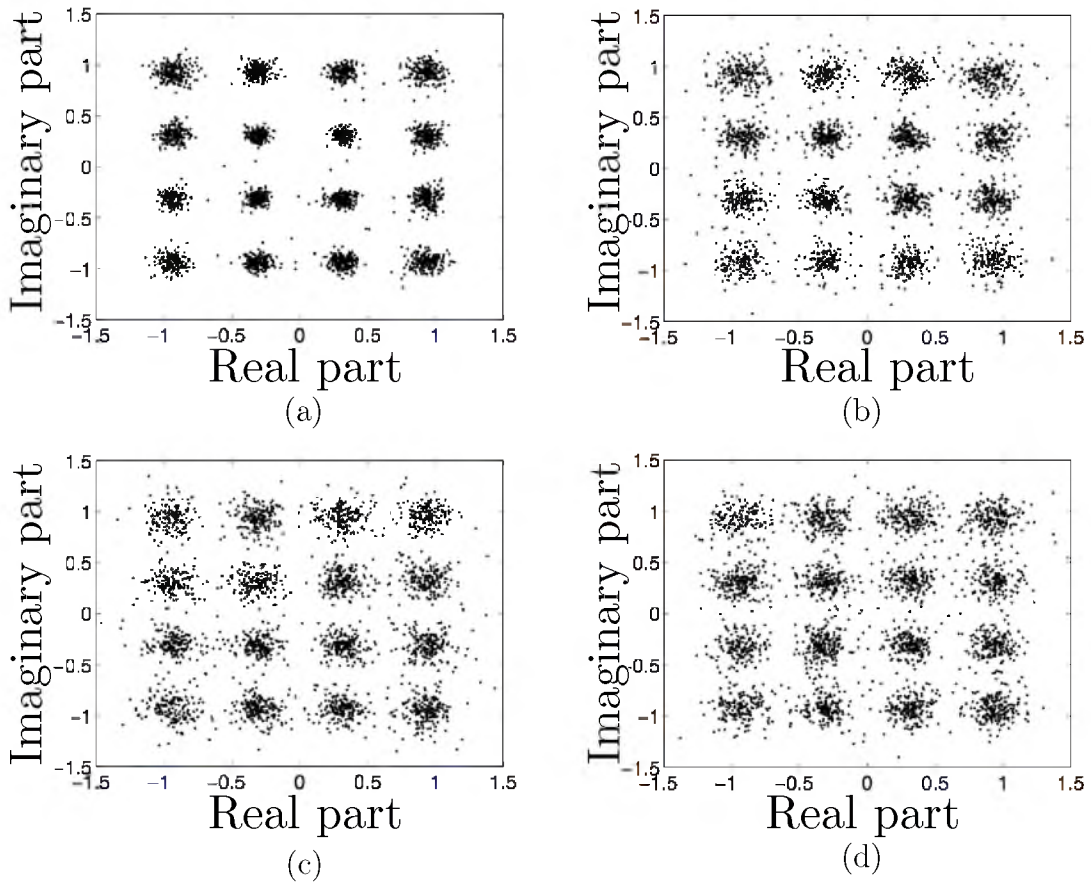


**Figure 7.6**: Eye diagram for 16QAM constellation. (a) 1 transmit hydrophone (b) 2 transmit hydrophone (c) 3 transmit hydrophone (d) 4 transmit hydrophone

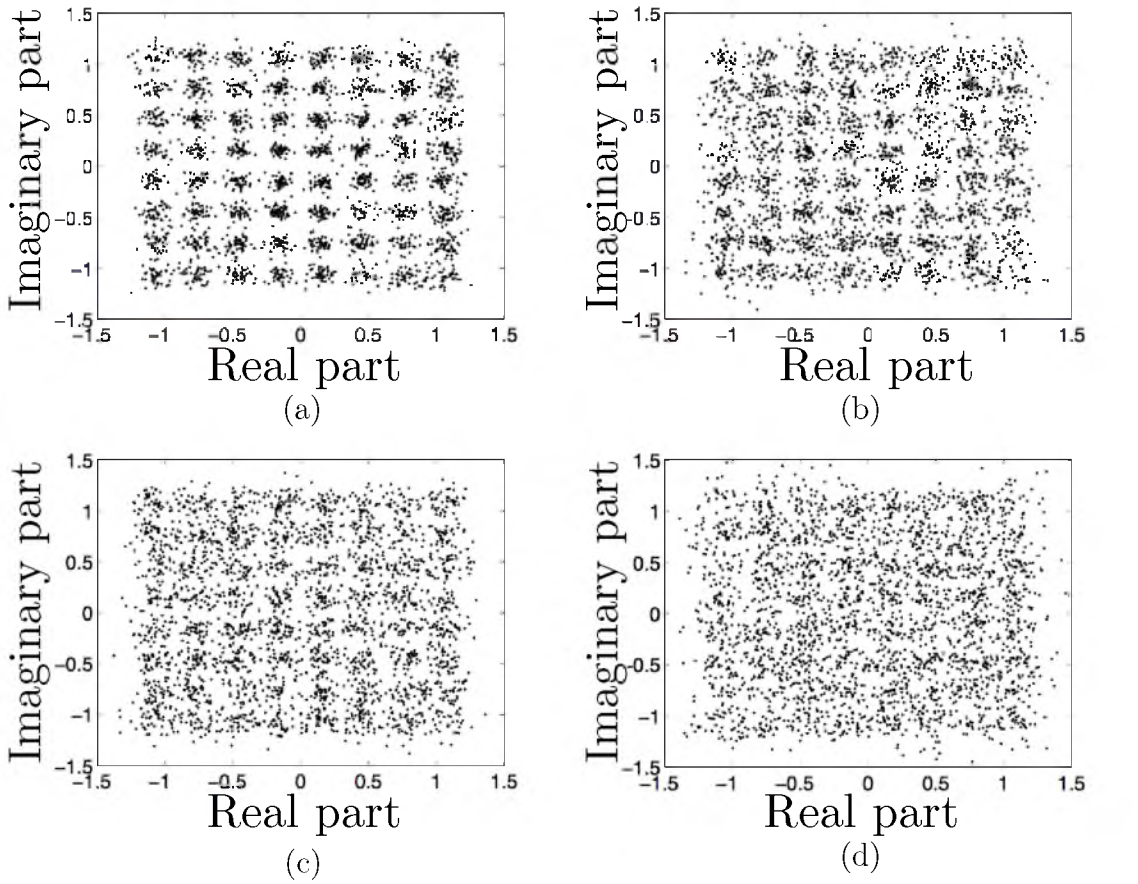


**Figure 7.7**: Eye diagram for 64QAM constellation. (a) 1 transmit hydrophone (b) 2 transmit hydrophone (c) 3 transmit hydrophone (d) 4 transmit hydrophone

Assuming the perfect knowledge of channel, the SIR performance difference between the single transmitter and multiple transmitter cases is reduced, as one would expect. These results are presented in Table 7.4. It can be seen that the SIR decreases 2 dB when the number of transmitters is increased from 1 to 4.

## 7.3 Summary

In this chapter, we analyzed the feasibility of implementing a MIMO system for multicarrier UWA communication channels. Our study emphasized the bandwidth efficiency of multicarrier MIMO communication in this application. We found that the bandwidth efficiency is increased very slowly by increasing the number of transmit antennas. On the other hand, this increase in the number of antennas results in poor SINR performance, so we conclude that the value of MIMO to UWA communication is very limited.

**Table 7.4**: SIR in dB for different constellations and number of transmitters when channel is known.

| $S$ | QPSK | 16QAM | 64QAM |
|---|---|---|---|
| 1 | 21.8 | 21.8 | 21.8 |
| 2 | 21.2 | 21.3 | 21.2 |
| 3 | 20.6 | 20.6 | 20.7 |
| 4 | 19.9 | 19.9 | 19.9 |

# CHAPTER 8

# CONCLUSIONS AND FUTURE RESEARCH

There is high demand for broadband communications which is increasing with a very fast pace. This has led to the use of multicarrier methods. Orthogonal frequency division multiplexing (OFDM) has been the most popular multicarrier method which enables high rate communications with simple equalizer design. However, OFDM might not be the best choice for some applications, such as doubly dispersive channels, cognitive radios, and multiple access. Specifically, for doubly dispersive channels that exhibit spreading in both time and frequency, OFDM suffers from a significant amount of ICI and has a very poor receiver performance. Therefore, to overcome these disadvantages, filterbank multicarrier (FBMC) has been suggested as an alternative to OFDM. FBMC methods use a bank of filters in the transmitter and receiver which are modulated versions of a prototype filter. The use of this prototype filter can overcome the disadvantages of OFDM. Filtered multitone (FMT) is a subset of FBMC methods which employs nonoverlapping filters and is simply generalizable to MIMO applications. In this dissertation, we studied the conventional FMT systems for slow fading channels. We also developed a novel FMT method for doubly dispersive channels was presented and examined.

We formulated the FMT transmitter in continuous and discrete time domains. An efficient implementation of FMT systems in discrete time domain was derived and the conditions for perfect reconstruction in an FBMC communication system was presented.

We derived equations for FMT in slow fading channels that allow evaluation of FMT when applied to mobile wireless communication systems. We considered using

fractionally spaced per tone channel equalizers with a different number of taps. The numerical results showed that single-tap equalizers suffice for typical wireless channels.

We furthered our equalizer design study by introducing adaptive equalizers which use channel estimation. We derived equations for an MMSE channel estimator. The results of optimum equalizers (when channel is known perfectly) were compared with those of the adaptive equalizers, and found that a loss of 1 dB incurs. This study considered the finite duration of the channel impulse response and used that to improve on the equalizers performance.

We introduced a new form of FMT which is specially designed to handle doubly dispersive channels by developing a prototype filter design method for robust performance. We called this FMT-dd. The proposed FMT-dd was applied to two common methods of data symbol orientation in the time-frequency space, namely, rectangular and hexagonal lattices. We found that our design outperforms both OFDM and the conventional FMT systems significantly. Moreover, hexagonal orientation expectedly outperformed the rectangular orientation.

The FMT-dd design was applied to real-world underwater acoustic (UWA) communication channels. The experimental results from an at-sea experiment (ACOMM10) demonstrated that this new design provided a significant gain over OFDM.

The feasibility of implementing a MIMO system for multicarrier UWA communication channels was analyzed. Our study emphasized the bandwidth efficiency of multicarrier MIMO communication in this application. We found that the bandwidth efficiency is increased very slowly by increasing the number of transmit antennas. On the other hand, this increase in the number of antennas resulted in poor SINR performance, so we conclude that the value of MIMO to UWA communication is very limited.

## 8.1 Outlook into Future Research

From this research, one can conclude that filtered multitone is a good choice for UWA communication systems. The work in this dissertation can be considered as a starting point for many other challenging problems in development of FMT systems for fading channels.

### 8.1.1 Nonuniform Doppler Scaling

In a communication system, when the transmitter and/or receiver are moving, the Doppler effect is introduced. In wireless channels, the Doppler effect can be modelled as a carrier frequency offset (CFO) in the receiver which is fixed for all of the bandwidth. On the other hand, due to the wideband nature of the UWA communication system, Doppler effect results in scaling the time-domain signal. Scaling the time-domain signal translates to a CFO that changes with respect to frequency in the frequency domain. This scaling may be different for different paths of the channel. Also, this scaling could change over time when the transmitter or receiver are accelerating or decelerating. Design of algorithms to find this scaling and compensate it should be investigated.

### 8.1.2 Channel Modelling

One of the most challenging parts of an UWA communication system is channel estimation. The UWA channel is characterized by the low speed of sound, large bandwidth relative to the carrier frequency, long delay spread, and fast time variations. Due to the low number of scatterers in UWA channels, they are considered to be sparse channels. A good channel model for UWA channels results in improved channel estimates as well as more efficient Doppler effect mitigation algorithms. Developing a good channel model for UWA is a research area that could be investigated in the future.

### 8.1.3 Iterative Decoding and Channel Estimation Methods

In order to estimate the channel for multicarrier UWA communication, pilot subcarriers are used. However, since UWA communications suffer from a significant amount of interference, estimated channel values are noisy. To improve these estimated values, one can create a loop by feeding the soft outputs from the channel decoder to the channel estimation algorithm. This iterative method can result in significant performance improvement of the receiver. Design and implementation of an iterative FMT receiver for UWA channels and analyzing its performance can be another interesting research topic.

# REFERENCES


[1] R. Haas and J.-C. Belfiore, "A time-frequency well-localized pulse for multiple carrier transmission," *Wireless Personal Communications*, vol. 5, pp. 1–18, 1997.

[2] S. Sesia, I. Toufik, and M. Baker, "LTE–The UMTS Long Term Evolution," *From Theory to Practice, published in*, vol. 66, 2009.

[3] L. Hommen, "The universal mobile telecommunications system (umts): Third generation," *The Internet and Mobile Telecommunications System of Innovation, Edward Elgar, Cheltenham*, pp. 129–61, 2003.

[4] M. Mouly, M. Pautet, and T. Foreword By-Haug, *The GSM system for mobile communications*. Telecom Publishing, 1992.

[5] T. Halonen, J. Romero, and J. Melero, *GSM, GPRS and EDGE performance: evolution towards 3G/UMTS*. Wiley, 2003.

[6] R. Van Nee, "Breaking the gigabit-per-second barrier with 802.11ac," *Wireless Communications, IEEE*, vol. 18, no. 2, p. 4, April 2011.

[7] "IEEE standard for information technology- telecommunications and information exchange between systems-local and metropolitan area networks-specific requirements-part 11: Wireless lan medium access control (MAC) and physical layer (PHY) specifications," *IEEE Std 802.11-1997*, pp. i –445, 1997.

[8] *Very high speed digital subscriber line transceivers 2 (VDSL2)*, ITU-T Recommendation G.993.2 Std., February 2006.

[9] *Air Interface for Fixed and Mobile Broadband Wireless Access Systems*, IEEE 802.16e Std., 2005.

[10] *Very-high bit-rate Digital Subscriber Lines (VDSL) Metallic Interface, Part 3: Technical Specification of a Multi-Carrier Modulation Transceiver*, Working Group R1E1.4 Std., 2000, document T1E1.4/2000-013R3.

[11] H. Holma and A. Toskala, *HSDPA/HSUPA For UMTS*. Wiley Online Library, 2006.

[12] A. Ghosh, R. Ratasuk, B. Mondal, N. Mangalvedhe, and T. Thomas, "LTE-advanced: next-generation wireless broadband technology," *Wireless Communications, IEEE*, vol. 17, no. 3, pp. 10 –22, June 2010.

[13] *IEEE Standard for Information technology–Telecommunications and information exchange between systems Local and metropolitan area networks–Specific requirements Part 11: Wireless LAN Medium Access Control (MAC) and Physical Layer (PHY) Specifications*, Std.

[14] J. Bingham, *ADSL, VDSL, and multicarrier modulation.* Wiley, 2000.

[15] V. Garg, *IS-95 CDMA and cdma2000: cellular/PCS systems implementation.* Prentice Hall, 1999.

[16] R. V. Nee and R. Prasad, *OFDM for Wireless Multimedia Communications.* Arthec House, Boston, MA, 2000.

[17] Y. Li and G. L. St, *Orthogonal Frequency Division Multiplexing for Wireless Communications.* Springer, New York, NY, 2006.

[18] "IEEE standard for local and metropolitan area networks part 16: Air interface for fixed and mobile broadband wireless access systems amendment 2: Physical and medium access control layers for combined fixed and mobile operation in licensed bands and corrigendum 1," *IEEE Std 802.16e-2005 and IEEE Std 802.16-2004/Cor 1-2005 (Amendment and Corrigendum to IEEE Std 802.16-2004)*, 2006.

[19] B. Farhang-Boroujeny and R. Kempter, "Multicarrier communication techniques for spectrum sensing and communication in cognitive radios," *IEEE Communications Magazine*, vol. 46, no. 4, pp. 80–85, April 2008.

[20] B. Farhang-Boroujeny, "Multicarrier modulation with blind detection capability using cosine modulated filter banks," *IEEE Trans. Commun.*, vol. 51, no. 12, pp. 2057–2070, December 2003.

[21] C. Siclet, P. Siohan, and D. Pinchon, "Perfect reconstruction conditions and design of oversampled DFT-modulated transmultiplexers," *EURASIP J. Appl. Signal Process.*, vol. 2006, pp. 94–94, January 2006. [Online]. Available: http://dx.doi.org/10.1155/ASP/2006/15756

[22] B. Farhang-Boroujeny, "OFDM versus filter bank multicarrier," *Signal Processing Magazine, IEEE*, vol. 28, no. 3, pp. 92 –112, May 2011.

[23] B. Saltzberg, "Performance of an efficient parallel data transmission system," *IEEE Trans. on Comm. Tech.*, vol. 15, no. 6, pp. 805–811, December 1967.

[24] R. Chang, "High-speed multichannel data transmission with bandlimited orthogonal signals," *Bell Sys. Tech. J.*, vol. 45, pp. 1775–1796, December 1966.

[25] S. Weinstein and P. Eber, "Data transmission by frequency-division multiplexing using the discrete Fourier transform," *IEEE Transactions on Communication Technology*, vol. 19, no. 5, pp. 628–634, October 1971.

[26] D. Pinchon, P. Siohan, and C. Siclet, "Design techniques for orthogonal modulated filterbanks based on a compact representation," *Signal Processing, IEEE Transactions on*, vol. 52, no. 6, pp. 1682 – 1692, June 2004.

[27] T. A. Weiss and F. K. Jondral, "Spectrum pooling: an innovative strategy for the enhancement of spectrum efficiency," vol. 42, no. 3, 2004.

[28] J. Proakis, *Digital Communications*, 3rd ed. McGraw-Hill, New York, NY, 1995.

[29] B. Hirosaki, "An orthogonally multiplexed QAM system using the discrete Fourier transform," *IEEE Transactions on Communications*, vol. 29, no. 7, pp. 982–989, July 1981.

[30] G. Cherubini, E. Eleftheriou, and S. Olcer, "Filtered multitone modulation for VDSL," in *Proc. IEEE Globecom'99*, vol. 2, 1999, pp. 1139–1144.

[31] G. Cherubini, E. Eleftheriou, S. Olcer, and J. Cioffi, "Filter bank modulation techniques for very high speed digital subscriber lines," *IEEE Commun. Mag.*, vol. 38, no. 5, pp. 98–104, May 2000.

[32] G. Cherubini, E. Eleftheriou, and S. Olcer, "Filtered multitone modulation for very high-speed digital subscriber lines," *IEEE Journal on Selected Areas in Commun.*, vol. 20, no. 5, pp. 1016–1028, June 2002.

[33] T. Wang, J. Proakis, and J. Zeidler, "Interference analysis of filtered multitone modulation over time-varying frequency- selective fading channels," *IEEE Transactions on Communications*, vol. 55, no. 4, April 2007.

[34] M. Tzannes, M. Tzannes, and H. Resnikoff, "The dwmt: A multicarrier transceiver for ADSL using M-band wavelet transforms," *ANSI Contribution T1E1.4/93-067*, vol. 1993, March.

[35] B. Farhang-Boroujeny and C. G. Yuen, "Cosine modulated and offset QAM filter bank multicarrier techniques: A continuous-time prospect," *Eurasip Journal on Advances in Signal processing*, vol. 2010, 2010.

[36] B. Li, S. Zhou, M. Stojanovic, L. Freitag, and P. Willett, "Multicarrier communication over underwater acoustic channels with nonuniform doppler shifts," vol. 33, no. 2, pp. 198–209, 2008.

[37] ——, "Non-uniform doppler compensation for zero-padded OFDM over fast-varying underwater acoustic channels," in *OCEANS 2007 - Europe*, June 2007, pp. 1 –6.

[38] B. Li, S. Zhou, M. Stojanovic, and L. Freitag, "Pilot-tone based ZP-OFDM demodulation for an underwater acoustic channel," in *OCEANS 2006*, September 2006, pp. 1 –5.

[39] B. L. Floch, M. Alard, and C. Berrou, "Coded orthogonal frequency division multiplex," *Proceedings of IEEE*, pp. 982–996, June 1995.

[40] M. Alard, "Construction of a multicarrier signal," Patent WO 96/35 278, 1996.

[41] K. Liu, T. Kadous, and A. Sayeed, "Orthogonal time-frequency signaling over doubly dispersive channels," *Information Theory, IEEE Transactions on*, vol. 50, no. 11, pp. 2583 – 2603, November 2004.

[42] S. Das and P. Schniter, "PMax-SINR ISI/ICI-shaping multicarrier communication over the doubly dispersive channel," *Signal Processing, IEEE Transactions on*, vol. 55, no. 12, pp. 5782 –5795, December 2007.

[43] G. Taubock, F. Hlawatsch, D. Eiwen, and H. Rauhut, "Compressive estimation of doubly selective channels in multicarrier systems: Leakage effects and sparsity-enhancing processing," vol. 4, no. 2, pp. 255–271, 2010.

[44] W. Kozek and A. F. Molisch, "Nonorthogonal pulseshapes for multicarrier communications in doubly dispersive channels," vol. 16, no. 8, pp. 1579–1589, 1998.

[45] S.-M. Phoong, Y. Chang, and C.-Y. Chen, "DFT-modulated filterbank transceivers for multipath fading channels," vol. 53, no. 1, pp. 182–192, 2005.

[46] P. Jung and G. Wunder, "WSSUS pulse design problem in multicarrier transmission," vol. 55, no. 9, 2007.

[47] B. Farhang-Boroujeny and C. Schlegel, "Efficient multicarrier realization of full-rate space-time orthogonal block coded systems," in *Communications, 2003. ICC '03. IEEE International Conference on*, vol. 4, 11-15 2003, pp. 2267 – 2271.

[48] C. Ll, P. Siohan, and R. Legouable, "The Alamouti Scheme with CDMA-OFDM/OQAM," *Eurasip Journal on Advances in Signal processing*, vol. 2010.

[49] M. Renfors, T. Ihalainen, and T. Stitz, "A block-alamouti scheme for filter bank based multicarrier transmission," in *Wireless Conference (EW), 2010 European*, 2010, pp. 1031 –1037.

[50] J. L. T. Ihalainen, A. Ikhlef and M. Renfors, "Channel equalization for multi-antenna FBMC/OQAM receivers," *Submitted to IEEE Transactions on Vehicular Technology*.

[51] B. M. Hochwald and S. ten Brink, "Achieving near-capacity on a multiple-antenna channel," *IEEE transactions on communications*, vol. 51, no. 3, pp. 389–399, March 2003.

[52] B. Farhang-Boroujeny, H. Zhu, and Z. Shi, "Markov chain monte carlo algorithm for CDMA and MIMO communication systems," *IEEE Trans. Signal Processing*, vol. 54, no. 5, pp. 1896 1896– 1909, May 2006.

[53] Pooyan Amini and B. Farhang-Boroujeny, "Per-tone equalizer design and analysis of filtered multitone communication systems over time-varying frequency-selective channels," in *IEEE International Conference on Communications, 2009. ICC '09.*, June 2009, pp. 1 –5.

[54] ——, "Tracking behavior of adaptive equalizers in filtered multitone communication systems," in *Signals, Systems and Computers, 2009 Conference Record of the Forty-Third Asilomar Conference on.* IEEE, 2009, pp. 903–907.

[55] Pooyan Amini, C. H. Yuen, R.-R. Chen, and B. Farhang-Boroujeny, "Isotropic filter design for MIMO filter bank multicarrier communications," in *Sensor Array and Multichannel Signal Processing Workshop (SAM), 2010 IEEE*, October 2010, pp. 89 –92.

[56] Pooyan Amini, C. Yuen, C. R.-R., and B. Farhang-Boroujeny, "Robust filter design for multicarrier communication over doubly dispersive channels," *2010 Symposium and Wireless Summer School at Virginia Tech.*, June 2010.

[57] Pooyan Amini and B. Farhang-Boroujeny, "Design and performance evaluation of filtered multitone (FMT) in doubly dispersive channels," in *Communications (ICC), 2011 IEEE International Conference on*, June 2011, pp. 1 –5.

[58] Pooyan Amini, R.-R. Chen, and B. Farhang-Boroujeny, "Filterbank multicarrier for underwater communications," in *Communication, Control, and Computing (Allerton), 2011 49th Annual Allerton Conference on*, September 2011, pp. 639 –646.

[59] B. Farhang-Boroujeny, *Signal processing techniques for software radios.* Lulu publishing house, 2008.

[60] B. Farhang-Boroujeny and R. Kempter, "Multicarrier communication techniques for spectrum sensing and communication in cognitive radios," vol. 46, no. 4, pp. 80–85, 2008.

[61] A. Tonello, "Exact matched filter performance bound for multitone modulation in fading channels," in *WPMC*, vol. 3, October 2003, pp. 361–365.

[62] M. Failli, "Digital land mobile radio communications COST 207," European Commission, Tech. Rep., 1989.

[63] Y. Li, J. Cimini, L.J., and N. Sollenberger, "Robust channel estimation for OFDM systems with rapid dispersive fading channels," *Communications, IEEE Transactions on*, vol. 46, no. 7, pp. 902 –915, July 1998.

[64] B. Farhang-Boroujeny, "A square-root Nyquist (M) filter design for digital communication systems," *IEEE Trans. on Signal Proc.*, vol. 56, no. 5, pp. 2127–2132, May 2008.

[65] I. Trigui, M. Siala, S. Affes, and A. Stephenne, "SIR optimized Hermite-based pulses for BFDM systems in doubly dispersive channels," in *Proc. Int. Symp. Signals, Systems and Electronics ISSSE '07*, 2007, pp. 587–590.

[66] I. Trigui, M. Siala, and H. Boujemaa, "Optimized pulse shaping for OFDM multi-user communications over doubly dispersive channels," in *Signal Processing and Its Applications, 2007. ISSPA 2007. 9th International Symposium on*, February 2007, pp. 1 –4.

[67] B. Boashash, Ed., *Time frequency signal analysis and processing: a comprehensive reference.* Elsevier, 2003.

[68] M. Rossi, J. Zhang, and W. Steenaart, "Iterative least squares design of perfect reconstruction QMF banks," in *Proc. Canadian Conference on Electrical and Computer Engineering*, vol. 2, 1996, pp. 762–765.

[69] T. Strohmer and S. Beaver, "Optimal OFDM design for time-frequency dispersive channels," *IEEE Transactions on Communications*, vol. 51, no. 7, pp. 1111–1122, July 2003.

[70] W. C. Jakes, *Microwave Mobile Communications*. IEEE Press, 1993.

[71] A. Singer, J. Nelson, and S. Kozat, "Signal processing for underwater acoustic communications," *Communications Magazine, IEEE*, vol. 47, no. 1, pp. 90 –96, January 2009.

[72] W. Li and J. Preisig, "Estimation of rapidly time-varying sparse channels," *Oceanic Engineering, IEEE Journal of*, vol. 32, no. 4, pp. 927 –939, October 2007.

[73] J. Gomes and M. Stojanovic, "Performance analysis of filtered multitone modulation systems for underwater communication," in *Proc. MTS/IEEE Biloxi - Marine Technology for Our Future: Global and Local Challenges OCEANS 2009*, 2009, pp. 1–9.

[74] S.-J. Hwang and P. Schniter, "Efficient multicarrier communication for highly spread underwater acoustic channels," vol. 26, no. 9, pp. 1674–1683, 2008.

[75] C. Berger, S. Zhou, J. Preisig, and P. Willett, "Sparse channel estimation for multicarrier underwater acoustic communication: From subspace methods to compressed sensing," *Signal Processing, IEEE Transactions on*, vol. 58, no. 3, pp. 1708–1721, 2010.

[76] T. Kang and R. Litis, "Matching pursuits channel estimation for an underwater acoustic OFDM modem," in *Acoustics, Speech and Signal Processing, 2008. ICASSP 2008. IEEE International Conference on*, 31 2008-April 4 2008, pp. 5296 –5299.

[77] J. Huang, C. Berger, S. Zhou, and J. Huang, "Comparison of basis pursuit algorithms for sparse channel estimation in underwater acoustic OFDM," in *OCEANS 2010 IEEE - Sydney*, May 2010, pp. 1 –6.

[78] J. Huang, S. Zhou, J. Huang, J. Preisig, L. Freitag, and P. Willett, "Progressive MIMO-OFDM reception over time-varying underwater acoustic channels," in *Signals, Systems and Computers (ASILOMAR), 2010 Conference Record of the Forty Fourth Asilomar Conference on.* IEEE, 2010, pp. 1324–1329.

[79] C. Qi, X. Wang, and L. Wu, "Underwater acoustic channel estimation based on sparse recovery algorithms," *Signal Processing, IET*, vol. 5, no. 8, pp. 739 –747, December 2011.

[80] S. Kim, "Angle-domain frequency-selective sparse channel estimation for underwater MIMO-OFDM systems," *Communications Letters, IEEE*, vol. 16, no. 5, pp. 685 –687, May 2012.

[81] Z. Wang, S. Zhou, J. Preisig, K. Pattipati, and P. Willett, "Clustered adaptation for estimation of time-varying underwater acoustic channels," *Signal Processing, IEEE Transactions on*, vol. 60, no. 6, pp. 3079 –3091, June 2012.

[82] T. Kang and R. Iltis, "Iterative carrier frequency offset and channel estimation for underwater acoustic OFDM systems," *Selected Areas in Communications, IEEE Journal on*, vol. 26, no. 9, pp. 1650–1661, 2008.

[83] K. Tu, D. Fertonani, T. Duman, M. Stojanovic, J. Proakis, and P. Hursky, "Mitigation of intercarrier interference for OFDM over time-varying underwater acoustic channels," *Oceanic Engineering, IEEE Journal of*, vol. 36, no. 2, pp. 156–171, 2011.

[84] J. Huang, S. Zhou, J. Huang, C. Berger, and P. Willett, "Progressive inter-carrier interference equalization for OFDM transmission over time-varying underwater acoustic channels," *Selected Topics in Signal Processing, IEEE Journal of*, vol. 5, no. 8, pp. 1524–1536, 2011.

[85] Z. Wang, S. Zhou, J. Catipovic, and P. Willett, "Parameterized cancellation of partial-band partial-block-duration interference for underwater acoustic OFDM," *Signal Processing, IEEE Transactions on*, vol. 60, no. 4, pp. 1782–1795, 2012.

[86] J. Huang, S. Zhou, and P. Willett, "Nonbinary ldpc coding for multicarrier underwater acoustic communication," vol. 26, no. 9, pp. 1684–1696, 2008.

[87] B. Li, J. Huang, S. Zhou, K. Ball, M. Stojanovic, L. Freitag, and P. Willett, "MIMO-OFDM for high-rate underwater acoustic communications," *Oceanic Engineering, IEEE Journal of*, vol. 34, no. 4, pp. 634–644, 2009.

[88] S. Mason, C. Berger, S. Zhou, K. Ball, L. Freitag, and P. Willett, "An OFDM design for underwater acoustic channels with doppler spread," in *Digital Signal Processing Workshop and 5th IEEE Signal Processing Education Workshop, 2009. DSP/SPE 2009. IEEE 13th.* IEEE, 2009, pp. 138–143.

[89] J. Gomes and V. Barroso, "Time-reversed OFDM communication in underwater channels," in *Signal Processing Advances in Wireless Communications, 2004 IEEE 5th Workshop on.* IEEE, 2004, pp. 626–630.

[90] X. Xu, G. Qiao, J. Su, P. Hu, and E. Sang, "Study on turbo code for multicarrier underwater acoustic communication," in *Wireless Communications, Networking and Mobile Computing, 2008. WiCOM'08. 4th International Conference on.* IEEE, 2008, pp. 1–4.

[91] P. Ceballos Carrascosa and M. Stojanovic, "Adaptive channel estimation and data detection for underwater acoustic MIMO-OFDM systems," *Oceanic Engineering, IEEE Journal of*, vol. 35, no. 3, pp. 635–646, 2010.

[92] Z. Wang, S. Zhou, G. Giannakis, C. Berger, and J. Huang, "Frequency-domain oversampling for zero-padded OFDM in underwater acoustic communications," *Oceanic Engineering, IEEE Journal of*, vol. 37, no. 1, pp. 14–24, 2012.

[93] S. Yerramalli and U. Mitra, "Optimal resampling of OFDM signals for multiscale–multilag underwater acoustic channels," *Oceanic Engineering, IEEE Journal of*, vol. 36, no. 1, pp. 126–138, 2011.

[94] P. Vaidyanathan, *Multirate systems and filter banks*. Pearson Education India, 1993.

[95] T. Schmidl and D. Cox, "Robust frequency and timing synchronization for OFDM," *Communications, IEEE Transactions on*, vol. 45, no. 12, pp. 1613 –1621, December 1997.

[96] P. Amini and B. Farhang-Boroujeny, "Packet format design and decision directed tracking methods for filter bank multicarrier systems," *EURASIP J. Adv. Sig. Proc.*, vol. 2010, 2010.

[97] D. Tse and P. Viswanath, *Fundamentals of wireless communication*. New York, NY, USA: Cambridge University Press, 2005.

[98] S. Lin and D. J. Costello, *Error Control Coding*, 2nd ed. Prentice Hall, June 2004.

[99] D. Kilfoyle, J. Preisig, and A. Baggeroer, "Spatial modulation experiments in the underwater acoustic channel," *Oceanic Engineering, IEEE Journal of*, vol. 30, no. 2, pp. 406–415, 2005.

[100] S. Roy, T. Duman, V. McDonald, and J. Proakis, "High-rate communication for underwater acoustic channels using multiple transmitters and space–time coding: Receiver structures and experimental results," *Oceanic Engineering, IEEE Journal of*, vol. 32, no. 3, pp. 663–688, 2007.

[101] H. Song, W. Hodgkiss, W. Kuperman, T. Akal, and M. Stevenson, "Multiuser communications using passive time reversal," *Oceanic Engineering, IEEE Journal of*, vol. 32, no. 4, pp. 915–926, 2007.

[102] A. Song, M. Badiey, and V. McDonald, "Multichannel combining and equalization for underwater acoustic MIMO channels," in *OCEANS 2008*, September 2008, pp. 1 –6.

[103] J. Tao, Y. Zheng, C. Xiao, T. Yang, and W.-B. Yang, "Time-domain receiver design for MIMO underwater acoustic communications," in *OCEANS 2008*, September 2008, pp. 1 –6.

[104] J. Zhang, Y. Zheng, and C. Xiao, "Frequency-domain turbo equalization for MIMO underwater acoustic communications," in *OCEANS 2009 - EUROPE*, May 2009, pp. 1 –5.

[105] F. Qu and L. Yang, "Basis expansion model for underwater acoustic channels," in *OCEANS 2008*, September 2008, pp. 1 –7.

[106] H. Wan, R.-R. Chen, J. W. Choi, A. Singer, J. Preisig, and B. Farhang-Boroujeny, "Stochastic expectation maximization algorithm for long-memory fast-fading channels," in *Global Telecommunications Conference (GLOBECOM 2010), 2010 IEEE*, December 2010, pp. 1 –5.

[107] X. Mao, R.-R. Chen, and B. Farhang-Boroujeny, "Decorrelation MIMO receiver for fast fading channels," *Submitted to IEEE Signal Processing Letters*, 2013.

[108] W. Shin, S. Lee, D. Kwon, and J. Kang, "LMMSE channel estimation with soft statistics for turbo-MIMO receivers," *Communications Letters, IEEE*, vol. 13, no. 8, pp. 585–587, 2009.